

THESIS ON NATURAL AND EXACT SCIENCES B196

Computational Study of Cyclohexylhemicucurbiturils

MARIO ÖEREN

TUT
PRESS

TALLINN UNIVERSITY OF TECHNOLOGY
Faculty of Science
Department of Chemistry

This dissertation was accepted for the defence of the degree of Doctor of Philosophy in Chemistry on October 28, 2015.

Supervisors: Assoc. Prof. Toomas Tamm, Department of Chemistry, Faculty of Science, Tallinn University of Technology, Estonia

Assoc. Prof. Riina Aav, Department of Chemistry, Faculty of Science, Tallinn University of Technology, Estonia

Reviewed by: Dr. Andre Lomaka, Department of Chemistry, Faculty of Science, Tallinn University of Technology, Estonia

Opponents: Assoc. Prof. Eric Masson, Department of Chemistry and Biochemistry, Ohio University, U. S. A.

Dr. Uko Maran, Institute of Chemistry, Faculty of Science and Technology, University of Tartu, Estonia

Defence of the thesis: 4th of December 2015

Declaration:

Hereby I declare that this doctoral thesis, my original investigation and achievement, submitted for the doctoral degree at Tallinn University of Technology has not been submitted for any academic degree.

/Mario Öeren/



Copyright: Mario Öeren, 2015

ISSN 1406-4723

ISBN 978-9949-23-859-0 (publication)

ISBN 978-9949-23-860-6 (PDF)

LOODUS- JA TÄPPISTEADUSED B196

Tsükloheksüülhemikukurbituriilide arvutuskeemiline modelleerimine

MARIO ÖEREN

Contents

List of Publications	7
Abbreviations.....	8
Introduction.....	9
1. Literature overview.....	10
1.1 Theoretical background	10
1.1.1 Quantum Chemical Methods	10
1.1.2 Density Functional Theory	11
1.1.3 Quantum Theory of Atoms in Molecules	12
1.1.4 Solvation effects	12
1.2 General Overview of Macrocycles	13
1.2.1 Cucurbiturils	14
1.2.2 Hemicucurbiturils	16
1.2.3 Cyclodextrins.....	18
1.3 Computational Methods Used in Host-Guest Chemistry.....	18
1.3.1 Geometry optimization	18
1.3.2 Electronic Structure	19
1.3.3 Host-Guest Interactions	19
1.3.4 Description of the Dimensions of Macrocycles.....	21
2. Aims of the present work.....	23
3. Methods	24
4. Results and discussion	26
4.1 Computational studies of complexation of Cyclohexylhemi- cucurbit[6]uril (Publication I).....	26
4.1.1 Geometry of cyclohexylhemicucurbit[6]uril	26
4.1.2 Electronic structure and potential binding sites of guests of cyclohexylhemicucurbit[6]uril.....	28
4.1.3 Complexes of cyclohexylhemicucurbit[6]uril with anions.....	29
4.1.4 Transition states of guest-host complex formation with anions as guests	33
4.1.5 Complexes of cyclohexylhemicucurbit[6]uril with H ⁺	33

4.1.6 Cyclohexylhemicucurbit[6]uril complexes with non-dissociated acids	35
4.1.7 Summary of studies of cycHC[6] and its complexes	36
4.2 Geometries (Publication II) and cavities of cycHC[<i>n</i>] homologues ..	36
4.3 The equilibrium and proposed mechanism of the reversible macrocyclization (Publication III)	47
4.3.1 Equilibrium between cycHC[6] and cycHC[8]	47
4.3.2 Simplified model system	48
4.3.3 Depropagation and propagation	50
4.3.4 Transition States TS2a and TS2b	51
4.3.5 Summary of the reversible macrocyclization mechanism	52
Conclusions	53
References	54
Publication I	61
Publication II	71
Publication III	79
Part of Supporting Info of Publication III	85
Abstract	93
Kokkuvõte	94
Acknowledgements	95
Elulookirjeldus	96
<i>Curriculum Vitae</i>	97
Original publications	98

List of Publications

- I** M. Öeren, E. Shmatova, T. Tamm and R. Aav “Computational and ion mobility MS study of (*all-S*)-cyclohexylhemicurbit[6]uril structure and complexes” *Physical Chemistry Chemical Physics*, 2014, **16**, 19198–19205.
- II** M. Fomitšenko, E. Shmatova, M. Öeren, I. Järving and R. Aav “New Homologues of Chiral Cyclohexylhemicurbit[*n*]urils” *Supramolecular Chemistry*, 2014, **26**, 698–703.
- III** E. Prigorchenko, M. Öeren, S. Kaabel, M. Fomitšenko, I. Reile, I. Järving, T. Tamm, F. Topić, K. Rissanen and R. Aav “Template Controlled Synthesis of Chiral Cyclohexylhemicurbit[8]uril” *Chemical Communications*, 2015, **51**, 10921–10924.

Author’s contribution to the Publications

The contributions by the author to the papers included in the thesis are as follows:

I – Planned and executed all computational experiments. Wrote the final manuscript.

II, III – Planned and executed all computational experiments. Participated in the final manuscript preparation (wrote paragraphs containing computational experiments).

Abbreviations

BCP	Bond Critical Point
CB[<i>n</i>]	Cucurbit[<i>n</i>]uril
CD	Cyclodextrin
COSMO	Conductor Like Screening Model
CycHC[<i>n</i>]	Cyclohexylhemicucurbit[<i>n</i>]uril
DCL	Dynamic Combinatorial Library
DFT	Density Functional Theory
HC[<i>n</i>]	Hemicucurbit[<i>n</i>]uril
HF	Hartree-Fock
HOMO	Highest Occupied Molecular Orbital
KS	Kohn-Sham
LUMO	Lowest Unoccupied Molecular Orbital
MEP	Map of Electrostatic Potential
MO	Molecular Orbital
MS	Mass Spectrometry
NMR	Nuclear Magnetic Resonance
PC _{cavity}	Packing Coefficient Ratio of a Cavity
QTAIM	Quantum Theory of Atoms in Molecules

Introduction

In 1987, Donald J. Cram, Jean-Marie Lehn, and Charles J. Pedersen were awarded with the Nobel Prize in Chemistry “for their development and use of molecules with structure-specific interactions of high selectivity”, which illustrates the overall significance of supramolecular chemistry.^{1,2} Host-guest chemistry is part of supramolecular chemistry, which describes complexes composed of two or more molecules or ions that are held together in particular structural relationships by non-covalent interactions.³ Host-guest chemistry has become an important discipline and there is a wide range of applications where the hosts can be used (*e.g.*, chemical sensors⁴, catalysts⁵, stabilizers⁶, traps to collect hazardous materials⁷, drug delivery vehicles⁸, enantiomer separation⁹, *etc.*).

A fine example of a host is the cucurbituril¹⁰, which, besides multiple homologues, has a variety of derivatives, analogues and congeners with diverse complexing abilities as described in a review by Lagona *et al*¹¹. The cucurbiturils form inclusion complexes with various cations, anions and neutral molecules which have been described in a review by Masson *et al*.¹² The first enantiomerically pure member of the cucurbituril family is the (*all-S*)- and (*all-R*)-cyclohexylhemicucurbituril,¹³ the computational study of which will be presented in the current thesis.

During the last decade, the use of computational methods for understanding and explaining the experimental data of host-guest chemistry has grown steadily. One of the reasons behind it is the increase of computational capabilities, which allows handling of supramolecular systems with relatively high accuracy and within a reasonable time frame. The best ratio between accuracy and cost has been achieved with the density functional theory, which has become the workhorse for studying the host-guest chemistry computationally.^{14a}

This thesis is composed of computational work on the geometries of empty cyclohexylhemicucurbituril homologues and their (inclusion) complexes with various guests. Besides the geometries, the electronic structure of the hosts is studied to explain the binding properties of cyclohexylhemicucurbiturils. In addition, the mechanism of the reversible macrocyclization from one homologue to another is proposed.

1. Literature overview

1.1 Theoretical background

1.1.1 Quantum Chemical Methods

The cornerstone of quantum chemistry is the time-independent Schrödinger equation. It is a partial differential equation which describes stationary states of atomic and molecular systems:

$$\hat{H}\psi = E\psi$$

A wave function (ψ) describes a quantum state of an isolated system of one or more particles. The Hamiltonian (\hat{H}), which acts on the wave function, is an operator corresponding to the total energy (E) of the system. The total energy is generally the sum of the kinetic and the potential energy, but it depends on the Hamiltonian being used.^{15a}

For hydrogen and hydrogen-like atoms (He^+ , Li^{2+} , *etc.*) the exact wave function is known and the Schrödinger equation is analytically solvable. If the system has more than one electron, the interelectronic repulsions must be taken into account which makes the Schrödinger equation insolvable without approximations.^{15b}

The Hartree-Fock (HF) method was developed to construct an approximate wave function, which could be solved using the Schrödinger equation. The Born-Oppenheimer approximation is inherently assumed, thus only the electronic Schrödinger equation is solved. The HF wave function is obtained by generating an initial wave function, which is a product of one-electron orbitals (neglecting the interelectronic repulsions). The orbitals are represented as linear combinations of a set of known functions (basis functions). To satisfy the antisymmetry principle, a Slater determinant is constructed from the one-electron orbitals and the spin-orbitals are used instead of spatial orbitals. While each electron moves independently, it still experiences the Coulomb repulsion due to the average positions of all other electrons. In addition, each electron experiences the exchange interaction due to the antisymmetrization (Slater determinant). To obtain better approximate wave functions the energy of the initial wave function is minimized using the variational method. The minimization process is iterative and for this reason the HF process is called a self-consistent-field approach.^{15b}

While the HF wave functions take into account the interactions between electrons in an average way (HF potential), it does not consider the instantaneous interactions between electrons (electron correlation). Due to that, the HF method has been superseded by several post-HF methods, which have been developed for further improvement of description of electron correlation.^{15b} The methods include configuration interaction¹⁶, coupled cluster¹⁷ and Møller-Plesset perturbation theory¹⁸ which are out of the scope of this thesis.

1.1.2 Density Functional Theory

The electronic wave function of an n -electron molecule in the HF method (and post-HF methods) depends on $3n$ spatial and n spin coordinates. In 1964, Hohenberg and Kohn proved that the ground-state molecular energy (and other molecular electronic properties) can be determined by the electron probability density ($\rho(x, y, z)$) alone, which depends only on three spatial coordinates.¹⁹ The theory states that the ground state energy (E_0) is a functional of ρ , thus $E_0 = E_0[\rho]$.^{15c} Therefore the theory is called density functional theory (DFT).

However, the Hohenberg-Kohn theorem does not state how to calculate E_0 from ρ and how to find ρ without finding the wave function.^{15c} This was solved by Kohn and Sham by using auxiliary functions, which are nowadays known as Kohn-Sham (KS) orbitals, and an exchange-correlation energy functional ($E_{xc}[\rho]$).²⁰ As a side note, Kohn shared the Nobel Prize in Chemistry in 1998 “for his development of the density functional theory”.²¹

In general, the steps involved in DFT calculations are similar to those of HF calculations and the procedure is called Kohn-Sham self-consistent field. The KS theory, like HF theory, uses spin-orbitals, but during minimization, an effective local potential is used instead of the HF potential. To distinguish these orbitals from their HF counterparts, they are referred to as KS orbitals. The aforementioned effective local potential incorporates the exchange-correlation energy potential to account for both the exchange and the correlation effects.^{14b} This potential, in turn, is expressed as the functional derivative of the exchange-correlation functional, E_{xc} with respect to ρ .

The only problem in finding the ground state energy with DFT is that the correct functional $E_{xc}[\rho]$ is not known.^{15c} A lot of approximate functionals have been developed for DFT calculations but the lack of a systematic procedure to improve the functionals is the main drawback of DFT. Nevertheless, DFT is a method used frequently due to its good ratio of computational cost and accuracy.^{14a}

1.1.3 Quantum Theory of Atoms in Molecules

The Quantum Theory of Atoms in Molecules (QTAIM) is a model, where the atoms and bonds in a molecule can be mapped through the topology of the electron density. The molecular structure is revealed by the critical points of the electron density (local maxima and saddle points) together with the gradient paths that originate and terminate at critical points. An example of a contour map of ethene with the gradient vectors is depicted in Figure 1. The maxima of the electron density on Figure 1 depict atoms (brown dots) and the saddle points depict bonds (blue dots). Besides studying chemical bonding and structures of chemical systems, QTAIM allows the calculation of certain physical properties on a per-atom basis. These properties include the strength and type of various bonds, the existence of aromaticity, the intramolecular interactions, *etc.*²²

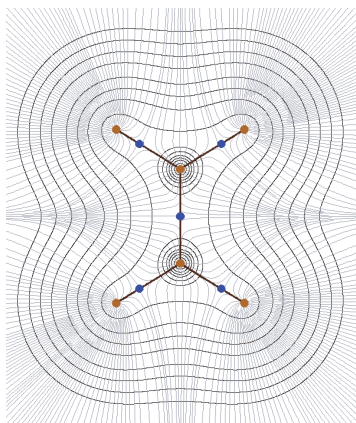


Figure 1. Map of a gradient vector field of the electron density of ethene (including electron density contour lines). Gradient vectors are depicted as grey lines. Atoms are depicted as brown dots and bond critical points (BCPs) are depicted as blue dots. The figure is generated using an example within the Multiwfn²³ program.

1.1.4 Solvation effects

Solvation effects are particularly challenging for computational chemistry. The reason for this is the difficulty of solving the Schrödinger equation for large, non-periodic systems. One way to tackle the problem is to model all or some parts of the studied system using molecular mechanics instead of quantum mechanics. The drawback of this approach is that it needs an efficient way to sample the potential energy hypersurface. Since the hypersurface has numerous local minima the sampling becomes the computational bottleneck.²⁴

If the solvent molecules are not of primary interest, continuum models, which model the solvent as an infinite medium characterized by a dielectric constant, can be used.²⁴ Amongst various solvation models of this kind, the conductor-like screening model (COSMO) is used in the current thesis. In the model, the solute molecule is embedded in a dielectric continuum and forms a cavity within the dielectric. The surface of the cavity is called the solvent accessible surface and is constructed using the sum of a van der Waals radius and an effective radius, which is empirically determined for each solvent.²⁵

The charge of the surface (surface segments) is calculated from the distribution of the electric charge of the studied molecule. From the calculated solvent charges and the charge distribution of the molecule, the energy of the interaction between the solvent and the solute molecule can be calculated.²⁵

1.2 General Overview of Macrocycles

The main subject of the computational study presented in the current thesis is the cyclohexylhemicucurbituril (cycHC)¹³, which is a substituted hemicucurbituril (HC)²⁶, which in turn is a subclass of cucurbiturils (CB)^{10,27}. Thus the macrocycles reviewed in the current overview are CBs, HCs and cycHCs with a minor exception. Since cycHC is one of the few enantiomerically pure members of the CB family, a chapter is also dedicated to the best known chiral macrocycle, cyclodextrine (CD)²⁸.

To compare and classify different macrocycles, a set of measurable parameters is required to describe them. The dimensions, solubility, acidity, stability and electrostatic potential are the fundamental properties of CBs.¹¹ The dimensions which are compared are the diameter of the opening, diameter of the cavity, height of the macrocycle and volume of the macrocycle. Measuring the dimensions of the host is also a part of the process to find suitable guests, which fit in the host's cavity.¹¹ In addition, the dimensions are used for comparing the experimentally isolated macrocycles with the calculated (non-isolated/theoretical) ones.²⁹ While solubility, acidity and thermal stability are, in general, measured experimentally, the electrostatic potential is calculated using computational chemistry.¹¹ Electrostatic effects play an important role in molecular recognition in various solutions and they also help to study the host-guest complexing.³⁰

In addition, the CBs are also characterized by their complexing properties, *e.g.*, binding interactions, binding affinities, guest exchange *etc.*¹¹ In computational studies such properties are researched using binding energies

of guest molecules.³¹⁻³³ Beside the binding energy, the energy of interactions between the host and the guest are studied using QTAIM.^{33,34}

In order to achieve uniform quality of presentation, all figures depicting molecular orbitals (MOs) in this chapter are based on calculations made by the author at the B97-D/TZVPD level of theory.

1.2.1 Cucurbiturils

CBs were first synthesized in 1905 by Behrend *et al*²⁷ and were described as “white, amorphous compounds, which are weakly soluble in dilute acid and base, and absorb large quantities of water without losing their dusty powdery character”¹². The structure of CB (Figure 2) was solved about 75 years later in 1981 by Freeman *et al*¹⁰ using X-ray crystallography. A trivial name – cucurbituril – was proposed based on its resemblance to a gourd or a pumpkin.

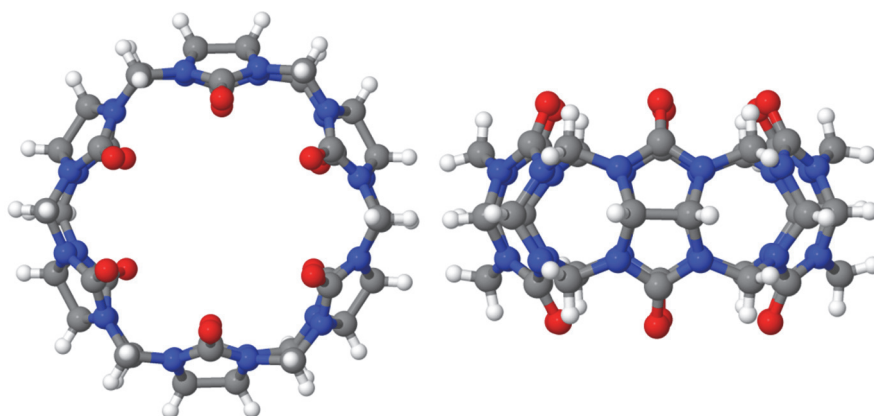


Figure 2. Top and side view of the crystal structure of CB[6].

The structure of CB consists of six glycoluril units linked together by twelve methylene bridges. The structure described by Freeman *et al*¹⁰ is now commonly known as CB[6], where the number refers to the six glycoluril units. Besides CB[6], homologues CB[5], CB[7], CB[8],³⁵ CB[10]^{36,37} and CB[14]³⁸ are known as well. The “white powder” described by Behrend *et al* was likely a mixture of CB[*n*].¹²

All CB[*n*]s possess hydrophilic carbonylated openings and a hydrophobic cavity. Due to these properties CBs are capable of forming complexes with cations, anions, metal clusters and organic guests. CB[*n*]s are bound to cations and clusters through their carbonylated portals, while anions occupy the void between stacks of CB[*n*]s. Some cations and organic guests are also

encapsulated, forming inclusion complexes with CB[*n*]s. The guest preferences can be understood by looking at the shape of the CB[*n*]s highest occupied molecular orbital (HOMO) (a) which is located on carbonylated openings and lowest unoccupied molecular orbital (LUMO) (b) which is distributed on hydrogen atoms pointing outwards the macrocycle (Figure 3).^{29,33}

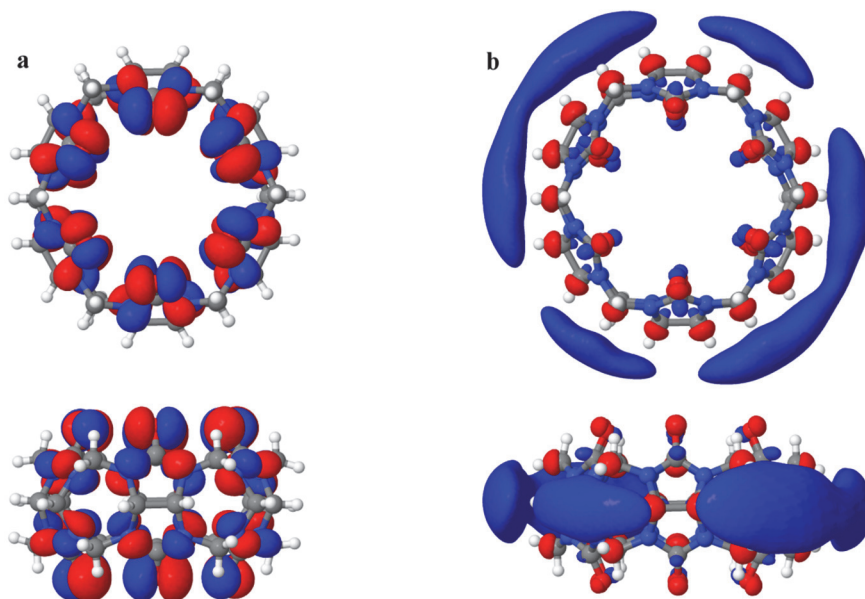


Figure 3. (a) HOMO and (b) LUMO of CB[6].

There is a wide area of applications for CB[*n*]s due to their outstanding recognition properties. In addition, they display strong non-covalent binding with various guests and hold a world record for the strongest association constant recorded – $K_a = 7,2 \cdot 10^{17} \text{ M}^{-1}$.³⁹ CB[*n*]s are used as molecular switches⁴⁰, drug delivery vehicles⁸, catalysts^{5,41}, *etc.*¹²

Beside different-sized homologues, the CB[*n*]s have also multiple derivatives such as inverted cucurbiturils⁴², *ns*-cucurbiturils⁴³ and various cyclic^{44–47} and acyclic congeners^{11,48}. In addition, a CB “cut” in half along the “equator” was synthesized by Miyahara *et al.*²⁶ which will be discussed in detail in the next chapter.

1.2.2 Hemicucurbiturils

In 2004, Miyahara *et al* synthesized an analogue of CB from ethyleneurea.²⁶ Miyahara *et al* assumed that HC should look like a CB which is cut along the “equator” and binds metal ions at the polar carbonyl side and organic molecules at the hydrophobic ethylene side (similarly to crown ethers). Conversely to the expectations, the monomers of HC had “zig-zag” conformation as depicted in Figure 4 and the macrocycle did not bind cations like CB did.

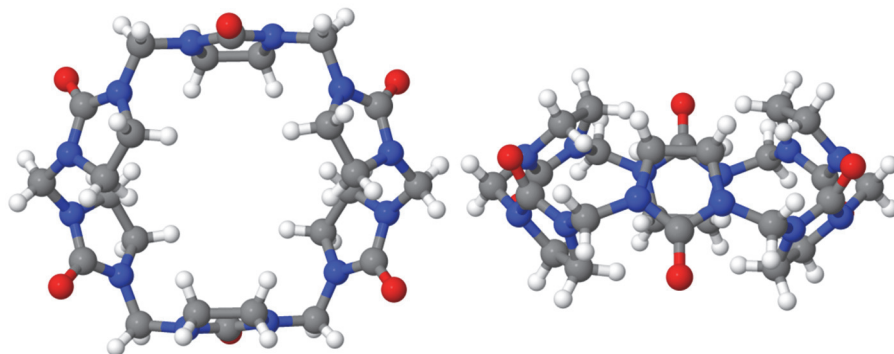


Figure 4. Top and side view of crystallographic structure of HC[6].²⁶

Due to the distinct geometry of HC, its electronic structure differs considerably from CB and therefore the binding properties differ as well. HOMO of the HC is distributed on the nitrogen and oxygen atoms, while LUMO is centred inside the cavity of the macrocycle as depicted in Figure 5.³³ The location of LUMO suggests that the HC binds anions. The fact that the first X-ray structure of HC[6] was an inclusion complex with a chloride anion illustrates its anion-binding properties well.^{26,33}

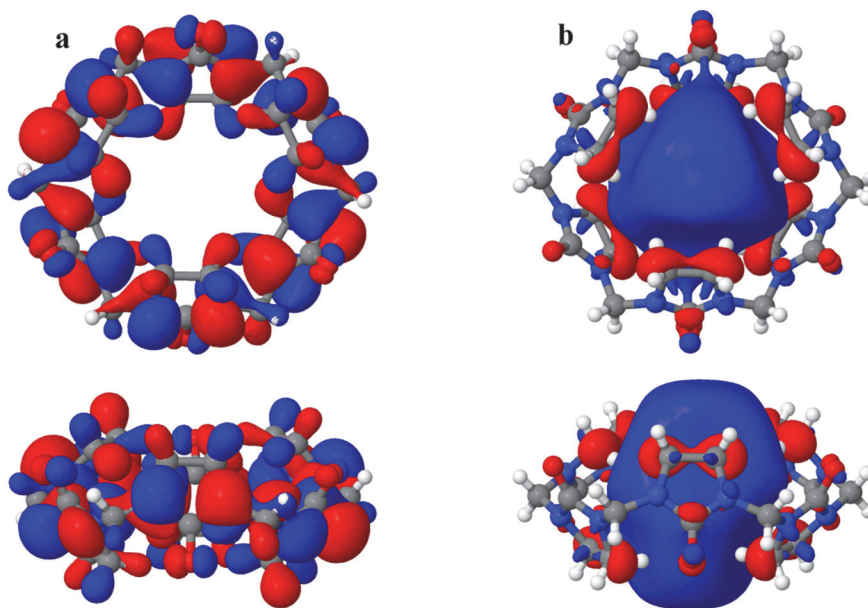


Figure 5. (a) HOMO and (b) LUMO of HC[6].³³

The known homologues of HC are HC[6] and HC[12].²⁶ In addition to the unsubstituted HCs, there are multiple substituted HCs *e.g.*, bambusurils⁴⁹, norbornahemicucurbiturils⁵⁰ and cycHCs¹³. The cycHC is the study subject of the current thesis and will be discussed in detail.

CycHC[6] is a derivate of HC[6], first synthesized by Aav *et al* in 2013.¹³ It can be synthesized from (*S,S*)- or (*R,R*)- (*N,N'*)-cyclohex-1,2-diylurea and it forms a chiral (*all-S*) or (*all-R*)-cycHC, respectively. Similarly to HC, it has a “zig-zag” conformation as depicted in Figure 6. Due to its similar structure, the cycHC[6] forms complexes with anions like HC. Binding with halides and carboxylic acids in 1:1 manner was observed. The formation of inclusion complexes was proposed. In addition, the diastereomeric complexes with enantiomers of chiral methoxyphenylacetic acids were studied and the binding affinities were distinguishable. These results indicate that cycHC may have chiral recognition properties.¹³

CycHC has multiple homologues, among which cycHC[6] and cycHC[8]⁵¹ have been isolated and cycHC[7], cycHC[9] and cycHC[10] have been detected by mass spectrometry (MS)⁵².

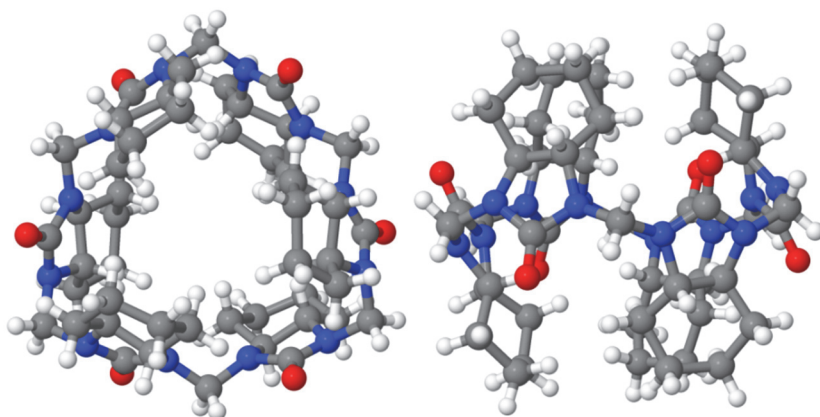


Figure 6. Top and side view of crystal structure of cycHC[6].¹³

1.2.3 Cyclodextrins

Since cycHC is chiral, the cyclodextrins (CDs), one of the most widely known chiral hosts, must be mentioned. CDs were synthesized in 1891 by Villiers²⁸ and have enjoyed wider interest since the 1980s. Applications of CDs can be found in practically all sectors of industry from pharmacy⁶ to agriculture^{53, 54}. One of the more specific properties of CDs is their chirality which generates different affinity for two enantiomers.⁹ CDs are readily soluble in water, come in a range of sizes, and are transparent to UV light. In addition to capillary electrophoresis, CDs are being used as chiral stationary phases in gas chromatography, high pressure liquid chromatography, *etc.*⁵⁴ The success of CDs illustrates the need for chiral hosts and host molecules in general.

1.3 Computational Methods Used in Host-Guest Chemistry

1.3.1 Geometry optimization

Geometry optimization is a process to minimize the forces acting on each atom in a molecule. Considering the relatively large size of the host molecules, the use of DFT during geometry optimization has proven to be a good choice. The popularity of DFT is due to the relatively low computational cost (compared to post-HF methods) while maintaining high accuracy (compared to semi-empirical methods).^{14a}

Sundararajan *et al*³³ and Pinjari *et al*^{55,56} have demonstrated that even at relatively low level of theory the optimization of macrocycles will yield a respectable result. The results were validated by comparing the computed

structure to the crystal structure. The density functionals which are often used for optimizing the geometry of macrocycles are B3LYP⁵⁷⁻⁶² and BP86^{57-60,63}. While both of these functionals are on the lower end of Jacob's ladder of density functional approximations⁶⁴, they are used due to the excellent computational cost and accuracy ratio. The basis sets suitable for geometry optimization of rigid macrocycles are usually small. It is known that the geometry optimization is not very dependent on the size of the basis set (especially if the studied structure is rigid).³³ Thus a smaller basis set is generally chosen.^{33,34,55,56,65-70}

1.3.2 Electronic Structure

Often, after the optimized geometry of the host is found, a study of the frontier orbitals (HOMO and LUMO) and the map of electrostatic potential (MEP) is performed. The study of the frontier orbitals leads to prediction of potential binding sites of guests.⁷¹ The MEP outlines electron-rich and electron-poor regions of a macrocycle, which are indicators of locations of possible electrostatic interactions between the host and the guest.⁷²

1.3.3 Host-Guest Interactions

The host and the guest form an inclusion complex if the host-guest complex has a lower overall Gibbs free energy compared to the non-complexed host and guest. Additionally, the barrier of the insertion reaction has to be low enough as well. The energy barrier of forming the host-guest complex is depicted in Figure 7. The overall Gibbs free energy of the complex depends on the interactions between the host and the guest, and the difference in the Gibbs free energies (ΔG) indicates the strength of the interactions (bigger difference means stronger interactions). While the ΔG might favour complex formation, the rate of reaction depends on the barrier height of the transition state ($[H\cdots G]^\ddagger$).^{73a}

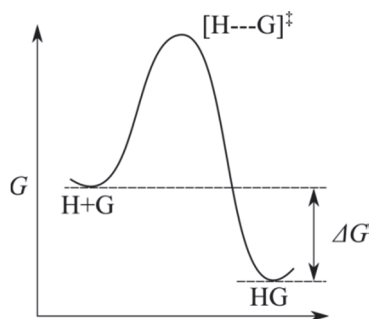


Figure 7. Gibbs free energy as a function of the reaction coordinate of HG complex formation.

In general, there is an equilibrium between the unbound (non-complexed) and bound (complexed) state:



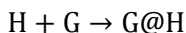
where H is the host and G is the guest and HG is the host-guest complex. In experiments, an association constant (K_a) of the reaction is measured. The association constant is equal to the concentration of the host-guest complex divided by the product of the concentrations of the individual host and guest molecules when the system is in equilibrium:

$$K_a = \frac{[HG]}{[H] \cdot [G]}$$

The K_a and ΔG are interrelated by the following formula^{73b}:

$$\Delta G = RT \ln K_a$$

The difference in Gibbs free energies can also be estimated using computational chemistry. The calculation results can be used for explaining the K_a of the experiment or evaluating if potential guests would form inclusion complexes with the host. This is done through multiple calculations, where the Gibbs free energy is calculated by subtracting the energy of products from the energy of reactants:



$$\Delta G = G_{G@H} - G_{H+G}$$

If the difference in Gibbs free energy is positive, the guest prefers not to bind and if the binding energy is negative, the guest prefers to form the inclusion complex.³³ The notation G@H indicates the inclusion complex where guest is inside the host.

To study the interactions between various guests and hosts QTAIM is used.²² The aims for the study using QTAIM are to find BCPs between the host and the guest and to characterize the bond strength through the potential energy density of the bond.⁷⁴

1.3.4 Description of the Dimensions of Macrocycles

To give a rough estimation of the size of a possible guest, the cavity and the openings of the macrocycle are measured. In addition, the measurements provide a way to categorize macrocycles based on their parameters of dimensions. The most studied geometric parameters are widths of the opening(s) of the macrocycle, width of the cavity, height of the macrocycle and cavity volume of the macrocycle. All of the parameters give a rough estimation of the size of possible guests the macrocycle could incorporate.

Two methods for measuring the widths and heights are used. In the case where the calculated structure can be compared to a crystal structure the distances from one atom centre to another are measured.³³ Another way to assess the widths and heights is to include van der Waals radii of the atoms used in the measuring process.¹³ There are no standard protocols for measuring these parameters, due to the different construction of the host molecules. In case of CBs with even number of monomeric units, the measuring of the opening is straightforward – from an oxygen atom to the opposite oxygen atom as depicted in Figure 8a. The same goes for the width of the cavity except a different atom is chosen. The measuring of the distance for CBs with odd number of monomers is often not explained in detail³⁵. In any case the radius of the opening and cavity of CBs can be measured from the chosen atom to the C_n symmetry axis of the molecule. While the openings of CBs are easily measured despite the number (even or odd) of composed monomers, the openings of HC[6] resemble a triangle, thus the measuring of their openings is not as trivial (Figure 8b). In that case both the distances between oxygen atoms and carbon atoms are measured, which gives a rough estimate of the size of the opening. The parameters describing the cavity have the same issues as the opening(s) and the atoms chosen for measurements vary between macrocycles. The height of the macrocycle imposes fewer difficulties and is uniquely determined for most macrocycles.³³

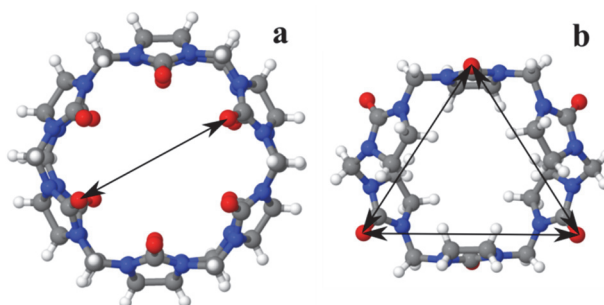


Figure 8. The measuring of the diameter of the opening of (a) CB[6] and (b) HC[6].

To measure the volume of the cavity, a three-dimensional model of the cavity is generated by rolling a probe on the van der Waals surface of the molecule (Figure 9). From the generated model the volume of the cavity (and the volume of the molecule) can be calculated. The radius of the probe, typically 1.4 Å, is chosen to avoid small dents which in large numbers would increase the volume significantly, but would be too small to house any part of the guest. Another variable is the grid size used to approximate the surface: the denser the grid size, the more accurate the results are. The surface of the model of the cavity is represented using triangles and using a finer grid results in smaller triangles representing the same area which in turn is more accurate.^{75,76}

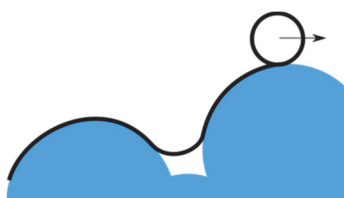


Figure 9. The probe rolls along the atoms' van der Waals spheres (blue).

Most cavities of macrocycles have openings which are large enough for a probe to pass through. To measure cavities, which are connected to the surroundings, a cap needs to be placed on the openings of the molecule to prevent the probe rolling out of the cavity. This is a procedure where inaccuracies and inconsistencies arise since there is no standard procedure for covering the openings. A plain way to solve the problem is to cover the openings with arbitrary carbon atoms.⁷⁷

In order to study the fit of the guest into the cycHC, the empirical 55% rule by Meccozi *et al* is used.⁷⁸ The rule states that encapsulation is largely determined by the relation between the volume of the guest and the volume of the cavity of the host. Binding is expected when the ratio of the guest volume to the cavity volume is roughly 0.55. This packing coefficient ratio for the cavity is abbreviated as PC_{cavity} .

2. Aims of the present work

Cyclohexylhemicucurbit[n]urils (cycHC[n]s) are recent additions to the popular cucurbituril family. Cucurbiturils have proven to be useful in various fields, thus the study of their chiral analogue is intriguing. Computational studies compliment experimental results and help to gain deeper understanding in host-guest chemistry. The present work aims to expand knowledge on the formation and binding properties of cycHC[n] to probe out its future applications.

The particular aims of the thesis are to:

- Study the geometry, cavity and electronic structure of both isolated and detected cycHC[n]s;
- Study the complexing properties of cycHC[n]s with anions, the proton and non-dissociated acids;
- Study the mechanism of the reversible macrocyclization between 6- and 8-membered homologues of cycHC.

3. Methods

The lightweight exchange-correlation functional BP86 has been used throughout the thesis due to its efficient time-cost ratio. The geometry optimization of macrocycles is a demanding process, but the results do not significantly depend on the basis set³³, thus the def2-SV(P)⁸⁰ basis set was used to obtain optimized geometries within an acceptable period of time. For further refinement of energies the def2-TZVPD⁸⁰ basis set was used. In publication III, the dispersion-corrected functional B97-D⁸¹ with the basis set def2-TZVPD⁸⁰ was used to get better accuracy of binding affinities. Dispersion corrected density functionals have been reported to yield binding affinities very close to the experimental estimates for similar systems⁸². The results of the latter combination have also been used for visualization of molecular orbitals in this thesis.

The solvation model COSMO²⁵ ($\epsilon = 51.1$ – formic acid) was used for the modelling of the chemical equilibrium between host-guest systems. Computational results which could be compared with crystal structures or gas-phase MS analyses were obtained without using any solvation model. In addition, solvation effects were also excluded from frontier orbital, MEP and binding energy calculations. Adding solvation effects (COSMO) to an empty cycHC creates a dielectric continuum inside the host. COSMO is based on the model where the studied molecule forms a cavity inside the dielectric and in the case of empty cycHC's a part of the dielectric is inside the created cavity which is not taken into account by the method.

Various methods have been used to speed up, enhance and verify the DFT calculations. To increase the speed of the geometry optimization the Resolution of Identity^{83–86} (also referred to as Density Fitting) technique was used during the process. For iodine, an appropriate Stuttgart pseudopotential was applied.^{87,88} To ensure that the chosen geometries were at minima or at first-order saddle points, as appropriate, vibrational frequency calculations were carried out. Following the vibrational frequency calculations, zero point vibrational energy was added to the energy of the molecule while comparing conformers and different binding locations as well as calculating binding energies. Gibbs free energy correction was added to the energy when the computational results were compared with the experiment. The counterpoise correction calculations were performed to assess the basis set superposition error when needed. The transition states were verified using intrinsic reaction coordinate calculations. All DFT calculations were performed using the Turbomole 6.4 and 6.5^{86,89–91} and Gaussian 09⁹² program packages.

The binding properties were studied *via* QTAIM using the program Multiwfn²³ (BP86/def2-SV(P)). Interactions between host and guest were studied by locating the BCPs as defined in the QTAIM model. The interaction energies were calculated using the potential energy density at the corresponding BCP using the equation $E=V(\mathbf{r}_{\text{BCP}})/2$.⁷⁴

To compare the stabilities of cycHC's of different sizes, the energy difference per monomeric unit was used. The energy per monomeric unit was obtained by dividing the energy of the macrocycle by the number of monomeric units it has. The differences were obtained by comparing energies per monomeric unit to the energy per monomeric unit of the six-membered cycHC.

Figures of geometries, molecular orbitals and cavities were generated with programs Jmol 14.2.13⁹³ and GIMP 2.8.0. Figures including vector graphics were generated using Inkscape 0.91. Two-dimensional chemical structures were generated using ChemDraw 14.

4. Results and discussion

This thesis focuses on the host-guest chemistry of cycHC[*n*]. The study is divided into three parts. The first part covers the study of cycHC[6] and its selected complexes. It features geometries, electronic structures, interactions between the host and the guest, and complexation reactions. The second part focuses on the homologues of cycHC, introducing their geometries and cavities. The third part describes the reversible macrocyclization mechanism where the number of monomeric units in the cycHC, and consequently the size of the host, is changed. The structures covered here consist of up to 230 atoms and some systems include heavier atoms such as bromine and iodine. In order to achieve the desired accuracy within a reasonable time frame, density functional theory (DFT) was used. Although DFT has some disadvantages compared to the post-HF methods,⁷⁹ the choice depended heavily on the size of the studied structures.

4.1 Computational studies of complexation of Cyclohexylhemicucurbit[6]uril (Publication I)

CycHC[6] had been synthesized by Aav *et al*¹³ by heating the (*R,R,N,N'*)-cyclohex-1,2-diylurea in hydrochloric acid or hydrobromic acid. The reaction products (1:1 halide complexes) had been isolated and characterized by electrospray ionization MS and quantitative nuclear magnetic resonance (NMR) spectroscopy. While the reaction products were stable in the solution, attempts to crystallize the complexes, to study their structure, had failed. Based on the literature, an assumption that the 1:1 halide complex is an inclusion complex had been made. According to the electrospray ionization MS, ¹³C NMR and diffusion NMR spectroscopy analyses, carboxylic acids and amines, which are very different in their complexation abilities, had exhibited affinity towards cycHC[6]. Therefore the mode of complexation had been ambiguous and it was not clear whether the guests had formed inclusion complexes. Furthermore, it was not clear whether the guests were bound as anions or non-dissociated neutral species.¹³ To understand and explain the various evasive experimental results, a computational study of the complexation properties of cycHC[6] was conducted.

4.1.1 Geometry of cyclohexylhemicucurbit[6]uril

The starting geometry for energy minimization of cycHC[6] was based on its crystal structure. The optimized geometry, like the crystal structure, had monomers in zig-zag orientation and exhibited D₃ point group symmetry. Attempts were made to find additional conformations of the cycHC[6], but

the distorted geometries optimized into the same structure as described above. The computed structure is depicted in Figure 10.

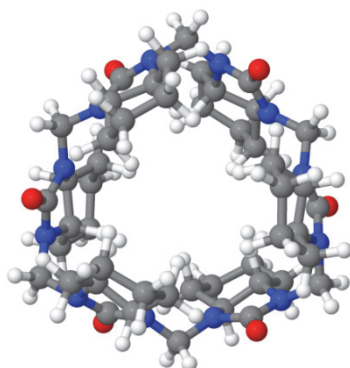


Figure 10. CycHC[6].

To validate the computed structure, its parameters were compared to the crystal structure. Since hydrogen atoms are difficult to detect with X-ray diffraction methods, the heavier atoms were chosen for measuring the various parameters. Six parameters were chosen to compare the computed geometry to the crystal structure. The parameters included the distances between the centre of the cavity (X), axis (Z) and selected atoms (O , C_2 , C_{4a} , C_5 and C_7) – $r(C_5-Z)$, $r(C_7-X)$, $r(C_{4a}-X)$, $r(C_2-X)$ and $r(O-X)$ – as depicted in Figure 11. The last parameter is the cavity volume (V_{cavity}) of the structure, which was determined using a probe with a radius of 1.4 Å (see section 1.3.4).

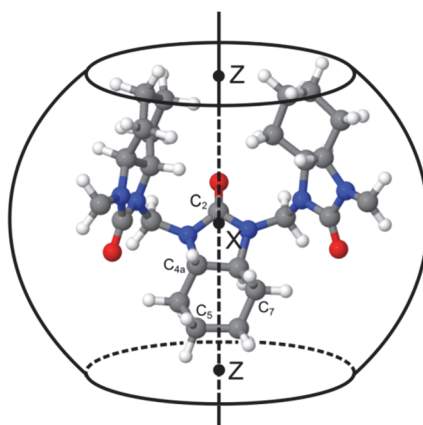


Figure 11. Atom numbers, centre of the cavity and Z-axis of cycHC[6].

The computed distances $r(C_2-X)$ and $r(O-X)$ are very similar to the distances in the experimental structure which hints that the “equator” of the macrocycle is relatively rigid (Table 1). Parameters $r(C_5-Z)$, $r(C_7-X)$ and

$r(\text{C}_{4a}-\text{X})$ differ by 0.4 Å between the computed structure and the crystal structure. The differences between the computed structure and the crystal structure are probably caused by the packing forces in the crystal structure and demonstrate the flexibility of the cyclohexyl groups. The cavity volume of the crystal structure is smaller as well, 36 Å³. The cavity volume of the cycHC[6] structure derived from our calculations is 53 Å³. The relatively large difference in the volumes is caused by the cyclohexyl groups, which by opening up (increasing the $r(\text{C}_5-\text{Z})$) generate a bigger cavity. This result hints that some movement is allowed for the cyclohexyl groups of the cycHC[6]. Thus cyclohexyl groups can make the opening of cycHC[6] wider, allowing bigger guests to move through the opening, and then by “closing the gate”, the guest is trapped inside the macrocycle.

Table 1. Selected distances and volumes of computed and experimental cycHC[6] in Å and Å³ respectively

	Computed parameters	Experimental parameters ^a
$r(\text{C}_5-\text{Z})$	3.1	2.7 ± 0.2
$r(\text{C}_7-\text{X})$	4.2	3.8 ± 0.1
$r(\text{C}_{4a}-\text{X})$	4.2	4.1 ± 0.1
$r(\text{C}_2-\text{X})$	4.4	4.4 ± 0.2
$r(\text{O}-\text{X})$	5.0	5.0 ± 0.1
V_{cavity}	53	36

^a Mean values for six atoms of each monomer given with maximum absolute deviation.

4.1.2 Electronic structure and potential binding sites of guests of cyclohexylhemicurbit[6]uril

The HOMO of cycHC[6] is mostly distributed between the heteroatoms of the molecule as depicted in Figure 12a. The probable location of the binding site for protons cannot be uniquely determined on the basis of HOMO (due to the various orbital parts pointing inside and outside the macrocycle). The LUMO is centred inside the cavity of the macrocycle as can be seen in Figure 12b. LUMO inside the cycHC[6] leads to the conclusion that the cavity of the macrocycle favours the interactions with anions which would result in the encapsulation of anionic guests.

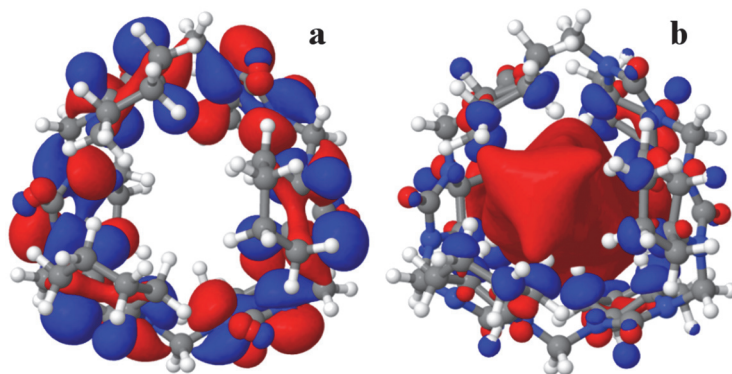


Figure 12. (a) HOMO and (b) LUMO of cycHC[6].

The MEP (see section 1.3.2) of cycHC[6] (Figure 13) can be interpreted as indication of locations where the non-dissociated guests would bind. The most electron-rich regions (red area) were found on oxygen atoms where the electron-poor regions of the guest would bind. The most electron-deficient areas (blue areas) were found on the methylene bridges. These are the regions where the electron-rich parts of the guest would bind.

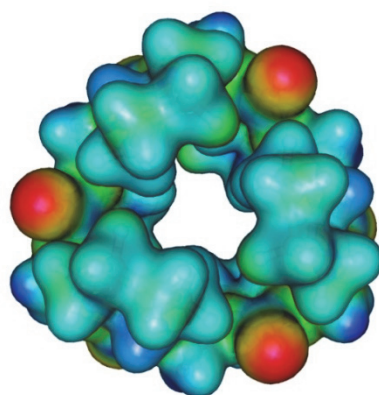


Figure 13. MEP of cycHC[6].

4.1.3 Complexes of cyclohexylhemicucurbit[6]uril with anions

A systematic search was conducted to study the potential binding sites of the anions. In order to achieve that, the macrocycle was depicted as a sphere, and considering its symmetry, it was divided into six identical sectors. The systematic analysis was based on only one sector. For a systematic analysis, five latitudes (with 36° increments) and five longitudes (with 10° increments) were mapped onto a sector of the sphere as depicted

in Figure 14. The crossing points of the meridians and parallels were used as initial locations for the guests in series of geometry optimizations. In addition, the locations inside the macrocycle and on the opening were added as well. The systematic search resulted in binding sites which were located, *e.g.*, on the methylene bridge, between two cyclohexyl groups or on the opening of the macrocycle. However, in the lowest energy geometry for smaller anions (Cl^- and Br^-), the anion is “hovering” above one of the cyclohexyl groups. In the lowest energy geometry for larger anions (HCOO^- and Γ^-), the anion is on the opening of the cycHC[6].

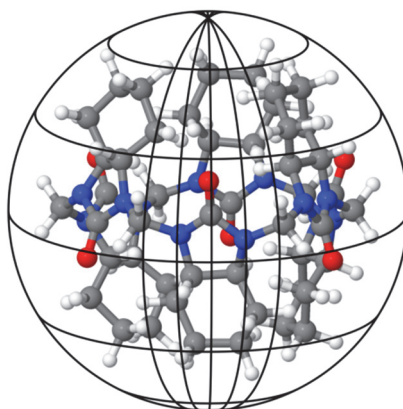


Figure 14. Latitudes and longitudes used in a systematic search for binding sites.

Out of all binding sites found, the one inside the macrocycle was favoured by all anions. The energy difference between the structure with the lowest energy and the second lowest one was over 11 kJ mol^{-1} for every anion. Thus the inclusion complexes were chosen for further study.

Parameters chosen to describe the cavity and the opening of the inclusion complexes were similar to the ones used in validating the computed structure. Instead of carbon atoms, the parameters were described using the axial hydrogen atoms (connected to the C_2 , C_{4a} , C_5 and C_7 carbon atoms). The distances from the $\text{H}_{4a\text{-ax}}$ and $\text{H}_{7\text{-ax}}$ to the centre of the cavity ($r(\text{H}_{4a\text{-ax}}-\text{X})$ and $r(\text{H}_{7\text{-ax}}-\text{X})$) describe the opening or closing movement of the cyclohexyl groups. The shortest distance of $\text{H}_{5\text{-ax}}$ from the axis (Z) ($r(\text{C}_{5\text{-ax}}-Z)$) describes the openings of the macrocycle. The distance between C_2 and X ($r(\text{C}_2-\text{X})$) indicates if the “equator” of the macrocycle is deformed by guests. The listed distances are graphically depicted in Figure 15. The fifth parameter is the size of the cavity of the inclusion complex. Additionally the $\text{PC}_{\text{cavity}}$ (see section 1.3.4) has been calculated for every anion.

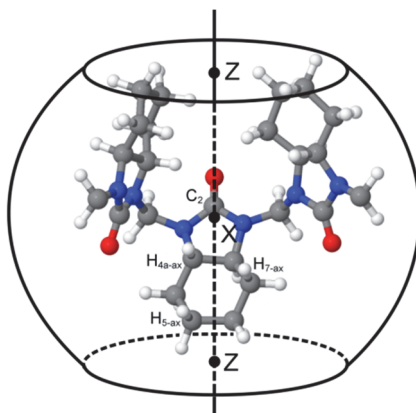


Figure 15. Atom labels, centre of the cavity and axis of cycHC[6].

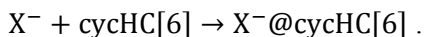
The relevant distances and other parameters of the inclusion complexes are presented in Table 2. During the formation of inclusion complexes, the flexible cyclohexyl groups covered the anions inside the macrocycle. Due to this the $C_{5-ax}-Z$ distance decreased while the $r(C_2-X)$ distance increased, making the openings smaller and the “equator” bigger. The biggest changes took place with the chloride ion and the smallest with iodine ion. Formic acid anion was the only guest which led to breaking of the D_3 symmetry by deforming the “equator” and making the macrocycle flatter.

Table 2. Distances between the centre of the cavity, axis and selected atoms of non-complexed and complexed cycHC[6] with anions (in Å). Cavity volumes are given without a guest in Å³ and PC_{cavity} is in percents

	Non-complexed cycHC[6]	Inclusion complex with:			
		Cl ⁻	Br ⁻	I ⁻	HCOO ⁻
$C_{5-ax}-Z$	2.4	2.2	2.3	2.4	2.3 – 2.4 ^a
$H_{7-ax}-X$	3.2	3.0	3.1	3.2	3.0 – 3.1 ^a
$H_{4a-ax}-X$	3.2	3.0	3.0	3.1	3.0 – 3.2 ^a
$r(C_2-X)$	4.4	4.5	4.5	4.5	4.4 – 4.5 ^a
Cavity volume	53	33	38	48	42
PC_{cavity}	-	62	72	91	79

^a Minimum and maximum distances are given due to the asymmetric geometry of the complexes with this anion.

Binding energies (ΔE) were calculated to determine, which anion forms the most stable inclusion complex with cycHC[6]. The energies were computed according to the reaction of cycHC[6] with anion X^- as shown below:



$$\Delta E = E(X^-@ \text{cycHC}[6]) - E(X^-) - E(\text{cycHC}[6])$$

Based on the calculated binding energies, chloride anion formed the strongest complex. The binding energy for chloride was -102 kJ mol^{-1} . According to the empirical 55% rule⁷⁸, chloride indeed fitted the best (Table 2). The bromide complex was the second in strength (-87 kJ mol^{-1}), closely followed by formic acid anion (-83 kJ mol^{-1}). Iodide formed the weakest inclusion complex with -65 kJ mol^{-1} of binding energy. According to QTAIM all halogen anions formed 12 bonding interactions with cycHC[6]. All interactions were with hydrogen atoms H_{4a-ax} and H_{7-ax} of each monomer of cycHC[6]. The strength of the interactions was close to 5 kJ mol^{-1} for all interactions, for all halogens. The formic acid anion interacted with the same hydrogen atoms, but the interaction strength ranged from $3 - 14 \text{ kJ mol}^{-1}$. These interactions were between the oxygen atoms of HCOO^- and H_{4a-ax} and H_{7-ax} of the macrocycle. In addition to the twelve interactions revealed by the QTAIM, the hydrogen atom of the formic acid anion formed BCPs with two nitrogen atoms. The interaction strengths of the N–H interactions were 7.3 and 4.5 kJ mol^{-1} . Chloride formed the strongest inclusion complex (Table 3), but the chloride forms the weakest interactions with cycHC[6]. This indicates that the size of the guest anion is an important factor influencing the stability and formation of inclusion complexes.

Table 3. Interaction and binding energies (kJ mol^{-1}) of anions with cycHC[6]

	Cl^-	Br^-	I^-	HCOO^-
Average interaction energies	4.7	4.9	4.8	9.7 ^a
H-N (a)	-	-	-	7.3
H-N (b)	-	-	-	4.5
Sum of interaction energies	56.7	59.1	58.0	127.8
Binding energy	-102	-87	-65	-83

^a The average interaction energy for HCOO^- does not contain energy contribution from H–N bonds.

4.1.4 Transition states of guest-host complex formation with anions as guests

While Cl^- and Br^- formed the inclusion complex spontaneously, the complexation of I^- and HCOO^- went through a transition state as depicted in Figure 16. The barrier heights were 12 kJ mol^{-1} and 22 kJ mol^{-1} for HCOO^- and I^- , respectively. At the start of the reaction coordinates (local minima in Figure 16), both anions were bound at the opening of the cycHC[6]. During the transition, anions moved along the Z axis and the cyclohexyl groups opened up. This indicates that the studied anions have low or no insertion barriers, which means that the formation of the inclusion complexes should be favourable.

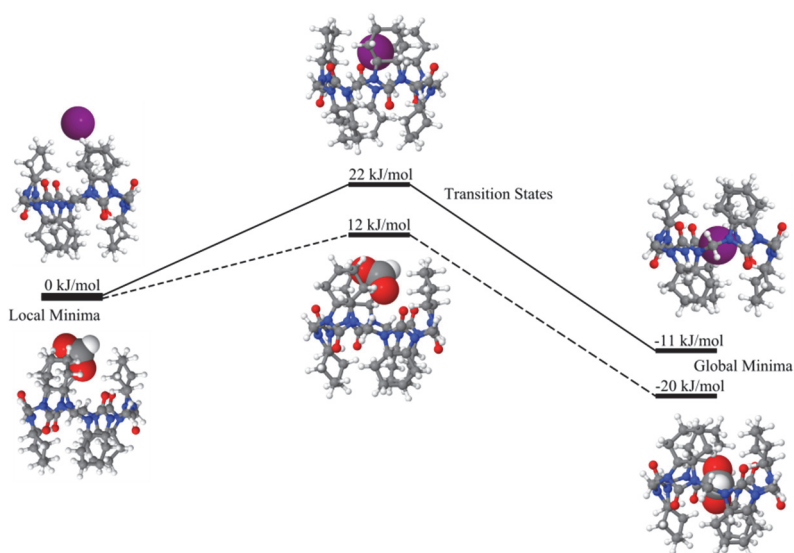


Figure 16. Reaction coordinates of I^- (solid line) and HCOO^- (dashed line) forming inclusion complexes with cycHC[6].

4.1.5 Complexes of cyclohexylhemicurbit[6]uril with H^+

The search for binding sites for the proton was analogous to the search for binding sites for anions. In addition to the automated search on the previously-shown grid (Figure 14), locations guided by the lobes of the HOMO were added as well. The resulting structures are depicted in Figure 17.

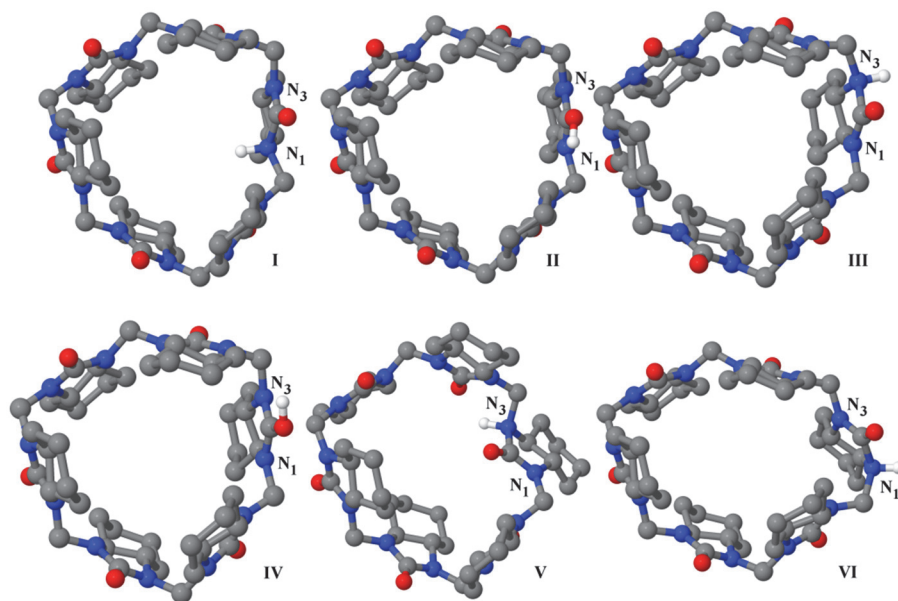
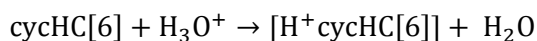


Figure 17. Structures of protonated cycHC[6]. Hydrogen atoms (except the added proton) are not shown.

The calculations for the binding energies of the proton for the structures in Figure 17 were based on the following reaction:



$$\Delta E = E([\text{H}^+ \text{cycHC[6]}]) + E(\text{H}_2\text{O}) - E(\text{cycHC[6]}) - E(\text{H}_3\text{O}^+)$$

The energetically lowest geometry lies 7 kJ mol^{-1} lower than the second-lowest geometry and according to the Boltzmann distribution (at 273 K) the population of geometry I is over 90%. The rest of the energy differences can be seen in Table 4. According to the energies, the favoured site for the proton is inside the macrocycle.

Table 4. Relative energies (kJ mol^{-1}) of the protonation of cycHC[6]

Geometry number	Protonation site of cycHC[6]	ΔE
I	At N ₁ , inside	0
II	O	7
III	At N ₃ , outside	9
IV	O	11
V	At N ₃ , inside	13
VI	At N ₁ , outside	34

Locations N₃ and N₁ (inside and outside respectively) have the highest energy because of the steric hindrance of the cyclohexyl group's hydrogen atom which points in the same direction as the proton (inward in case of N₃ and outward in case of N₁).

4.1.6 Cyclohexylhemicucurbit[6]uril complexes with non-dissociated acids

The binding sites towards non-dissociated acids were found by taking geometries of various local minima of anion and cycHC[6] complexes and adding a proton to the anion. Similarly, geometries of local minima of proton and cycHC[6] complexes were complemented with anions. The combination of binding sites resulted in set of geometries, where the non-dissociated acid was inside or outside the macrocycle. Energetically, the outside binding sites were favoured for all guests. The inclusion complexes with all guests were more than 14 kJ mol^{-1} higher in energy. The favoured geometries of cycHC[6] complex with HCl are depicted in Figure 18. The geometries with other guests were similar. The geometry (a) in Figure 18 is favoured for all studied hydrogen halides (Table 5). The formic acid favoured geometry (b) due to its different shape compared to hydrohalic acids.

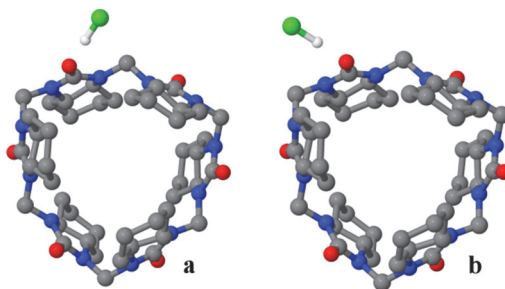


Figure 18. Lowest-energy geometries of cycHC[6] and HCl complexes. Hydrogen atoms of the cycHC[6] are not shown.

Table 5. Energies of cycHC[6] and non-dissociated guest complexes

Guest	Geometry	ΔE	Binding energy
HCl	a	0	-67
	b	2	-65
HBr	a	0	-26
	b	1	-25
HI	a	0	-31
	b	1	-30
HCOOH	a	5	-16
	b	0	-21

4.1.7 Summary of studies of cycHC[6] and its complexes

The computational study reveals that cycHC[6] can form inclusion complexes with all studied anions, as well as the proton. All anions in the study preferred to form an inclusion complex with cycHC[6] which agrees with the experimental results. Amongst all anions, chloride forms the strongest complex and its size is closest to the empirical 55% rule⁷⁸. The cycHC has multiple binding sites for the proton. The most preferable ones are located inside the cycHC[6]. All non-dissociated acids prefer to bind outside the macrocycle.

The computationally obtained structures have been verified via ion mobility mass spectroscopy, also reported in paper I. The collision cross-section values measured by ion-mobility MS and calculated from minimum energy conformers of anion complexes were found to agree with each other and the deviation of the calculated collision cross-section from the experimental data was within 2%, confirming that anions formed inclusion complexes with cycHC[6].

4.2 Geometries (Publication II) and cavities of cycHC[n] homologues

Chapter 4.2 is omitted from the electronic version of this thesis due to the unpublished results.

4.3 The equilibrium and proposed mechanism of the reversible macrocyclization (Publication III)

CycHC[6] and cycHC[8] are the only cycHCs which have been isolated. CycHC[8] was first observed as a byproduct in small quantities, but after dissolving cycHC[6] in formic acid, cycHC[6] was found to be slowly converted into cycHC[8]. During the optimization of reaction conditions, the reaction time had been decreased (using CF₃COOH as a template) and the yield increased (using NaPF₆ as a template). Analogous results had been also obtained in the synthesis starting from (*R,R,N,N'*)-cyclohex-1,2-diylurea.

To study the reversible macrocyclization, the equilibrium between cycHC[6] and cycHC[8] was modelled. The equilibrium was modelled with and without a guest molecule to understand the importance of the template in the reversible macrocyclization mechanism. In addition, a simplified model system for the study of the reaction mechanism was constructed.

4.3.1 Equilibrium between cycHC[6] and cycHC[8]

According to the experimental studies, the equilibrium constant (K_{eq}) between cycHC[6] and cycHC[8] in DCOOD and CD₃CN 1:1 mixture is $3.0 \cdot 10^5$. The difference in experimental Gibbs free energies, corresponding to the K_{eq} , is roughly -31 kJ mol^{-1} in favour of cycHC[8]. High-resolution MS analysis of the reaction mixture demonstrated the presence of large number of various oligomers (up to an octamer) forming a dynamic combinatorial library (DCL). As mentioned earlier, the computationally estimated energy difference per monomeric unit, comparing cycHC[8] to cycHC[6] is 2 kJ mol^{-1} in favour of cycHC[6]. The negligible difference in energies of the homologues indicates that the equilibrium shift towards cycHC[8] is caused by an external factor.

In the case of DCL, it has been suggested that the different-sized macrocycles are obtained by the aid of template molecules.⁹⁷ From previous studies it is known that the formic acid anion forms an inclusion complex with cycHC[6]. According to our calculations, the formic acid anion also forms an inclusion complex with cycHC[8] (Figure 19).

To verify if the guest anion shifts the equilibrium towards cycHC[8], the difference in Gibbs free energies (ΔG) was calculated for the following reversible macrocyclization reaction:



The calculated ΔG is -177 kJ mol^{-1} in favour of cycHC[8]. The result qualitatively agrees with the experiment (-31 kJ mol^{-1}), but considerably overestimates the difference between Gibbs free energies. The difference might be caused by the non-complexed formic acid anion which is more stabilised in the continuum than inside the macrocycle. Thus it can be concluded that, although the calculated ΔG is purely qualitative, the equilibrium shifts towards cycHC[8] due to formation of inclusion complex with formic acid anion.

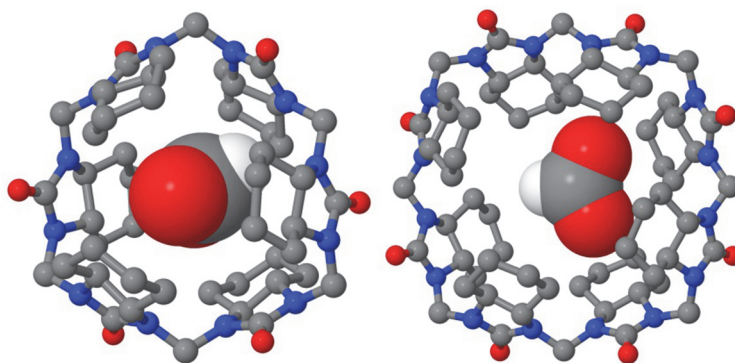


Figure 19. $\text{HCOO}^-@\text{cycHC}[6]$ and $\text{HCOO}^-@\text{cycHC}[8]$. Hydrogen atoms of the cycHC[6] and cycHC[8] are not shown.

4.3.2 Simplified model system

While the shift towards cycHC[8] is induced by the guest anion, it does not explain the reaction mechanism. Data obtained from studying reaction mixtures with high-resolution MS, demonstrated a wide variety of intermediate compounds which are depicted in Figure 20. According to the structure of intermediate compounds, the methylene bridge is continuously broken and formed during the reversible macrocyclization reaction. In the process, the substituting groups (R_1 and R_2) for oligomers with different lengths remain the same; therefore it can be presumed that the reaction mechanism for breaking or forming the methylene bridge should not depend significantly on the length of the oligomer. Thus in the interest of computational speed the compound **1b** was picked for further studies.

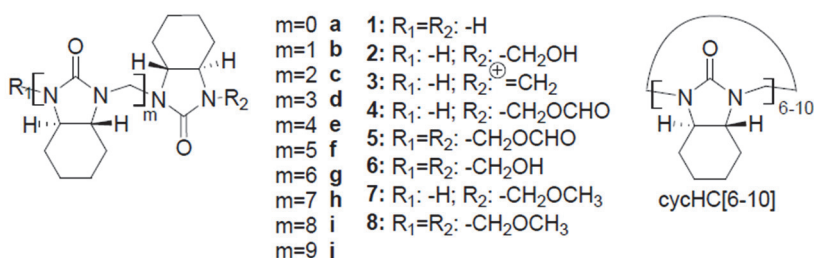


Figure 20. DCL of the reversible macrocyclization reaction.⁵¹

The reversible macrocyclization has been found to take place only in specific acidic conditions. From our previous studies (see section 4.1.5) it is known that cycHC can be protonated, and the preferable location for the proton is one of the nitrogen atoms. In dimer **1b**, nitrogen, which is connected to the carbon atom of the methylene bridge, represents the protonation site of the macrocycle. Taking into account the experimental and computational data, the protonated form of **1b** (**1bH⁺**, Figure 21) was chosen as the simplified model system to study the reaction mechanism.

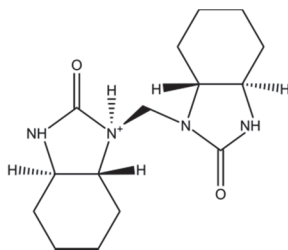


Figure 21. Protonated form of **1b**.

The protonation reaction itself was not modelled. Based on the fact, that all intermediates in reaction mixture were present in very minor amounts, it was concluded, that the rate limiting step of the overall reversible macrocyclization reaction is the first step of the mechanism, the protonation. Therefore the transition state barrier height (ΔG^\ddagger) of the protonation was estimated using the Eyring equation:

$$\Delta G^\ddagger = -\ln\left(\frac{kh}{k_B T}\right) RT,$$

where k is the experimental reaction rate constant ($5.3 \cdot 10^{-5} \text{ s}^{-1}$), h is Planck's constant, k_B is the Boltzmann constant, T is the temperature (293.15 K) and R is the gas constant in kJ mol^{-1} . According to the Eyring equation, the ΔG^\ddagger of the protonation reaction is 96 kJ mol^{-1} .

4.3.3 Depropagation and propagation

The depropagation and propagation are depicted in Figure 22. The propagation begins by protonation of **1b**. The energy difference of **1b** and **1bH⁺** is 85 kJ mol⁻¹ and the transition state for the protonation is at 96 kJ mol⁻¹. After the protonation of **1b**, the depropagation can advance through two different reaction paths, both of which agree with the observed intermediates.

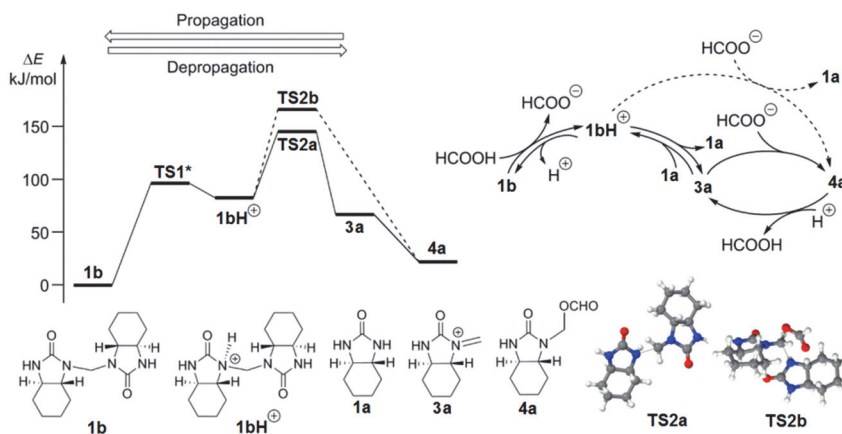


Figure 22. Reaction coordinates of the model reaction.

Along one of the reaction paths (through **TS2a**) the bond between the protonated nitrogen atom and the carbon atom of the methylene bridge dissociates, generating **1a** and **3a**. The transition state **TS2a** barrier for this reaction is 64 kJ mol⁻¹. **3a** in turn reacts with HCOO⁻ and forms **4a**. The reaction path is depicted in Figure 23.

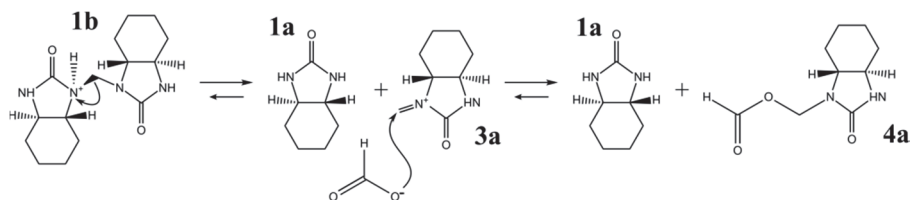


Figure 23. Energetically favoured reaction path.

The other reaction path (through **TS2b**) includes the formic acid anion in the step after the protonation. The anion attacks the carbon atom of the methylene bridge, forming the compounds **4a** and **3a** and the step with the

iminium ion is skipped. In this path, transition state energy **TS2b** is 80 kJ mol⁻¹. From the two choices, the path going through dissociation of C–N bond is energetically favoured due to the lower energy transition state by 16 kJ mol⁻¹. The non-favoured reaction path is depicted in Figure 24.

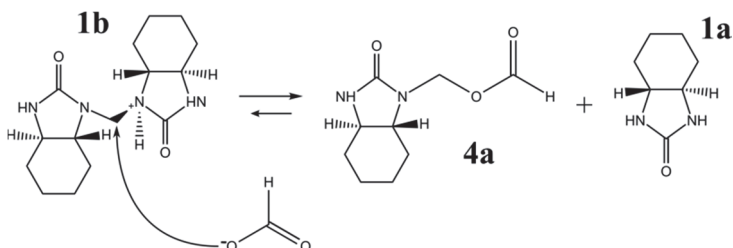


Figure 24. Energetically non-favoured reaction path.

According to the calculated reaction coordinates, the protonation of the **1b** is the rate limiting step of the process, because the transition state **TS1*** has the highest barrier in the reaction coordinate. This result agrees with the results of NMR and MS experiments as well. In the NMR study, only the compounds **1b** and **4a** had been observed, which means that the reaction goes through **1bH⁺** and **3a** fast enough that they do not accumulate. In MS the intermediate **3a** had been seen, which also suggests that the protonation is indeed the rate limiting step of the reaction.

4.3.4 Transition States **TS2a** and **TS2b**

The difference between the transition states depicted in Figure 25 is the lack of or presence of the formic acid anion which in the case of **TS2b** attacks the methyl bridge carbon atom and generates compounds **4a** and **1a**. In **TS2a**, the bond between the methyl bridge carbon atom and the protonated nitrogen atom dissociates without the formic acid anion. The possible reason why the **TS2b** is energetically not favoured might be the distortion of its monomers towards each other. The distortion is caused by the formic acid anion's oxygen atom, which has interactions with the hydrogen atoms of both fragments (marked with an asterisk in Figure 25).

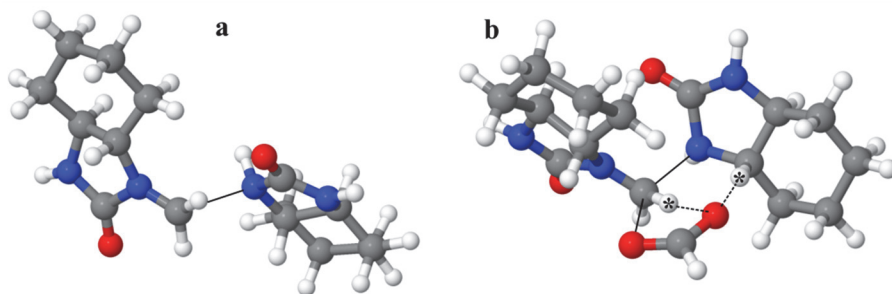


Figure 25. Transition states (a) TS2a and (b) TS2b. Broken and formed bonds are depicted with continuous lines. Interactions between formic acid anion and hydrogen atoms are depicted with dashed lines.

4.3.5 Summary of the reversible macrocyclization mechanism

Due to the dynamic character of the methylene bridges, it is possible to break the macrocycle into smaller oligomers, which can be rearranged to form other homologues. The protonation of the macrocycle is the rate-limiting step of the process, thus the C–N bond dissociation needs acidic conditions. The equilibrium between the macrocycles is directed by the energy difference of the anion inclusion complexes of cycHCs, and as a result of that the size of the macrocycle can be controlled with the size of the anionic template.

Conclusions

Cyclohexylhemicucurbit[*n*]urils and their complexes with guests were studied using computational chemistry. Based on the results of DFT calculations the following conclusions have been made:

- I. The computational study reveals that cycHC[6] can form inclusion complexes with anions.
- II. All studied anions preferred to form an inclusion complex with cycHC[6], which agrees with the experimental results.
- III. The cycHC has multiple binding sites for the proton, the most preferable being inside the cycHC[6].
- IV. All non-dissociated acids preferred to form non-inclusion complexes with cycHC[6].
- V. The electronic properties of cycHC[*n*] indicate that generally the cycHC[*n*]s are similar (HOMO is smeared across the “equator”; LUMO is concentrated inside the cavity).
- VI. The order of stability of cycHC[*n*], based on relative energies of non-complexes cycHC[*n*] is the following: cycHC[6] > cycHC[8] > cycHC[7] = cycHC[9] > cycHC[10].
- VII. The energies per monomeric unit of cycHC[6] and cycHC[8] were similar, but with the HCOO⁻ as a guest, the equilibrium shifted towards cycHC[8]. This indicates templating effect of the guest.
- VIII. Based on dimer to monomer depropagation study, which proceeds through protonation and iminium formation, homologue reversible macrocyclization mechanism is proposed.
- IX. Methylene bridges in the hemicucurbiturils are dynamic covalent bonds. This finding allows to direct the outcome of the synthesis with noncovalent interactions.

References

- 1 *The Nobel Prize in Chemistry 1987*, www.nobelprize.org/nobel_prizes/chemistry/laureates/1987 - accessed in September 2015.
- 2 J.-M. Lehn, *Science*, 1993, **260**, 1762–1763.
- 3 E. P. Kyba, R. C. Helgeson, K. Madan, G. W. Gokel, T. L. Tarnowski, I. S. S. Moore and D. J. Cram, *J. Am. Chem. Soc.*, 1977, **99**, 2564–2571.
- 4 C. Zhu and L. Fang, *Curr. Org. Chem.*, 2014, **18**, 1957–1964.
- 5 M. Pattabiraman, A. Natarajan, R. Kaliappan, T. Mague and V. Ramamurthy, *Chem. Commun.*, 2005, 4542–4544.
- 6 T. Loftsson and D. Duchene, *Int. J. Pharm.*, 2007, **329**, 1–11.
- 7 S. Erdemir, M. Bahadir and M. Yilmaz, *J. Hazard. Mater.*, 2009, **168**, 1170–6.
- 8 S. Walker, R. Oun, F. J. McInnes and N. J. Wheate, *Isr. J. Chem.*, 2011, **51**, 616–624.
- 9 L. Szenté and J. Szemán, *Anal. Chem.*, 2013, **85**, 8024–30.
- 10 W. A. Freeman, W. L. Mock and N.-Y. Shih, *J. Am. Chem. Soc.*, 1981, **103**, 7367–7368.
- 11 J. Lagona, P. Mukhopadhyay, S. Chakrabarti and L. Isaacs, *Angew. Chem. Int. Ed. Engl.*, 2005, **44**, 4844–4870.
- 12 E. Masson, X. Ling, R. Joseph, L. Kyeremeh-Mensah and X. Lu, *RSC Adv.*, 2012, **2**, 1213–1247.
- 13 R. Aav, E. Shmatova, I. Reile, M. Borissova, F. Topić and K. Rissanen, *Org. Lett.*, 2013, **15**, 3786–3789.
- 14 W. Koch and M. C. Holthausen, *A Chemist's Guide to Density Functional Theory*, Wiley-VCH, Weinheim, 2nd edn., 2001, pages (a) V and (b) 41–47.
- 15 I. N. Levine, *Quantum Chemistry*, Pearson Prentice Hall, Upper Saddle River, 6th edn., 2009, pages (a) 12–13, (b) 281–292, (c) 520–525.
- 16 C. D. Sherrill and H. F. Schaefer, *Adv. Quantum Chem.*, 1999, **34**, 143–269.
- 17 R. J. Bartlett and M. Musial, *Rev. Mod. Phys.*, 2007, **79**, 291–352.
- 18 D. Cremer, *Wiley Interdiscip. Rev. Comput. Mol. Sci.*, 2011, **1**, 509–530.
- 19 P. Hohenberg and W. Kohn, *Phys. Rev.*, 1964, **136**, 864–871.

- 20 W. Kohn and J. Sham, L., *Phys. Rev.*, 1965, **140**, 1133–1138.
- 21 *The Nobel Prize in Chemistry 1998*, http://www.nobelprize.org/nobel_prizes/chemistry/laureates/1998/ - accessed in September 2015.
- 22 R. F. W. Bader, *Atoms in Molecules: A Quantum Theory*, Oxford University Press, Oxford, United Kingdom, United Kingdom, 1990.
- 23 T. Lu, *Multiwfn version 3.2.1*, University of Science and Technology Beijing, Beijing, China, China.
- 24 C. J. Cramer and D. G. Truhlar, *Solvent Effects and Chemical Reactivity*, Kluwer Academic Publishers, Dordrecht, 1st edn., 1996, pages 2–5.
- 25 A. Klamt and G. Schüürmann, *J. Chem. Soc. Perkin Trans. 2*, 1993, **5**, 799–805.
- 26 Y. Miyahara, K. Goto, M. Oka and T. Inazu, *Angew. Chem. Int. Ed. Engl.*, 2004, **43**, 5019–5022.
- 27 R. Behrend, E. Meyer and F. Rusche, *Justus Liebigs Ann. Chem.*, 1905, **339**, 1–37.
- 28 A. Villiers, *Compt. Rend. Fr. Acad. Sci.*, 1891, 435–438.
- 29 F. Pichierri, *Chem. Phys. Lett.*, 2004, **390**, 214–219.
- 30 B. Honig and A. Nicholls, *Science*, 1995, **268**, 1144–1149.
- 31 K. S. Oh, J. Yoon and K. S. Kim, *J. Phys. Chem. B*, 2001, **105**, 9726–9731.
- 32 H. Cong, L.-L. Tao, Y.-H. Yu, Z. Tao, F. Yang, Y.-J. Zhao, S.-F. Xue, G. a Lawrance and G. Wei, *J. Phys. Chem. A*, 2007, **111**, 2715–2721.
- 33 M. Sundararajan, R. V. Solomon, S. K. Ghosh and P. Venuvanalingam, *RSC Adv.*, 2011, **1**, 1333.
- 34 S. R. Peerannawar, V. V. Gobre and S. P. Gejji, *Comput. Theor. Chem.*, 2012, **983**, 16–24.
- 35 J. Kim, I. Jung, S. Kim, E. Lee, J. Kang, S. Sakamoto, K. Yamaguchi and K. Kim, *J. Am. Chem. Soc.*, 2000, **122**, 540–541.
- 36 A. Day, A. P. Arnold, R. J. Blanch and B. Snushall, *J. Org. Chem.*, 2001, **66**, 8094–8100.
- 37 A. I. Day, R. J. Blanch, A. P. Arnold, S. Lorenzo, G. R. Lewis and I. Dance, *Angew. Chem., Int. Ed.*, 2002, **41**, 275–277.

- 38 X. J. Cheng, L. L. Liang, K. Chen, N. N. Ji, X. Xiao, J. X. Zhang, Y. Q. Zhang, S. F. Xue, Q. J. Zhu, X. L. Ni and Z. Tao, *Angew. Chemie - Int. Ed.*, 2013, **52**, 7252–7255.
- 39 L. Cao, M. Šekutor, P. Y. Zavalij, K. Mlinarić-Majerski, R. Glaser and L. Isaacs, *Angew. Chemie - Int. Ed.*, 2014, **53**, 988–993.
- 40 T. Minami, N. A. Esipenko, B. Zhang and P. Anzenbacher, *Chem. Commun.*, 2014, **50**, 61–63.
- 41 L. Zheng, S. Sonzini, M. Ambarwati, E. Rosta, O. A. Scherman and A. Herrmann, *Angew. Chemie Int. Ed.*, 2015, **54**, DOI: 10.1002/anie.201505628.
- 42 L. Isaacs, S. Park, S. Liu, Y. H. Ko, N. Selvapalam, Y. Kim, H. Kim, P. Y. Zavalij, G. Kim, H. Lee and K. Kim, *Molecules*, 2005, **8**, 18000–18001.
- 43 W. Huang, S. Liu, P. Y. Zavalij and L. Isaacs, *JACS Commun.*, 2006, 1–47.
- 44 J. Lagona, J. C. Fettinger and L. Isaacs, *J. Org. Chem.*, 2005, **70**, 10381–10392.
- 45 J. Zhao, H. J. Kim, J. Oh, S. Y. Kim, J. W. Lee, S. Sakamoto, K. Yamaguchi and O. Kim, *Angew. Chemie - Int. Ed.*, 2001, **40**, 4233–4235.
- 46 H. Isobe, S. Sato and E. Nakamura, *Society*, 2002, **7**, 1214–1215.
- 47 A. I. Day, A. P. Arnold and R. J. Blanch, *Molecules*, 2003, **8**, 74–84.
- 48 C. A. Burnett, D. Witt, J. C. Fettinger and L. Isaacs, *J. Org. Chem.*, 2003, **68**, 6184–6191.
- 49 J. Svec, M. Necas and V. Sindelar, *Angew. Chem. Int. Ed. Engl.*, 2010, **49**, 2378–2381.
- 50 T. Fiala and V. Sindelar, *Synlett*, 2013, **24**, 2443–2445.
- 51 E. Prigorchenko, M. Öeren, S. Kaabel, M. Fomitšenko, I. Reile, I. Järving, T. Tamm, F. Topić, K. Rissanen and R. Aav, *Chem. Commun.*, 2015, **51**, 1092–10924.
- 52 M. Fomitšenko, E. Shmatova, M. Öeren, I. Järving and R. Aav, *Supramol. Chem.*, 2014, **26**, 698–703.
- 53 R. Villalonga, R. Cao and A. Fragoso, *Chem. Rev.*, 2007, **107**, 3088–3116.
- 54 J. F. Stoddard, *Annu. Reports Sect. 'B'*, 1988, **85**, 353–386.
- 55 R. V Pinjari and S. P. Gejji, *J. Phys. Chem. A*, 2008, **112**, 12679–12686.

- 56 R. V Pinjari and S. P. Gejji, *J. Phys. Chem. A*, 2009, **113**, 1368–1376.
- 57 P. A. M. Dirac, *Proc. R. Soc. A*, 1929, **123**, 714–733.
- 58 J. C. Slater, *Phys. Rev.*, 1951, **81**, 385–390.
- 59 S. H. Vosko, L. Wilk and M. Nusair, *Can. J. Phys.*, 1980, **58**, 1200–1211.
- 60 A. D. Becke, *Phys. Rev. A*, 1988, **38**, 3098–3100.
- 61 C. Lee, W. Yang and R. G. Parr, *Phys. Rev. B*, 1988, **37**, 785–789.
- 62 A. D. Becke, *J. Chem. Phys.*, 1993, **98**, 5648.
- 63 J. P. Perdew, *Phys. Rev. B*, 1986, **33**, 8822–8824.
- 64 J. P. Perdew, *AIP Conf. Proc.*, 2001, **577**, 1–20.
- 65 M. Sundararajan, V. Sinha, T. Bandyopadhyay and S. K. Ghosh, *J. Phys. Chem. A*, 2012, **116**, 4388–4395.
- 66 S. Pan, S. Mondal and P. K. Chattaraj, *New J. Chem.*, 2013, **37**, 2492–2499.
- 67 P. H. Dixit, R. V Pinjari and S. P. Gejji, *J. Phys. Chem. A*, 2010, **114**, 10906–10916.
- 68 V. V Gobre, R. V Pinjari and S. P. Gejji, *J. Phys. Chem. A*, 2010, **114**, 4464–4470.
- 69 V. V. Gobre, P. H. Dixit, J. K. Khedkar and S. P. Gejji, *Comput. Theor. Chem.*, 2011, **976**, 76–82.
- 70 S. R. Peerannawar and S. P. Gejji, *J. Mol. Model.*, 2013, **19**, 5113–5127.
- 71 K. Fukui and H. Fujimoto, *Frontier Orbitals and Reaction Paths*, World Scientific Publishing Co. Pte. Ltd., Singapore, 1997, pages 13–14.
- 72 J. Tomasi, B. Mennucci and R. Cammi, *Molecular Electrostatic Potentials: Concepts and Applications*, Elsevier B.V., New Orleans, 1996, vol. 3.
- 73 P. Atkins and J. de Paula, *Physical Chemistry*, Pearson Education, San Francisco, 2006, pages (a) 599, (b) 822.
- 74 E. Espinosa, E. Molins and C. Lecomte, *Chem. Phys. Lett.*, 1998, **285**, 170–173.
- 75 N. Guex and M. C. Peitsch, *Electrophoresis*, 1997, **18**, 2714–2723.
- 76 The DeepView Team, *Deep. - Swiss-Pdb Viewer User Guid. version 3.7*.
- 77 W. M. Nau, M. Florea and K. I. Assaf, *Isr. J. Chem.*, 2011, **51**, 559–577.

- 78 S. Mecozzi and J. Rebek, *Chem. - A Eur. J.*, 1998, **4**, 1016–1022.
- 79 K. Burke, *J. Chem. Phys.*, 2012, **136**, 150901.
- 80 F. Weigend and R. Ahlrichs, *Phys. Chem. Chem. Phys.*, 2005, **7**, 3297–3305.
- 81 S. Grimme, *J. Comput. Chem.*, 2006, **27**, 1787–1799.
- 82 M. Sundararajan, *J. Phys. Chem. B*, 2013, **117**, 13409–13417.
- 83 P. Deglmann, K. May, F. Furche and R. Ahlrichs, *Chem. Phys. Lett.*, 2004, **384**, 103–107.
- 84 M. Sierka, A. Hogeckamp and R. Ahlrichs, *J. Chem. Phys.*, 2003, **118**, 9136–9148.
- 85 K. Eichkorn, O. Treutler, H. Öhm, M. Häser and R. Ahlrichs, *Chem. Phys. Lett.*, 1995, **240**, 283–290.
- 86 K. Eichkorn, F. Weigend, O. Treutler and R. Ahlrichs, *Theor. Chem. Acc.*, 1997, **97**, 119–124.
- 87 K. A. Peterson, D. Figgen, E. Goll, H. Stoll and M. Dolg, *J. Chem. Phys.*, 2003, **119**, 11113–11123.
- 88 K. A. Peterson, B. C. Shepler, D. Figgen and H. Stoll, *J. Phys. Chem. A*, 2006, **110**, 13877–13883.
- 89 O. Treutler and R. Ahlrichs, *J. Chem. Phys.*, 1995, **102**, 346–354.
- 90 M. Von Arnim and R. Ahlrichs, *J. Comput. Chem.*, 1998, **19**, 1746–1757.
- 91 R. Ahlrichs, M. Bär, M. Häser, H. Horn and C. Kölmel, *Chem. Phys. Lett.*, 1989, **162**, 165–169.
- 92 M. J. Frisch, G. W. Trucks, H. B. Schlegel, G. E. Scuseria, M. A. Robb, J. C. Cheeseman, J. R. Montgomery, Jr., J. A. Vreven, T. Kudin, K. N. Burant, J. M. Millam, S. S. Iyengar, J. Tomasi, V. Barone, B. Mennucci, M. Cossi, G. Scalmani, N. Rega, G. A. Petersson, H. Nakatsuji, M. Hada, M. Ehara, K. Toyota, R. Fukuda, J. Hasegawa, M. Ishida, T. Nakajima, Y. Honda, O. Kitao, H. Nakai, M. Klene, X. Li, J. E. Knox, H. P. Hratchian, J. B. Cross, V. Bakken, C. Adamo, J. Jaramillo, R. Gomperts, R. E. Stratmann, O. Yazyev, A. J. Austin, R. Cammi, C. Pomelli, J. W. Ochterski, P. Y. Ayala, K. Morokuma, G. A. Voth, P. Salvador, V. G. Dannenberg, J. J. Zakrzewski, S. Dapprich, A. D. Daniels, M. C. Strain, O. Farkas, D. K. Malick, J. B. Rabuck, A. D. Raghavachari, K. Foresman, J. V. Ortiz, Q. Cui, A. G. Baboul, S. Clifford, J. Cioslowski, B. B. Stefanov, G. Liu, A. Liashenko, P. Piskorz, I. Komaromi, R. L. Martin, D. J. Fox, T. Keith, M. A. Al-

- Laham, C. Y. Peng, M. Nanayakkara, A. Challacombe, P. M. W. Gill, B. Johnson, W. Chen, M. W. Wong, C. Gonzalez and J. A. Pople, *Gaussian 09, Revision C.01*, Gaussian, Inc., Wallingford CT, 2004.
- 93 *Jmol: an open-source Java viewer for chemical structures in 3D*, <http://www.jmol.org/> - accessed August 2015.
- 94 M. Öeren, E. Shmatova, T. Tamm and R. Aav, *Phys. Chem. Chem. Phys.*, 2014, **16**, 19198–19205.
- 95 M. Xue, Y. Yang, X. Chi, X. Yan and F. Huang, *Chem. Rev.*, 2015, **115**, 7398–7501.
- 96 G. Gil-Ramírez, D. a. Leigh and A. J. Stephens, *Angew. Chemie Int. Ed.*, 2015, **54**, 6110–6150.
- 97 H. Jacobson and W. H. Stockmayer, *J. Chem. Phys.*, 1950, **18**, 1600–1606.

Reprinted with permission from Royal Society of Chemistry

Publication I

M. Öeren, E. Shmatova, T. Tamm and R. Aav “Computational and ion mobility MS study of (*all-S*)-cyclohexylhemicucurbit[6]uril structure and complexes” *Phys. Chem. Chem. Phys.*, 2014, **16**, 19198–19205.

Computational and ion mobility MS study of (*all-S*)-cyclohexylhemicucurbit[6]uril structure and complexes†

Cite this: *Phys. Chem. Chem. Phys.*, 2014, 16, 19198

Mario Öeren, Elena Shmatova, Toomas Tamm and Riina Aav*

A computational study of (*all-S*)-cyclohexylhemicucurbit[6]uril and its complexes with anions (Cl^- , Br^- , I^- and HCOO^-), the proton (H^+) and non-dissociated acid (HCl , HBr , HI and HCOOH) guests was performed. The geometries of guest–host complexes were optimized *via* density functional theory using the BP86 functional, SV(P) basis set and Stuttgart pseudopotentials for iodide. Binding affinities and their trends were evaluated at the BP86/TZVPD level of theory. In addition, the quantum theory of atoms in molecules was used to gain insight into guest–host interactions. A computational study in the gas phase and ion-mobility mass-spectrometry analysis revealed that the studied macrocycle formed inclusion complexes with anions. Protonation of the macrocycle is preferred at the nitrogen atom pointing inside of the cavity. In the studied conditions, non-dissociated acids formed complexes at the oxygen atom pointing outside of the macrocycle.

Received 20th May 2014,
Accepted 8th July 2014

DOI: 10.1039/c4cp02202e

www.rsc.org/pccp

1. Introduction

Although the first cucurbituril (CB) was synthesized more than 100 years ago,¹ and characterized over 30 years ago,² this macrocyclic compound has gained wider attention only in recent decades. Applications of CBs³ are based on their ability to bind guest molecules, mainly alkylammonium cations. CBs are widely used as catalysts,⁴ nanomaterials and as drug delivery vehicles.⁵ Hemicucurbiturils (HCs) are a relatively new branch in the diverse CB family.³ The first HCs (HC[*n*] with *n* = 6, 12) were synthesized by Miyahara *et al.*⁶ in 2004 and since then only a few new HCs have been reported.^{7–9} Amongst new HCs, the first enantiomerically pure member of the cucurbituril family, (*all-S*)- and (*all-R*)-cyclohexylhemicucurbit[6]uril (cycHC[6]), has been synthesized in our group.¹⁰ Unsubstituted HCs have been reported to catalyse organic reactions,^{11–13} although their mode of action is still unknown. In contrast to CBs, in which the urea units are aligned, HCs adopt a ‘zig-zag’ orientation, causing a substantial difference in the electronic structure of the macrocycle and thereby allowing for the binding of anions.^{6,14} The anion binding properties of structurally close relatives of hemicucurbiturils, namely bambus[*n*]urils¹⁵ (BU[*n*], *n* = 4–6) have also been reported.^{16–18}

Since the pioneering computational study of Kim and co-workers in 2001,¹⁹ there has been a steady increase in the

number and quality of computational treatments of cucurbiturils and related systems. In many cases, complexation with various guest molecules has been among the goals of the studies. The size of the system, which is further increased by inclusion of a guest, initially necessitated the use of relatively simple models (Hartree–Fock) and small basis sets (STO-3G, 3-21G).^{19–21} Recent advances in computer technology have made treatments with more sophisticated models (DFT with hybrid functionals, up to triple-zeta basis sets) feasible.^{22–32} Use of the density fitting (also known as resolution of identity) approximation is routinely used, especially because the associated loss in accuracy is negligible.

Several researchers have paid close attention to the frontier molecular orbitals – the highest occupied MO (HOMO) and lowest unoccupied MO (LUMO) – of the macrocyclic systems,^{24,25,33} as well as the electrostatic potential generated by the molecule.^{26–32} These properties lead to the prediction of binding sites and modes of guests, and HOMO–LUMO energy gaps can be used as indicators of relative reactivities. The map of electrostatic potential (MESP) outlines electron-rich and electron-poor regions of a macrocycle, which are indicators of locations of possible electrostatic interactions between the host and the guest.

Binding modes and binding energies of various guest molecules have also received research attention.^{19,21,25,34–36} Such models can also provide insight into the probable location of the binding site, including whether binding inside or outside of the macrocycle is preferred. Additional information about the nature of chemical bonds between the host and guests has been obtained from the quantum theory of atoms in molecules (QTAIM).^{23,31} This model also provides an estimate of the strength of host–guest interactions.

Department of Chemistry, Tallinn University of Technology, Ehitajate tee 5, 19086 Tallinn, Estonia. E-mail: riina@chemet.ee

† Electronic supplementary information (ESI) available: Computational and IM-MS CCS details, including optimized geometries. See DOI: 10.1039/c4cp02202e

It has been reported that the HC binds anions^{9,23,37} and a few cations.^{38,39} In addition, Cong *et al.* have suggested that the binding of a proton inside of HC occurs during catalysis with HC.¹² The chiral hemicucurbituril (*all-S*)-cycHC[6] was isolated as a hydrogen halide complex. Additionally, based on the results of a diffusion NMR study of (*all-S*)-cycHC[6] complexes, it was proposed that substituted hemicucurbituril forms inclusion complexes with carboxylic acids.¹⁰ So far, there is no crystal structure of (*all-S*)-cycHC[6] complexes and it is not known whether the acids are bound as dissociated anions or as non-dissociated neutral species. A computational study of the structure and mode of complexation of cycHC[6] would increase our knowledge in this field.

In this paper, we report the geometry and electronic structure of cycHC[6] and its complexes with the anions Cl^- , Br^- , I^- and HCOO^- and the proton and non-dissociated (HCl , HBr , HI and HCOOH) guests. Different binding sites were evaluated and selected complexes were studied using QTAIM analysis. Additionally, a study of ion mobility mass-spectrometric analysis of cycHC[6] complexes was performed.

2. Experimental section

2.1 Computational details

2.1.1 Description of the opening and the cavity of cycHC[6]. Four parameters were chosen to describe the geometric changes of the macrocycle upon complexation with guests. The distances from the carbon C_2 and oxygen O to the centre of the cavity X ($r(\text{C}_2\text{-X})$ and $r(\text{O-X})$) describe the changes of the geometry at the equator of the macrocycle. The distances from the C_{4a} and C_7 to the centre of the cavity ($r(\text{C}_{4a}\text{-X})$ and $r(\text{C}_7\text{-X})$) describe the opening or closing movement of the cyclohexyl groups. The shortest distance of C_5 from the axis (Z) ($r(\text{C}_5\text{-Z})$) describes the openings of the macrocycle. The listed distances are graphically depicted in Fig. 1. The cavity size of the optimized structures was studied using the program Swiss-PdbViewer.⁴⁰

2.1.2 Electronic structure calculations. All molecular structures in this work were built using the program Avogadro⁴¹ and pre-optimized therein using the MMFF94 molecular-mechanical model. Further geometry optimizations were conducted with

density functional theory (DFT), using the BP86 functional^{42–46} along with the def2-SV(P)⁴⁷ basis set. The interactions between guest and host were expected to be prevalently electrostatic; hence, in the interest of computational speed, the choice of the lightweight, thus fast functional without dispersion correction was justified. To speed up the geometry optimization, the resolution of identity (RI) approximation was used.^{48–51} Vibrational frequency calculations were performed to ensure that all chosen geometries were at minima, and to estimate the zero-point vibrational energies (ZPE). The energies of local minima were refined by single-point calculations with the def2-TZVPD⁴⁷ basis set. The iodine atoms were described with the inclusion of the appropriate Stuttgart pseudopotential.^{52,53} In addition, counterpoise correction calculations were performed to obtain basis set superposition error (BSSE) corrected energies for host-guest complexes.⁵⁴ The transition states were verified using dynamic reaction coordinate calculations. All calculations were performed in the gas phase. Solvation effects were omitted because cycHC[6] complexation was previously studied in hydrophobic solvent (CDCl_3)¹⁰ and to model that one should include the first shell explicitly and use a continuum model to describe the bulk solvent. Currently, little information is available about the structure of the first explicit solvation shell of chloroform for the calculated species. Also, in this work complexes were experimentally studied in the gas phase by mass-spectrometric analysis. The density functional theory calculations were performed using the Turbomole 6.4 program package.^{55–58}

2.1.3 Search for binding sites. The search for binding sites for guests was done systematically, where outside of the macrocycle five latitudes (with 36° increments) and five longitudes (with 10° increments) were combined (Fig. 2).

The crossing points of the meridians and parallels were used as initial locations for the guests in the geometry optimizations. For each guest type, a few locations were added manually as well. The centre of the macrocycle was added to the set for anions and locations on the HOMO were added for the proton. The combinations of anion and proton locations were added for the non-dissociated guest.

2.1.4 Binding energy of the guest. The binding energy (BE) was calculated by subtracting the sum of the total energies of

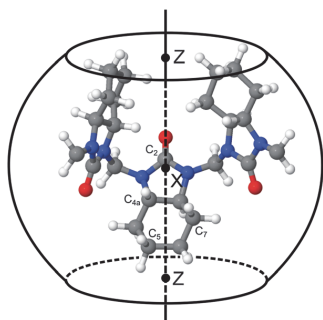


Fig. 1 Atom numbers, centre of the cavity and axis of cycHC[6].

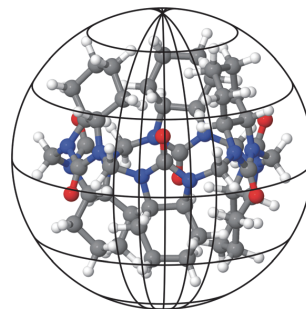


Fig. 2 Latitudes and longitudes used in a systematic search for binding sites.

the reagents from the sum of the total energies of the products. The total energies for each geometry were calculated as sums of DFT energies (DE) and basis set superposition error (BSSE) corrections from def2-TZVPD calculations and the zero-point energy (ZPE) correction from def2-SV(P) calculations. The binding energy of anions and non-dissociated guests with the host were calculated according to eqn (1).

$$BE = (DE_{GH} + ZPE_{GH} + BSSE_{GH}) - (DE_G + ZPE_G + DE_H + ZPE_H), \quad (1)$$

where the equation components with the subscripts GH, G and H denote the aforementioned energies of the guest–host complex, guest and host, respectively.

The calculation of the binding energy of a proton to the macrocycle is shown in eqn (2), and it was found *via* the reaction of an oxonium ion with a host molecule, producing water as the secondary product.

$$BE = (DE_{GH} + ZE_{GH} + DE_{H_2O} + ZE_{H_2O}) - (DE_{H_3O^+} + ZE_{H_3O^+} + DE_H + ZE_H), \quad (2)$$

where the equation components with the subscripts GH, H₂O, H₃O⁺ and H denote the aforementioned energies of the guest–host complex, water, oxonium ion and host, respectively.

2.1.5 Post-processing of the results. For visualization of the map of electrostatic potential (MESP), single-point calculations were repeated at the def2-SV(P) level of theory using Gaussian 09⁵⁹ software. Visualizations of geometries, frontier orbitals and MESP were generated from the output files with Jmol⁶⁰ and Molekel.⁶¹ The binding properties of the macrocycle were studied *via* QTAIM,⁶² using the program Multiwfn⁶³ with def2-SV(P) density. The required .wfx file for iodine with ECP information was generated with Gaussian 09. Interactions between the host and the guest were investigated *via* locating the bond critical points (BCPs) as defined in the QTAIM model. The interaction energies (*E*) were calculated using the potential energy density (*V*) at the corresponding BCP, as in this case $E = V/2$.⁶⁴

2.2 Ion-mobility mass-spectrometric analysis

Hemicucurbituril cycHC[6] HCl and HBr adducts were synthesized as previously described.¹⁰ 40 μM solutions of cycHC[6] + HCl and cycHC[6] + HBr in a solvent mixture of H₂O (47.5%), MeOH (47.5%) and HCOOH (5%) were prepared and analyzed by electrospray ionization ion mobility mass spectrometry (ESI-IM-MS). All of the MS experiments were performed using a Waters Synapt G2 HDMS quadrupole travelling wave ion mobility orthogonal acceleration time-of-flight mass spectrometer (Waters, Manchester, UK), equipped with a normal Z-spray ESI source in both positive and negative ion modes. A source temperature of 100 °C, capillary voltage of 2 kV, desolvation temperature of 150 °C, and cone voltage of 20 V were set as the ESI parameters. All experiments were performed under conditions of 280 m s⁻¹ wave velocity and 18 V wave height by traveling wave ion-mobility mass spectrometry (TWIM-MS). The experimental collision cross-sections (Ω_D) of cycHC[6] complexes were calculated by the calibration method of Thalassinou *et al.*,⁶⁵ with

polyalanine as a calibrant. The published Ω_D values of the polyalanine were obtained from the database of the Clemmer group.⁶⁶ The theoretical Ω_D values were calculated by the projection approximation method, using the radius of each atom⁶⁷ from the hard sphere mode.⁶⁸

3. Results and discussion

3.1 Geometry and electronic structure of cyclohexylhemicucurbit[6]uril

The calculated structure of cycHC[6] had monomers in 'zig-zag' orientation and exhibited D₃ point group symmetry. Validation of the computed structure was done *via* comparison of the shortest distances between the centre of the cavity, axis and selected atoms – $r(C_5-Z)$, $r(C_7-X)$, $r(C_{4a-X})$, $r(C_2-X)$ and $r(O-X)$ – of the calculated and crystallographic structure¹⁰ (Table 1).

As can be seen from Table 1, the distances $r(C_2-X)$ and $r(O-X)$ of the computed structure were very close to the experimental ones, while the difference increased for the atoms that were located closer to the opening from $r(C_{4a-X})$ to $r(C_5-Z)$. The differences between the computed and experimental structure were probably caused by the flexibility of cyclohexyl groups, which were influenced by the packing forces in the crystal structure. The volume of the internal cavity was 22 Å³ for the calculated structure and 18 Å³ for the experimental structure.

The highest occupied molecular orbital (HOMO) was mostly distributed over the polar cyclic urea functional groups, and its bulkiest lobes were on the nitrogen atoms (Fig. 3a). Nitrogen atoms were not planar, adopting quasi-sp²/quasi-sp³ geometry, and therefore the HOMO lobes on nitrogen atoms were present both inside and outside of the macrocycle. The HOMO was also located on the cyclohexyl moiety and this orbital only slightly covered the oxygen atoms. The location of the binding site for cations was not uniquely determined by the orbital structure. The binding of a cation could take place inside or outside of the macrocycle, where the HOMO of the latter was delocalized. The lowest unoccupied molecular orbital (LUMO), on the other hand, was concentrated mostly inside the macrocycle (Fig. 3b).

This positioning of the LUMO in the centre of the cavity creates a potential binding site for anions. Therefore, we could expect interaction between the HOMO of the anionic guests and the LUMO of macrocycle, which would result in encapsulation of the anionic guest molecule. The HOMO–LUMO gap was

Table 1 Distances between the centre of the cavity and axis and selected atoms of computed and experimental cycHC[6] in Å

	Computed parameters	Experimental parameters ^a
$r(C_5-Z)$	3.1	2.7 ± 0.2
$r(C_7-X)$	4.2	3.8 ± 0.1
$r(C_{4a-X})$	4.2	4.1 ± 0.1
$r(C_2-X)$	4.4	4.4 ± 0.2
$r(O-X)$	5.0	5.0 ± 0.1

^a Radii were the mean values for six atoms of each monomer given with maximum absolute deviation.

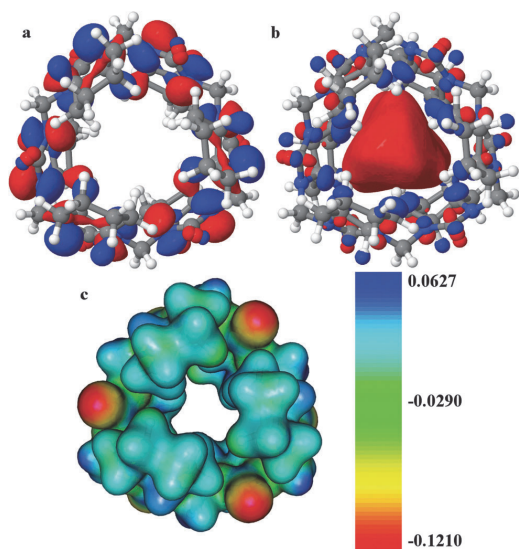


Fig. 3 Electronic structure of cycHC[6]: (a) HOMO; (b) LUMO; (c) MESP.

4.93 eV (SV(P)), making it the lowest amongst analogous macrocycles (6.04–6.58 eV).^{2,3}

The map of electrostatic potential (MESP) of cycHC[6] is shown in Fig. 3c. The most electron-rich regions (red area) were on oxygen atoms, while the most electron-deficient areas (blue areas) were found on the methylene bridges and the centres of cyclohexyl groups. Besides oxygen atoms, nitrogen atoms were found to be electron-rich as well (yellow area) and, due to the chirality of the monomer, one electron-rich nitrogen was pointing outside of the macrocycle and the other one inside. The MESP on nitrogen atoms agreed with the HOMO being located on the nitrogen atoms. The openings of the macrocycle were rather electron-poor. The listed characteristics of cycHC[6] electronic structure and frontier orbitals made it possible to visualize possible binding sites of guest molecules. However the complexation of both an anion and a proton inside the cavity of macrocycle is feasible. Further computations of the interaction strengths and binding energies of non-dissociated and dissociated acids with cycHC[6] were carried out.

3.2 Structure of cycHC[6]-anion complexes

In the search for the binding sites for anions, geometry optimization of all generated initial structures led to multiple distinct local minima for all anions. In all cases, anions strongly preferred the binding site inside the macrocycle. The energy difference between the lowest-energy minimum, having an anion inside, and the second-lowest one, having an anion outside, was always over 25 kJ mol⁻¹ and reached 100 kJ mol⁻¹ for some higher-lying minima. Based on these results, we propose that all anions prefer to reside inside the macrocycle. The lowest energy complexes are shown in Fig. 4. All possible molecular geometries of different binding sites and their energies can be found in the ESI.†

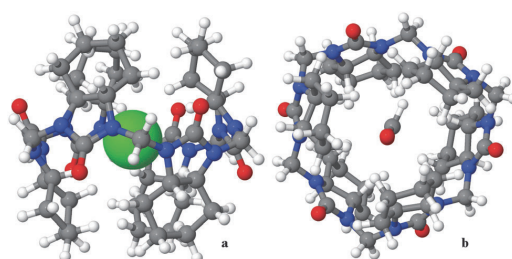


Fig. 4 Lowest energy complexes of cycHC[6] with anions Cl⁻ (a) and HCOO⁻ (b).

Table 2 Distances between the centre of the cavity, axis and selected atoms of non-complexed and complexed cycHC[6] with anions in Å. Cavity volumes are given without a guest in Å³

	Non-complexed cycHC[6]	cycHC[6] complexed with			
		Cl ⁻	Br ⁻	I ⁻	HCOO ⁻
$r(\text{H5}_{\text{ax}}-\text{Z})$	2.4	2.2	2.3	2.4	2.3–2.4 ^a
$r(\text{H7}_{\text{ax}}-\text{X})$	3.2	3.0	3.1	3.2	3.0–3.1
$r(\text{H4a}_{\text{ax}}-\text{X})$	3.2	3.0	3.0	3.1	3.0–3.2
$r(\text{C}_2-\text{X})$	4.4	4.5	4.5	4.5	4.4–4.5
Cavity volume	22	21	21	22	21

^a Minimum and maximum distances are given due to the asymmetrical geometry of the complexes with this anion.

The shortest distances between inside-pointing axial hydrogens (H5_{ax}, H7_{ax}, H4a_{ax}), carbonyl carbon (C₂) and the centre of the cavity (X) and axis (Z) were measured to compare the geometries of anion complexed macrocycles and non-complexed macrocycles. The relevant distances $r(\text{H5}_{\text{ax}}-\text{Z})$, $r(\text{H7}_{\text{ax}}-\text{X})$, $r(\text{H4a}_{\text{ax}}-\text{X})$ and $r(\text{C}_2-\text{X})$ are given in Table 2.

All spherical halogen anions caused symmetrical changes in the geometry of cycHC[6], while the non-spherical formic acid anion led to deformation of the macrocycle. Upon adopting the anions inside the cavity of the macrocycle, the distance $r(\text{C}_2-\text{X})$ increased, showing that the equator of the cycHC[6] had expanded slightly. At the same time, the distances between the inside-pointing hydrogens of the cyclohexyl rings and axis, as well as the centre of the cavity ($r(\text{H5}_{\text{ax}}-\text{Z})$, $r(\text{H7}_{\text{ax}}-\text{X})$, $r(\text{H4a}_{\text{ax}}-\text{X})$) decreased, indicating that flexible cyclohexyl rings covered the anions, causing a slight shrinkage of the opening. The biggest changes in cavity size took place in the case of the chloride and the smallest with the iodine complex.

According to QTAIM analysis, halogen anions had 12 bonding interactions with the macrocycle. All halogen anions interacted with the same hydrogens (H4a_{ax} and H7_{ax}) of each monomer of the macrocycle. The calculated interaction energies were close to 5 kJ mol⁻¹ for both interacting hydrogens and similar for each halogen anion. The HCOO⁻ ion interacted with the same hydrogen atoms, although the interaction energies showed large variability (3.0–14 kJ mol⁻¹). Additionally, the HCOO⁻ formed two extra bonding interactions between the formate hydrogen atom and two nitrogen atoms of different monomers of the macrocycle (H–N interactions (a) and (b) in Table 3).

Table 3 Interaction and binding energies (kJ mol^{-1}) of anions with cycHC[6]

	Cl^-	Br^-	I^-	HCOO^-
Average interaction energies	4.7	4.9	4.8	9.7 ^a
H–N (a)	—	—	—	7.3
H–N (b)	—	—	—	4.5
Sum of interaction energies	56.7	59.1	58.0	127.8
Binding energy	–102	–87	–65	–83

^a The average interaction energy for HCOO^- does not contain H–N energies.

The binding energies of the four anions with the host molecule were computed according to the reaction of cycHC[6] with anion X^- , as shown below. The binding and interaction energies of anion complexes are listed in Table 3.



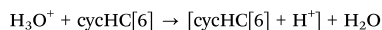
Despite the fact that formate had the highest interaction energy with cycHC[6] ($127.8 \text{ kJ mol}^{-1}$), the binding energy showed the strongest interaction with chloride (-102 kJ mol^{-1}), in the gas phase, as chlorides fit best into the macrocycle. Distortion of the macrocycle geometry by the HCOO^- ion partially cancelled the effect of the strong interactions by increasing tension in the macrocycle. In the case of halides, the interaction energies decreased with the increase in the size of the halide, which could have been caused by the repulsive force between the anion and heavy atoms of the macrocycle. These computational results agree well with the LUMO localization inside of the

non-complexed macrocycle and confirm that cycHC[6] forms inclusion complexes with halogen and formate anions.

In addition to binding energy, the transition states of ion insertion were studied as well. While Cl^- and Br^- insertion is spontaneous, the transition state energies for I^- and HCOO^- insertion are 22 kJ mol^{-1} and 12 kJ mol^{-1} respectively (Fig. 5). At the start of the ion insertion both anions were bound at the opening of the macrocycle. Energies of the corresponding local minima at the opening were higher than the global minima by 11 kJ mol^{-1} for I^- and 20 kJ mol^{-1} for HCOO^- , respectively. During the transition, anions moved along the Z axis, the cyclohexyl groups opened up: the $r(\text{H5}_{\text{ax}}\text{-Z})$ increased from the value of 2.4 \AA up to 3.6 \AA . This indicates that the studied anions have low or no insertion barriers, which means that the formation of the inclusion complexes is favored.

3.3 Structure of cycHC[6] with a proton

The search for possible binding sites yielded six local minima for the proton. The lowest energy geometries with covalently bound protons are shown in Fig. 6. Energetically, the binding of the proton to the macrocycle was favoured for all local minima, as shown in Table 4. The binding energy of the proton with the cycHC[6] was computed according to the reaction of cycHC[6] with oxonium as shown below:



The results show that, in reaction with an oxonium ion, cycHC[6] is preferably protonated at the nitrogen N_1 atom

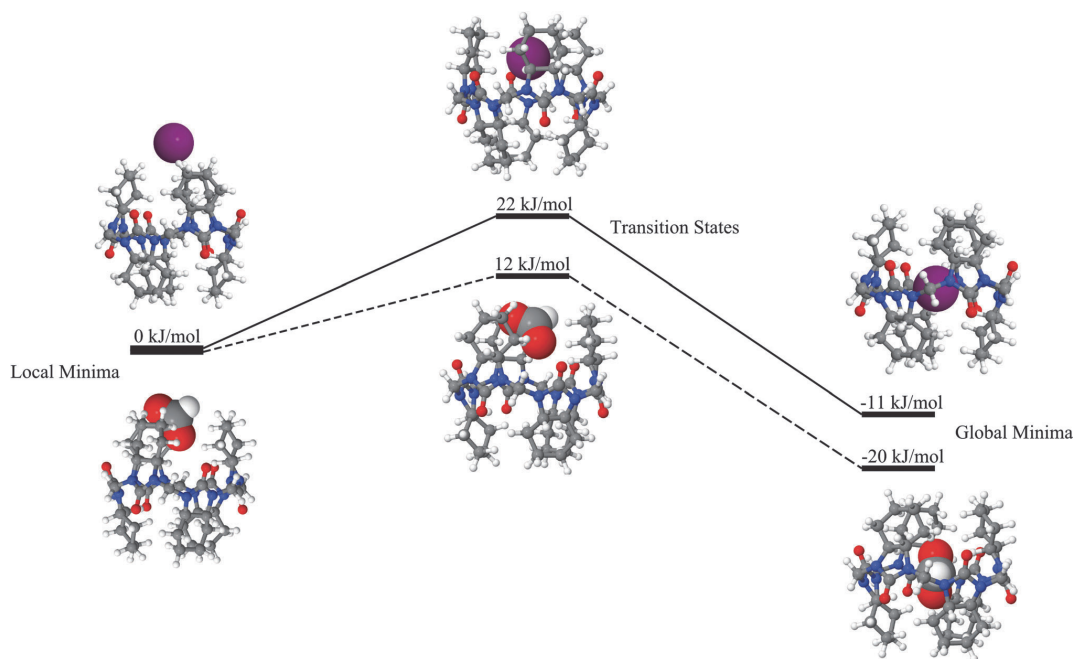


Fig. 5 Reaction coordinates of I^- (solid line) and HCOO^- (dashed line) forming inclusion complexes with cycHC[6].

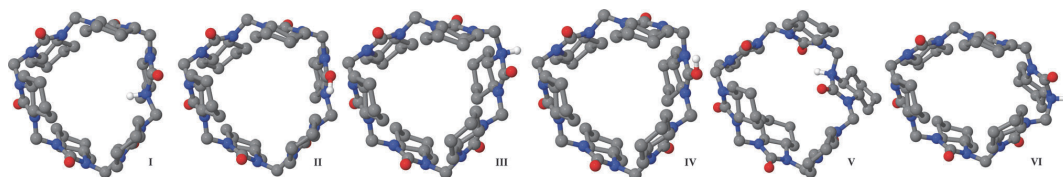


Fig. 6 Structures of protonated cycHC[6]. Hydrogen atoms (except the added proton) were removed.

positioned inside of the macrocycle. According to the Boltzmann distribution, the population of protonated geometry I will be over 90%. Favourable protonation sites were in good agreement with the analysis of the electronic structure of cycHC[6]. However, it should be noted that the binding of bulkier cations inside the cavity of the macrocycle is much less probable, due to the position and size of non-complexed cycHC[6] LUMO.

3.4 Structure of cycHC[6] with HCl, HBr, HI or HCOOH

The non-dissociated guests can bind both inside and outside of the macrocycle. Energetically, the outside binding sites were favoured for all guests. The inclusion complexes were at least 14 kJ mol^{-1} higher in energy. The representative energetically favored geometries of the complex with hydrogen chloride are shown in Fig. 7; the complexes with HBr, HI and HCOOH were similar. In contrast to the favourable binding site of the proton at the nitrogen of cycHC[6], there was binding of electron-poor hydrogens of non-dissociated acids at the oxygen atom of the macrocycle outside the cavity. This change in the preferred interaction site is most probably caused by steric factors. The binding energies of these complexes confirm that complexation with non-dissociated acids was energetically favourable in the studied conditions (Table 5). The binding energies

Table 4 Energies (kJ mol^{-1}) of the protonation of cycHC[6]

Geometry nr	Protonation site of cycHC[6]	Energy difference from minima	Binding energy
I	At N_1 inside	0	-244
II	O	7	-238
III	At N_3 outside	9	-236
IV	O	11	-233
V	At N_3 inside	13	-232
VI	At N_1 outside	34	-211

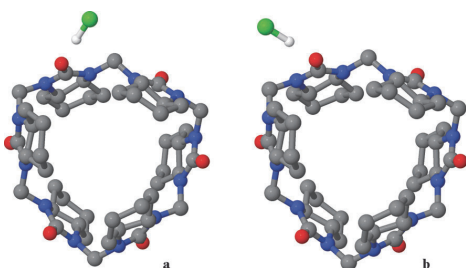
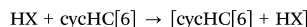


Fig. 7 Lowest energy geometries of cycHC[6] and HCl complexes.

Table 5 Binding energy (kJ mol^{-1}) of the non-dissociated guests with cycHC[6]

Non-dissociated guest	Geometry	Energy difference from minima	Binding energy
HCl	a	0	-67
	b	2	-65
HBr	a	0	-26
	b	1	-25
HI	a	0	-31
	b	1	-30
HCOOH	a	5	-16
	b	0	-21

of the non-dissociated guests with cycHC[6] were computed according to the reaction shown below, where HX denotes the non-dissociated acid:



The results indicate that the cycHC[6] was able to bind the studied non-dissociated guests in the gas phase, although inclusion complexes were not formed.

3.5 Ion-mobility mass-spectrometric analysis of cycHC[6] ion complexes

The computationally obtained structures were verified *via* TWIM-MS spectroscopy. The collision cross-section (CCS) values measured by ion-mobility mass spectrometry and calculated from minimum energy conformers of Cl^- , Br^- and HCOO^- anion complexes were found to agree with each other well (Table 6). The deviation of the calculated CCS from the experimental data was 2%, confirming that anions formed inclusion complexes with cycHC[6]. The lowest-energy protonated cycHC[6] theoretical CCS value also coincided with the experimental data. It should be noted that the CCS of the $[\text{cycHC[6]} + \text{Na}]^+$ complex was significantly larger than all other ion CCS values, showing that sodium is positioned outside of the macrocycle.

Table 6 Collision cross section value of each *trans*-cycHC[6] complex

Complex	Experimental CCS (\AA^2)	Theoretical CCS (\AA^2)
$[\text{cycHC[6]} + \text{Cl}]^-$	182	185
$[\text{cycHC[6]} + \text{Br}]^-$	183	186
$[\text{cycHC[6]} + \text{HCOO}]^-$	183	187
$[\text{cycHC[6]} + \text{H}]^+$	194	197 ^a
$[\text{cycHC[6]} + \text{Na}]^+$	225	—

^a For geometry I in Fig. 6.

4. Conclusions

The electronic structure of *trans*-cyclohexylhemicucurbit[6]uril and its complexes with ionic (H^+ , Cl^- , Br^- , I^- and HCOO^-) and non-dissociated (HCl , HBr , HI , HCOOH) guests was studied. It was shown that cyclohexylhemicucurbituril had numerous possible binding sites for all guests. The conclusions based on our study *in vacuo* are as follows:

(i) Non-complexed cyclohexylhemicucurbituril exhibited D_3 symmetry, and the computed geometry was in good agreement with the crystal structure. Calculations showed electron-rich areas on the oxygen atoms of each of the cyclohexylurea units, while the HOMO was located at the equator of the macrocycle. The largest lobes of the HOMO were on nitrogen atoms, pointing inside and outside the macrocycle. Electron-deficient areas were located on methylene bridges and the centres of cyclohexyl groups. The LUMO was concentrated inside the macrocycle, filling the cavity.

(ii) All of the studied anions favoured binding inside the macrocycle. QTAIM analysis showed that twelve bonding interactions existed between the macrocycle and halogen anions, and fourteen such interactions were found between the macrocycle and HCOO^- . The order of the binding preference of the studied anions was $\text{Cl}^- > \text{Br}^- > \text{HCOO}^- > \text{I}^-$. The formation of the inclusion complex of anions with cycHC[6] was also confirmed by ion-mobility mass-spectrometry.

(iii) The systematic search for a binding site for a proton resulted in six possible locations. In the lowest-energy geometry, the proton was attached inside of the macrocycle to the nitrogen atom. Proton binding in the reaction of cycHC[6] with oxonium cation was favourable by -244 kJ mol^{-1} .

(iv) Non-dissociated acids preferred binding outside of the macrocycle through electron-poor hydrogens of the acids at the oxygen of cycHC[6]. There were two energetically close and structurally similar binding sites for all of the studied non-dissociated acids. According to the binding energy, -65 kJ mol^{-1} , the strongest complex was formed with hydrogen chloride.

Acknowledgements

This research was supported by the Estonian Science Foundation through Grant Nos 8255 and 8698 and the Tallinn University of Technology basic financing grant No. B25. The Estonian Ministry of Education and Research through Grants IUT19-32 and the EU European Regional Development Fund (3.2.0101.08-0017) also provided financial support. Computations were performed on the HPC cluster at Tallinn University of Technology, which is part of the ETAIS project. The authors thank Prof. Hugh I. Kim and Ms Hyun Hee Lee L. Lee at the Pohang University of Science and Technology, Korea, for IM-MS data and helpful discussions. The authors would also like to thank Dr Merle Uudsemaa at the Tallinn University of Technology for helpful discussions.

Notes and references

- 1 R. Behrend, E. Meyer and F. Rusche, *Justus Liebigs Ann. Chem.*, 1905, **339**, 1–37.

- 2 W. A. Freeman, W. L. Mock and N.-Y. Shih, *J. Am. Chem. Soc.*, 1981, **103**, 7367–7368.
- 3 E. Masson, X. Ling, R. Joseph, L. Kyeremeh-Mensah and X. Lu, *RSC Adv.*, 2012, **2**, 1213–1247.
- 4 B. C. Pemberton, R. Raghunathan, S. Volla and J. Sivaguru, *Chemistry*, 2012, **18**, 12178–12190.
- 5 S. Walker, R. Oun, F. J. McInnes and N. J. Wheate, *Isr. J. Chem.*, 2011, **51**, 616–624.
- 6 Y. Miyahara, K. Goto, M. Oka and T. Inazu, *Angew. Chem., Int. Ed.*, 2004, **43**, 5019–5022.
- 7 Y. Li, L. Li, Y. Zhu, X. Meng and A. Wu, *Cryst. Growth Des.*, 2009, **9**, 4255–4257.
- 8 T. Fiala and V. Sindelar, *Synlett*, 2013, 2443–2445.
- 9 M. Lisbjerg, B. M. Jessen, B. Rasmussen, B. Nielsen, A. Ø. Madsen and M. Pittelkow, *Chem. Sci.*, 2014, **5**, 2591–2908.
- 10 R. Aav, E. Shmatova, I. Reile, M. Borissova, F. Topić and K. Rissanen, *Org. Lett.*, 2013, **15**, 3786–3789.
- 11 H. Cong, T. Yamato, X. Feng and Z. Tao, *J. Mol. Catal. A: Chem.*, 2012, **365**, 181–185.
- 12 H. Cong, T. Yamato and Z. Tao, *J. Mol. Catal. A: Chem.*, 2013, **379**, 287–293.
- 13 H. Cong, T. Yamato and Z. Tao, *New J. Chem.*, 2013, **37**, 3778–3783.
- 14 H.-J. Buschmann, E. Cleve and E. Schollmeyer, *Inorg. Chem. Commun.*, 2005, **8**, 125–127.
- 15 J. Svec, M. Necas and V. Sindelar, *Angew. Chem., Int. Ed.*, 2010, **49**, 2378–2381.
- 16 V. Havel, J. Svec, M. Wimmerova, M. Dusek, M. Pojarova and V. Sindelar, *Org. Lett.*, 2011, **13**, 4000–4003.
- 17 A. Révész, D. Schröder, J. Svec, M. Wimmerová and V. Sindelar, *J. Phys. Chem. A*, 2011, **115**, 11378–11386.
- 18 V. Havel, V. Sindelar, M. Necas and A. E. Kaifer, *Chem. Commun.*, 2014, **50**, 1372–1374.
- 19 K. S. Oh, J. Yoon and K. S. Kim, *J. Phys. Chem. B*, 2001, **105**, 9726–9731.
- 20 H. Cong, Q.-J. Zhu, H.-B. Hou, S.-F. Xue and Z. Tao, *Supramol. Chem.*, 2006, **18**, 523–528.
- 21 H. Cong, L.-L. Tao, Y.-H. Yu, Z. Tao, F. Yang, Y.-J. Zhao, S.-F. Xue, G. a. Lawrance and G. Wei, *J. Phys. Chem. A*, 2007, **111**, 2715–2721.
- 22 F. Pichierri, *Dalton Trans.*, 2013, **42**, 6083–6091.
- 23 M. Sundararajan, R. V. Solomon, S. K. Ghosh and P. Venuvanalingam, *RSC Adv.*, 2011, **1**, 1333–1341.
- 24 M. Sundararajan, V. Sinha, T. Bandyopadhyay and S. K. Ghosh, *J. Phys. Chem. A*, 2012, **116**, 4388–4395.
- 25 S. Pan, S. Mondal and P. K. Chattaraj, *New J. Chem.*, 2013, **37**, 2492–2499.
- 26 R. V. Pinjari and S. P. Gejji, *J. Phys. Chem. A*, 2008, **112**, 12679–12686.
- 27 R. V. Pinjari and S. P. Gejji, *J. Phys. Chem. A*, 2009, **113**, 1368–1376.
- 28 P. H. Dixit, R. V. Pinjari and S. P. Gejji, *J. Phys. Chem. A*, 2010, **114**, 10906–10916.
- 29 V. V. Gobre, R. V. Pinjari and S. P. Gejji, *J. Phys. Chem. A*, 2010, **114**, 4464–4470.

- 30 V. V. Gobre, P. H. Dixit, J. K. Khedkar and S. P. Gejji, *Comput. Theor. Chem.*, 2011, **976**, 76–82.
- 31 S. R. Peerannawar, V. V. Gobre and S. P. Gejji, *Comput. Theor. Chem.*, 2012, **983**, 16–24.
- 32 S. R. Peerannawar and S. P. Gejji, *J. Mol. Model.*, 2013, **19**, 5113–5127.
- 33 H. Cong, Y.-J. Zhao, S.-F. Xue, Z. Tao and Q.-J. Zhu, *J. Mol. Model.*, 2007, **13**, 1221–1226.
- 34 J. W. Lee, S. Samal, N. Selvapalam, H.-J. Kim and K. Kim, *Acc. Chem. Res.*, 2003, **36**, 621–630.
- 35 T. S. Choi, J. Y. Ko, S. W. Heo, Y. H. Ko, K. Kim and H. I. Kim, *J. Am. Soc. Mass Spectrom.*, 2012, **23**, 1786–1793.
- 36 D. H. Noh, S. J. C. Lee, J. W. Lee and H. I. Kim, *J. Am. Soc. Mass Spectrom.*, 2014, **25**, 410–421.
- 37 H.-J. Buschmann and A. Zielesny, *Comput. Theor. Chem.*, 2013, **1022**, 14–22.
- 38 H.-J. Buschmann, A. Zielesny and E. Schollmeyer, *J. Inclusion Phenom. Macrocyclic Chem.*, 2006, **54**, 181–185.
- 39 D.-D. Xiang, Q.-X. Geng, H. Cong, Z. Tao and T. Yamato, *Supramol. Chem.*, 2014, 1–8.
- 40 N. Guex and M. C. Peitsch, *Electrophoresis*, 1997, **18**, 2714–2723.
- 41 M. D. Hanwell, D. E. Curtis, D. C. Lonie, T. Vandermeersch, E. Zurek and G. R. Hutchison, *J. Cheminf.*, 2012, **4**, 1–17.
- 42 P. A. M. Dirac, *Proc. R. Soc. A*, 1929, **123**, 714–733.
- 43 J. C. Slater, *Phys. Rev.*, 1951, **81**, 385–390.
- 44 S. H. Vosko, L. Wilk and M. Nusair, *Can. J. Phys.*, 1980, **58**, 1200–1211.
- 45 A. D. Becke, *Phys. Rev. A: At., Mol., Opt. Phys.*, 1988, **38**, 3098–3100.
- 46 J. P. Perdew, *Phys. Rev. B: Condens. Matter Mater. Phys.*, 1986, **33**, 8822–8824.
- 47 F. Weigend and R. Ahlrichs, *Phys. Chem. Chem. Phys.*, 2005, **7**, 3297–3305.
- 48 P. Deglmann, K. May, F. Furche and R. Ahlrichs, *Chem. Phys. Lett.*, 2004, **384**, 103–107.
- 49 M. Sierka, A. Hogekamp and R. Ahlrichs, *J. Chem. Phys.*, 2003, **118**, 9136–9148.
- 50 K. Eichkorn, O. Treutler, H. Öhm, M. Häser and R. Ahlrichs, *Chem. Phys. Lett.*, 1995, **240**, 283–290.
- 51 K. Eichkorn, F. Weigend, O. Treutler and R. Ahlrichs, *Theor. Chem. Acc.*, 1997, **97**, 119–124.
- 52 K. A. Peterson, D. Figgen, E. Goll, H. Stoll and M. Dolg, *J. Chem. Phys.*, 2003, **119**, 11113–11123.
- 53 K. A. Peterson, B. C. Shepler, D. Figgen and H. Stoll, *J. Phys. Chem. A*, 2006, **110**, 13877–13883.
- 54 P. Taylor, S. F. Boys and F. Bernardi, *Mol. Phys.*, 1970, **19**, 553–566.
- 55 O. Treutler and R. Ahlrichs, *J. Chem. Phys.*, 1995, **102**, 346–354.
- 56 M. Von Arnim and R. Ahlrichs, *J. Comput. Chem.*, 1998, **19**, 1746–1757.
- 57 R. Ahlrichs, M. Bär, M. Häser, H. Horn and C. Kölmel, *Chem. Phys. Lett.*, 1989, **162**, 165–169.
- 58 K. Eichkorn, F. Weigend, O. Treutler and R. Ahlrichs, *Theor. Chem. Acc.*, 1997, **97**, 119–124.
- 59 M. J. Frisch, G. W. Trucks, H. B. Schlegel, G. E. Scuseria, M. A. Robb, J. C. Cheeseman, J. R. Montgomery, Jr., J. A. Vreven, T. Kudin, K. N. Burant, J. M. Millam, S. S. Iyengar, J. Tomasi, V. Barone, B. Mennucci, M. Cossi, G. Scalmani, N. Rega, G. A. Petersson, H. Nakatsuji, M. Hada, M. Ehara, K. Toyota, R. Fukuda, J. Hasegawa, M. Ishida, T. Nakajima, Y. Honda, O. Kitao, H. Nakai, M. Klene, X. Li, J. E. Knox, H. P. Hratchian, J. B. Cross, V. Bakken, C. Adamo, J. Jaramillo, R. Gomperts, R. E. Stratmann, O. Yazyev, A. J. Austin, R. Cammi, C. Pomelli, J. W. Ochterski, P. Y. Ayala, K. Morokuma, G. A. Voth, P. Salvador, V. G. Dannenberg, J. J. Zakrzewski, S. Dapprich, A. D. Daniels, M. C. Strain, O. Farkas, D. K. Malick, J. B. Rabuck, A. D. Raghavachari, K. Foresman, J. V. Ortiz, Q. Cui, A. G. Baboul, S. Clifford, J. Cioslowski, B. B. Stefanov, G. Liu, A. Liashenko, P. Piskorz, I. Komaromi, R. L. Martin, D. J. Fox, T. Keith, M. A. Al-Laham, C. Y. Peng, M. Nanayakkara, A. Challacombe, P. M. W. Gill, B. Johnson, W. Chen, M. W. Wong, C. Gonzalez and J. A. Pople, *Gaussian 09, Revision C.01*, Gaussian, Inc., Wallingford, CT, USA, 2004.
- 60 *Jmol: an open-source Java viewer for chemical structures in 3D*, <http://www.jmol.org/>, accessed February 2014.
- 61 U. Varetto, *Molekel version 5.4.0.8*, Swiss National Supercomputing Centre, Lugano, Switzerland, 2006.
- 62 R. F. W. Bader, *Atoms in Molecules: A Quantum Theory*, Oxford University Press, Oxford, United Kingdom, 1990.
- 63 T. Lu, *Multwfn version 3.2.1*, University of Science and Technology Beijing, Beijing, China, 2009.
- 64 E. Espinosa, E. Molins and C. Lecomte, *Chem. Phys. Lett.*, 1998, **285**, 170–173.
- 65 K. Thalassinou, M. Grabenauer, S. E. Slade, G. R. Hilton, M. T. Bowers and J. H. Scrivens, *Anal. Chem.*, 2009, **81**, 248–254.
- 66 www.indiana.edu/~clemmer, accessed December 2013.
- 67 R. S. Rowland and R. Taylor, *J. Phys. Chem.*, 1996, **100**, 7384–7391.
- 68 T. Wyttenbach, G. Von Helden, J. J. Batka and M. T. Bowers, *J. Am. Soc. Mass Spectrom.*, 1997, **8**, 275–282.

Reprinted with permission from Taylor & Francis

Publication II

M. Fomitšenko, E. Shmatova, M. Öeren, I. Järving and R. Aav “New Homologues of chiral cyclohexylhemicurbit[*n*]urils” *Supramolecular Chemistry*, 2014, **9**, 698–703.

New homologues of chiral cyclohexylhemicucurbit[*n*] jurils

Maria Fomitšenko, Elena Shmatova, Mario Öeren, Ivar Järving and Riina Aav*

Department of Chemistry, Tallinn University of Technology, Akadeemia tee 15, 12618 Tallinn, Estonia

(Received 21 February 2014; accepted 16 May 2014)

The existence of new 7-, 8-, 9- and 10-membered homologues of chiral cyclohexylhemicucurbituril is reported. The barrel-shaped (*all-R*)-cyclohexylhemicucurbit[8]juril ((*all-R*)-cycHC[8]) was isolated and its complexes with anions were detected in negative ion mode MS. Here, 7-, 9- and 10-membered homologues were detected by HPLC–HRMS. Geometries of all reported macrocycles were calculated using quantum chemical methods, which showed that even-numbered homologues were barrel-shaped and odd-numbered homologues were asymmetrical barrel-shaped with unequal dimensions of the openings. The size of the ((*all-R*)-cycHC[8]) cavity was comparable to CB[8] and it probably can serve as a chiral host.

Keywords: hemicucurbiturils; cucurbiturils; chiral macrocycles; NMR; host–guest complex

Introduction

Hemicucurbiturils are members of the cucurbituril (1) family, which has grown enormously in this century (2, 3). There are several homologues (4–6) of normal cucurbiturils and a wide variety of analogues (7–13). In general, glycoluril monomers in these macrocyclic compounds are joined together by two methylene bridges and form strong host–guest pairs with cationic ammonium compounds (3, 14, 15). In hemicucurbiturils, on the other hand, monomers are linked together via one bridge, causing a zigzag orientation of the urea functionalities (16–18). This structural change, compared with the normal cucurbiturils, drastically influences the electronic structure of macrocycles and allows complexation of anions inside the cavity (19, 20). The zigzag orientation of the single-bridged glycoluril monomers in bambusurils (21) exhibits similar anion binding properties (22–24). Presently, the ring sizes of cucurbituril family macrocycles range from 4-membered bambusurils (25) to 14-membered twisted normal cucurbituril (26). The most widely applied normal cucurbituril homologues have six to eight monomers joined together and the inner dimensions of these macrocycles allow for selective complexation of a large number of useful small molecules (2, 3, 14). Until now, only 6- and 12-membered hemicucurbiturils have been isolated. Ten years ago, Miyahara et al. (16) reported that, in strongly acidic conditions, ethyleneurea, in the presence of formalin, can selectively produce two homologues of unsubstituted hemicucurbiturils in very high yields. Hemicucurbit[6]juril (HC[6]) is formed in concentrated HCl at lower temperatures and hemicucurbit[12]juril (HC[12]) in diluted acid at higher temperatures (Figure 1). It has been shown that unsubstituted hemicucurbituril can catalyse organic

reactions (27–29). The structure of the first substituted hemicucurbituril – achiral *meso*-cyclohexylhemicucurbit[6]juril (*meso*-cycHC[6]) – was reported by Li et al. (17) and, due to introduced rigidity in the formed macrocycle, it required much harsher conditions than HC[6] for high-yielding synthesis. In the same conditions, its more rigid analogue, norbornahemicucurbit[6]juril (norHC[6]), was formed in significantly lower yield (30). Together with norHC[6], traces of 4-, 5-, 7- and 8-membered norbornahemicucurbiturils were detected by mass-spectrometric analysis (30). The only presently known chiral analogue of substituted hemicucurbiturils, (*all-S*) or (*all-R*)-cyclohexylhemicucurbit[6]juril (*chiral*-cycHC[6]) (18), has cyclohexyl and urea cycles joined in *trans*-fashion. High-yielding synthesis of the latter required a much longer (24 h) reaction time at the same temperature, compared with other substituted hemicucurbiturils (Figure 1).

In this paper, we report the isolation of a new chiral homologue of substituted hemicucurbituril, enantiomerically pure (*all-R*)-cyclohexylhemicucurbit[8]juril ((*all-R*)-cycHC[8]) and analytical evidence of the existence of its 7-, 9- and 10-membered homologues ((*all-R*)-cycHC[7], (*all-R*)-cycHC[9] and (*all-R*)-cycHC[10]). The calculated geometries of all reported macrocycles are also presented.

Results and discussion

The formation of hemicucurbiturils occurs as a result of a polymerisation reaction; therefore, in addition to the most favourable 6-membered macrocycles, the existence of homologues was expected. A reaction mixture of previously reported (*all-R*)-cycHC[6] was carefully examined by reverse-phase (RP)-HPLC–MS analysis, and 7-, 8-,

*Corresponding author. Email: riina@chemnet.ee

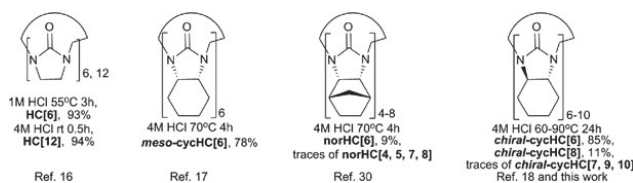


Figure 1. Hemicucurbit[*n*]urils structures and reaction conditions for their synthesis from Refs (16–18, 30) and this work.

9- and 10-membered homologues of (*all-R*)-cycHC[6] were found. A chromatogram of cycHC[6–10] is shown in Figure 2, in which peaks were detected by ultraviolet (UV) light and positive ion mode high-resolution mass spectrometry. The order of homologue elution in RP column was cycHC[9], cycHC[8] and cycHC[7] as one cluster, followed by cycHC[6] and cycHC[10] further apart from each other. The elution order shows that 10- and 6-membered homologues were less polar than their 7-, 8- and 9-membered homologues.

Preliminary attempts were made to increase the degree of formation of higher homologues, by varying the reaction temperature of cyclisation between 60 and 90°C. According to the ¹H NMR analysis, cycHC[6] still remained the main product in all reactions performed in 4 M HCl solution and the reaction temperature did not influence significantly the content of crude product. Additional study is necessary to find out conditions that could drive macrocyclisation towards formation of higher homologues. Nevertheless, the purification of crude product by RP flash chromatography afforded (*all-R*)-cycHC[8] in 11% yield. NMR spectra of (*all-R*)-cycHC[8] showed high symmetry; therefore, signals belonging to all monomers of the macrocycle were identical, adopting the same averaged conformation as in the case of *chiral*-cycHC[6] (18). The chemical shifts of relevant atoms of *chiral*-cycHC[6] and (*all-R*)-cycHC[8] were distinguishable and their assignment is presented in Figure 3.

NMR observations are in good agreement with the calculated geometry of (*all-R*)-cycHC[8] (Figure 4).

The equatorial belt of the macrocycle adopted a square-like shape, having methylene bridges with carbon number C9 on the corners of the macrocycle. Carbon C9 is situated between the stereogenic carbons C2, in which protons H(in) point inside the cavity. According to the optimised structure, all cyclohexyl rings were in chair conformation, which was also supported by the high value of ³*J*_(HH)-coupling constants (> 11 Hz) between the cyclohexyl axial protons. Monomers were in zigzag orientation and cyclohexyl rings leaned slightly over the opening, as in the case of cycHC[6]. The diameter of (*all-R*)-cycHC[8] opening was 4.6 Å, which is within the corresponding values of normal cucurbiturils (31) CB[6] (3.9 Å) and CB[7] (5.4 Å). The cavity diameter at the equator of cycHC[8] macrocycle was 8.5 Å, which is comparable to the 8.8 Å of the CB[8] cavity size. (*all-R*)-cycHC[8] had a barrel shape as do normal cucurbiturils, and its cavity dimensions were comparable to the most widely applied normal cucurbiturils. In the negative ion mode of MS analysis, complexes of (*all-R*)-cycHC[8] with chloride and formate anions were detected, confirming that the new substituted hemicucurbituril can bind anions as do other zigzag-oriented cucurbituril family members.

To get a better understanding of the structures of other existing chiral cyclohexylhemicucurbiturils, geometries of

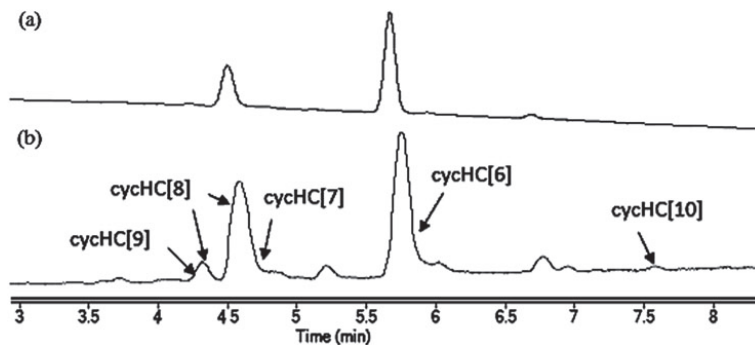


Figure 2. RP-HPLC–MS chromatograms of (*all-R*)-cycHC[9], (*all-R*)-cycHC[8], (*all-R*)-cycHC[7], (*all-R*)-cycHC[6] and (*all-R*)-cycHC[10] (a) detected by UV at 210 nm and (b) detected by (+)ESI-MS.

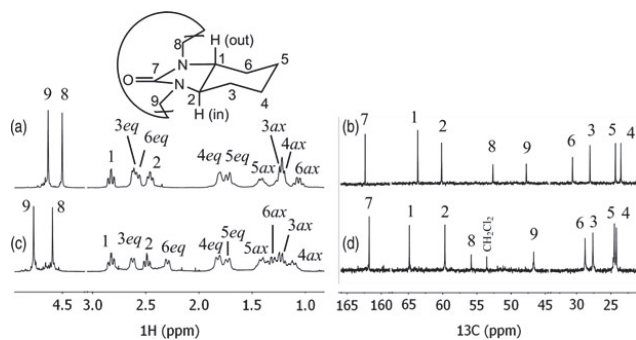


Figure 3. Assigned ^1H and ^{13}C NMR spectra of (a), (b) *chiral*-cycHC[6] and (c), (d) (*all-R*)-cycHC[8], respectively.

7-, 9- and 10-membered homologues were also calculated (Figure 5).

Macrocycles with odd numbers of monomers (cycHC[7], cycHC[9]) still formed almost barrel-like shapes. Cyclohexyl rings of zigzag-oriented monomers leaned over the openings, but two aligned urea cycles distorted the symmetry of the macrocycle, leading to two different sized openings (Table 1). The 10-membered homologue was a symmetrical five-cornered barrel. In 7-, 9- and 10-membered macrocycles, the cyclohexyl rings adopted both twisted and chair conformations. The dimensions describing the sizes of the cavities of the chiral hemicucurbiturils are outlined in Table 1.

Conclusions

As a result of RP liquid chromatography of the crude product of previously known *chiral*-cycHC[6], new 7-, 8-, 9- and 10-membered homologues of chiral cyclohexylhemicucurbituril were found. The barrel-shaped (*all-R*)-cyclohexylhemicucurbit[8]uril was isolated and

its complexes with anions were detected in negative ion mode MS. Here, 7-, 9- and 10-membered homologues were detected by HPLC–HRMS. The geometries of all reported macrocycles were calculated using the density functional theory, which showed that even-numbered homologues were barrel-shaped and odd-numbered homologues were asymmetrical barrel-shaped with unequal dimensions of the openings. The isolated (*all-R*)-cycHC[8] was more polar than its 6-membered homologue. The cavity of (*all-R*)-cycHC[8] was comparable with CB[7] and CB[8]; therefore, it probably will serve as a chiral host for anions of small molecules.

Experimental section

General

All used instruments are located at Tallinn University of Technology, Department of Chemistry. RP-HPLC-MS was performed on an Agilent 6540 UHD Accurate-Mass Q-TOF LC/MS spectrometer (Agilent Technologies, Santa Clara, CA, USA) with AJ-ESI ionisation and a Zorbax

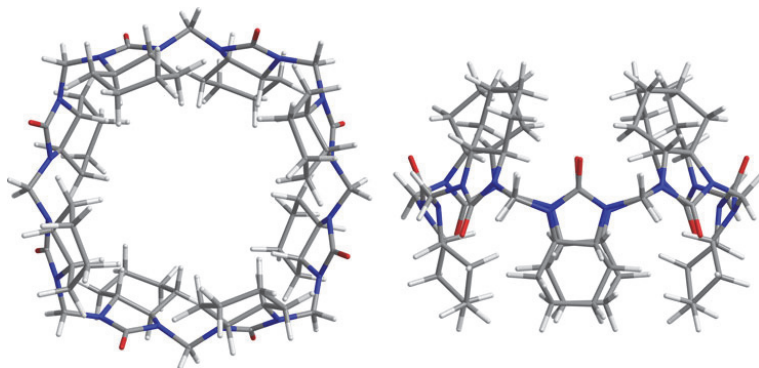


Figure 4. (Colour online) Calculated structures of (*all-R*)-cycHC[8].

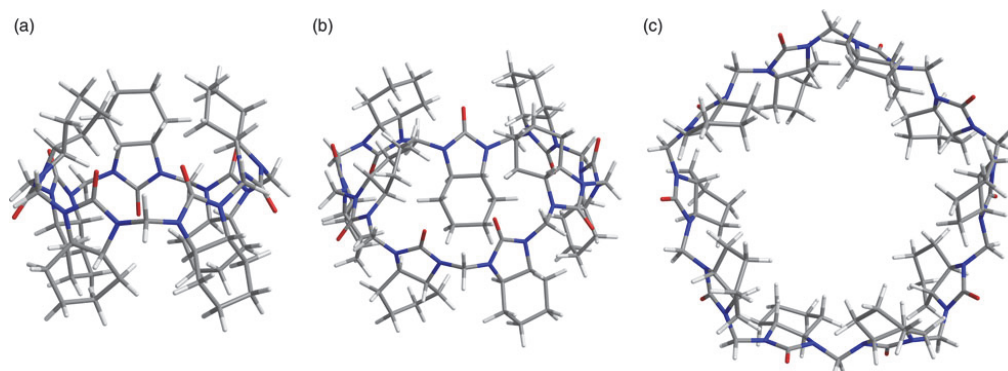


Figure 5. (Colour online) Calculated structures of (a) (*all-R*)-cycHC[7], (b) (*all-R*)-cycHC[9] and (c) (*all-R*)-cycHC[10].

Eclipse Plus C18 column (2.1 mm × 150 mm, 1.8 μm) and is reported as *m/z* ratios. RP flash column chromatography was performed on a Biotage Isolera™ Prime purification system using a Biotage SNAP KP-C18-HS Cartridge (60 g, 50 μm) (Biotage®, Uppsala, Sweden). NMR spectra were recorded using a Bruker Avance III 400 MHz spectrometer (Bruker BioSpin GmbH, Rheinstetten, Germany), and chemical shifts are referenced in carbon spectrum by CDCl₃ at 77.16 ppm and proton spectrum by CDCl₃ at 7.26 ppm. Infrared (IR) spectra were obtained on a Bruker Tensor 27 FT-IR spectrometer (Bruker Optik GmbH, Ettlingen, Germany) and are reported in wave numbers. The intensities of the peaks are reported using the following abbreviations: s: strong, m: medium and w: weak. Optical rotation was measured using an Anton Paar MCP 500 polarimeter (Anton Paar GmbH, Graz, Austria). The melting point was detected using a Nagema melting point microscope.

Experimental procedures

Synthesis of (*all-R*)-cyclohexylhemicurbiturils was performed as described in an earlier publication (18), except for varying the temperature between 60 and 90°C.

An RP-HPLC-MS analysis of 1 mg/mL crude sample in 0.1% formic acid in acetonitrile was performed using a 10-min gradient from 70% to 100% of eluent A, which was acetonitrile, and eluent B was a 0.1% formic acid aqueous solution. The flow rate was set at 0.4 mL/min and the UV detection at 210 nm. Mass-to-charge ratios were measured using ESI-Q-TOF MS.

RP flash chromatography was performed with 200 mg of crude product (18), which was dissolved in 1 ml of formic acid before loading it into the column. The sample was purified using gradient from 50% to 100% of eluent A with the same eluents as described in the HPLC conditions. The flow rate was adjusted to 40 ml/min, and the sample detection was measured at 210 nm. Here, 22 mg of cycHC[8] was obtained in 11% yield.

Characterisation data

Compound (*all-R*)-cycHC[8]: It is a white solid (22 mg, 0.018 mmol, yield 11%). Mp = 245–250°C (dec). IR (KBr, cm⁻¹) 3502 w, 2936 m, 2858 m, 1711 s, 1435 m, 1359 s, 1332 m, 1232 s, 1134 w, 1058 w, 1014 w, 988 w, 919 w, 830 w, 774 m, 667 w, 628 w, 532 w, 516 w, 476 w. ¹H NMR (400 MHz, CDCl₃) δ = 1.18–1.05 (m, H_{4ax}, 1H), 1.23 (qd, H_{3ax}, *J* = 11.0, 2.9, 1H), 1.29 (qd, H_{6ax},

Table 1. Dimensions^a of (*all-R*)-cyclohexylhemicurbit[6–10]urils in Å.

	cycHC[6] ^b	cycHC[7] ^c	cycHC[8] ^c	cycHC[9] ^c	cycHC[10] ^c
Diameter at the opening	2.2	2.3 4.2	4.6	4.9 7.3	6.6
Diameter at the equator of the cavity	5.3	6.8	8.5	9.8	11.5
Height	12.1	12.8	12.5	12.7	12.4

^aTaking van der Waals radii into account.

^bFrom Ref. (18).

^cFrom calculated structures.

$J = 11.3, 3.3, 1\text{H}$), 1.47–1.35 (m, **H5ax**, 1H), 1.73 (bd, **H5eq**, $J = 12.7, 1\text{H}$), 1.82 (bd, **H4eq**, $J = 12.5, 1\text{H}$), 2.30 (dd, $J = 11.5, 2.7$, **H6eq**, 1H), 2.49 (td, $J = 11.0, 2.9$, **H2** (in), 1H), 2.62 (dd, $J = 11.6, 2.7$, **H3eq**, 1H), 2.83 (td, $J = 11.1, 3.1$, **H1**(out), 1H), 4.59 (s, **H8**, 8H), 4.77 (s, **H9**, 8H). ^{13}C NMR (101 MHz, CDCl_3) $\delta = 161.77$ (C7), 64.86 (C1), 59.68 (C2), 55.83 (C8), 46.69 (C9), 28.76 (C6), 27.63 (C3), 24.48 (C5), 24.19 (C4). HRMS (ESI +): calculated for $(\text{C}_{64}\text{H}_{97}\text{N}_{16}\text{O}_8)^+$ $[\text{M} + \text{H}]^+$ 1217.7670, found 1217.7670. HRMS (ESI -): calculated for $(\text{C}_{65}\text{H}_{97}\text{N}_{16}\text{O}_{10})$ $[\text{M} + \text{HCOO}]$ 1261.7579, found 1261.7607. HRMS: calculated for $\text{C}_{64}\text{H}_{96}\text{N}_{16}\text{O}_8\text{Cl}$ $[\text{M} + \text{Cl}]$ 1251.7291, found 1251.7283. $[\alpha]_{\text{D}}^{25} = 60^\circ$ (c 0.62, $\text{CDCl}_3/\text{CHCl}_3$).

Compound (*all-R*)-cycHC[7]: HRMS (ESI +): calculated for $(\text{C}_{56}\text{H}_{85}\text{N}_{14}\text{O}_7)^+$ $[\text{M} + \text{H}]^+$ 1065.6720, found 1065.6720. HRMS (ESI -): calculated for $(\text{C}_{57}\text{H}_{85}\text{N}_{14}\text{O}_9)$ $[\text{M} + \text{HCOO}]$ 1109.6341, found 1109.6621.

Compound (*all-R*)-cycHC[9]: HRMS (ESI +): calculated for $(\text{C}_{72}\text{H}_{109}\text{N}_{18}\text{O}_9)^+$ $[\text{M} + \text{H}]^+$ 1369.8619, found 1369.8621. HRMS (ESI -): calculated for $(\text{C}_{73}\text{H}_{109}\text{N}_{18}\text{O}_{11})$ $[\text{M} + \text{HCOO}]$ 1413.8529, found 1413.8490.

Compound (*all-R*)-cycHC[10]: HRMS (ESI +): calculated for $(\text{C}_{80}\text{H}_{121}\text{N}_{20}\text{O}_{10})^+$ $[\text{M} + \text{H}]^+$ 1521.9569, found 1521.9551.

Calculation studies

All structures were built and optimised on an MMFF94 (32) level of theory, using the programme Avogadro (33). Further geometry optimisations were conducted using density functional theory, combining BP86 (34–38) functional with a def2-SV(P) (39) basis set. Density functional theory calculations were performed with the program package Turbomole 6.4 (40).

The dimensions of (*all-R*)-cyclohexylhemicucurbiturils were measured using the lengths from the chosen atoms to the centre of the opening or to the centre of the cavity. For the opening, a hydrogen atom closest to the centre was chosen from each monomer. For the cavity, the carbonyl carbon of each monomer was chosen. Next, the average radius for both atom sets was found. For both dimensions, the Van der Waals radius was subtracted from the average radius and the diameter was obtained by multiplying the radius by two. The centre points were arithmetic averages of the Cartesian coordinates of chosen atom sets. Heights are distances between opening centres, positioned closest to the edge with two added Van der Waals radii of the hydrogens.

Funding

This work was supported by Estonian Science Foundation [grant number 8698], Tallinn University of Technology base financing

[grant number B25], the Ministry of Education and Research [grant numbers IUT19-32, IUT19-9] and the EU European Regional Development Fund [grant number 3.2.0101.08-0017].

Supplementary data

Supplementary data for this article can be accessed at <http://dx.doi.org/10.1080/10610278.2014.926362>.

References

- Freeman, W.A.; Mock, W.L.; Shih, N.-Y. *J. Am. Chem. Soc.* **1981**, *103*, 7367–7368.
- Isaacs, L. *Chem. Commun.* **2009**, *6*, 619–629.
- Lagona, J.; Mukhopadhyay, P.; Chakrabarti, S.; Isaacs, L. *Angew. Chem. Int. Ed.* **2005**, *44*, 4844–4870.
- Day, A.; Arnold, A.P.; Blanch, R.J.; Snushall, B. *J. Org. Chem.* **2001**, *66*, 8094–8100.
- Kim, J.; Jung, I.-S.; Kim, S.-Y.; Lee, E.; Kang, J.-K.; Sakamoto, S.; Yamaguchi, K.; Kim, K. *J. Am. Chem. Soc.* **2000**, *122*, 540–541.
- Day, A.I.; Blanch, R.J.; Arnold, A.P.; Lorenzo, S.; Lewis, G.R.; Dance, I. *Angew. Chem. Int. Ed.* **2002**, *41*, 275–277.
- Lagona, J.; Fettingler, J.C.; Isaacs, L. *Org. Lett.* **2003**, *5*, 3745–3747.
- Flinn, A.; Hough, G.C.; Stoddart, J.F.; Williams, D. *J. Angew. Chem.* **1992**, *31*, 1475–1477.
- Isobe, H.; Sato, S.; Nakamura, E. *Org. Lett.* **2002**, *4*, 1287–1289.
- Zhao, Y.J.; Xue, S.F.; Zhu, Q.J.; Tao, Z.; Zhang, J.X.; Wei, Z.B.; Long, L.S.; Hu, M.L.; Xiao, H.P.; Day, A.I. *Chin. Sci. Bull.* **2004**, *49*, 1111–1116.
- Zhao, J.; Kim, H.-J.; Oh, J.; Kim, S.-Y.; Lee, J.W.; Sakamoto, S.; Yamaguchi, K.; Kim, K. *Angew. Chem. Int. Ed.* **2001**, *40*, 4233–4235.
- Lucas, D.; Minami, T.; Iannuzzi, G.; Cao, L.; Wittenberg, J. B.; Anzenbacher, Jr, P.; Isaacs, L. *J. Am. Chem. Soc.* **2011**, *133*, 17966–17976.
- Ma, D.; Zavalij, P.Y.; Isaacs, L. *J. Org. Chem.* **2010**, *75*, 4786–4795.
- Masson, E.; Ling, X.; Joseph, R.; Kyeremeh-Mensah, L.; Lu, X. *RSC Adv.* **2012**, *2*, 1213–1247.
- Chernikova, E.Yu.; Fedorov, Yu.V.; Fedorova, O.A. *Russ. Chem. Bull. Int. Ed.* **2012**, *61*, 1363–1390.
- Miyahara, Y.; Goto, K.; Oka, M.; Inazu, T. *Angew. Chem. Int. Ed.* **2004**, *43*, 5019–5022.
- Li, Y.; Lin, L.; Zhu, Y.; Meng, X.; Wu, A. *Cryst. Growth Des.* **2009**, *9*, 4255–4257.
- Aav, R.; Shmatova, E.; Reile, I.; Borissova, M.; Topic, F.; Rissanen, K. *Org. Lett.* **2013**, *15*, 3786–3789.
- Buschmann, H.-J.; Cleva, E.; Schollmeyer, E. *Inorg. Chem. Commun.* **2005**, *8*, 125–127.
- Buschmann, H.-J.; Zielesny, A.; Schollmeyer, E. *J. Incl. Phenom. Macrocyc. Chem.* **2006**, *54*, 181–185.
- Svec, J.; Necas, M.; Sindelar, V. *Angew. Chem. Int. Ed.* **2010**, *49*, 2378–2381.
- Svec, J.; Dusek, M.; Fejfarova, K.; Stacko, P.; Klán, P.; Kaifer, A.E.; Li, W.; Hudeckova, E.; Sindelar, V. *Chem. Eur. J.* **2011**, *17*, 5605–5612.
- Havel, V.; Sindelar, V.; Necas, M.; Kaifer, A.E. *Chem. Commun.* **2014**, *50*, 1372–1374.
- Révész, Á.; Schröder, D.; Svec, J.; Wimmerov, M.; Sindelar, V. *J. Phys. Chem. A* **2011**, *115*, 11378–11386.
- Havel, V.; Svec, J.; Wimmerova, M.; Dusek, M.; Pojarova, M.; Sindelar, V. *Org. Lett.* **2011**, *13*, 4000–4003.

- (26) Cheng, X.-J.; Liang, L.-L.; Chen, K.; Ji, N.-N.; Xiao, X.; Zhang, J.-X.; Zhang, Y.-Q.; Xue, S.-F.; Zhu, Q.-J.; Ni, X.-L.; et al. *Angew. Chem. Int. Ed.* **2013**, *52*, 7252–7255.
- (27) Cong, H.; Yamato, T.; Feng, X. *J. Mol. Catal. A Chem.* **2012**, 181–185.
- (28) Cong, H.; Yamato, T.; Zhu Tao *J. Mol. Catal. A Chem.* **2013**, 287–293.
- (29) Cong, H.; Yamato, T.; Zhu Tao *New J. Chem.* **2013**, *37*, 3778–3783.
- (30) Fiala, T.; Sindelar, V. *Synlett* **2013**, *24*, 2443–2445.
- (31) Lee, J.W.; Samal, S.; Selvapalam, N.; Kim, H.-J.; Kim, K. *Acc. Chem. Res.* **2003**, *36*, 621–630.
- (32) Halgren, T.A. *J. Comput. Chem.* **1998**, *17*, 490–519.
- (33) Hanwell, M.D.; Curtis, D.E.; Lonie, D.C.; Vandermeersch, T.; Zurek, E.; Hutchison, G.R. *J. Cheminform.* **2012**, *4* (1), 17–33.
- (34) Dirac, P.A.M. *Proc. Roy. Soc. (Lond.) A* **1929**, *123*, 714–733.
- (35) Slater, J.C. *Phys. Rev.* **1951**, *81*, 385–390.
- (36) Vosko, S.H.; Wilk, L.; Nusair, M.; *Can J. Phys.* **1980**, *58*, 1200–1211.
- (37) Becke, A.D. *Phys. Rev. A* **1988**, *38*, 3098–3100.
- (38) Perdew, J.P. *Phys. Rev. B* **1986**, *33*, 8822–8824.
- (39) Weigend, F.; Ahlrichs, R. *Phys. Chem. Chem. Phys.* **2005**, *7*, 3297–3305.
- (40) Ahlrichs, R.; Bär, M.; Häser, M.; Horn, H.; Kölmel, C. *Chem. Phys. Lett.* **1989**, *162*, 165–169.

Reprinted with permission from Royal Society of Chemistry

Publication III

E. Prigorchenko, M. Öeren, S. Kaabel, M. Fomitšenko, I. Reile, I. Järving, T. Tamm, F. Topić, K. Rissanen and R. Aav “Template-controlled synthesis of chiral cyclohexylhemicucurbit[8]uril” *Chem. Comm.*, 2015, 51, 10921–10924.



Cite this: DOI: 10.1039/c5cc04101e

Received 18th May 2015,
Accepted 3rd June 2015

DOI: 10.1039/c5cc04101e

www.rsc.org/chemcomm

Template-controlled synthesis of chiral cyclohexylhemicucurbit[8]uril†

E. Prigorchenko,^a M. Öeren,^a S. Kaabel,^a M. Fomitšenko,^a I. Reile,^b I. Järving,^a
T. Tamm,^a F. Topić,^c K. Rissanen^c and R. Aav*^a

Enantiomerically pure cyclohexylhemicucurbit[8]uril (cycHC[8]), possessing a barrel-shaped cavity, has been prepared in high yield on a gram scale from either (*R,R,N,N'*)-cyclohex-1,2-diyurea and formaldehyde or cycHC[6]. In either case, a dynamic covalent library is first generated from which the desired cycHC can be amplified using a suitable anion template.

Research on new and selective host–guest systems and their applications is currently progressing very quickly.¹ Along with the search for new selective host–guest pairs, new and more efficient synthesis methods for hosts are being developed. Based on the recent success in the field of reversible non-covalent interactions in supramolecular chemistry,² the concept of dynamic covalent chemistry (DCC) has been established.³ Controlling covalent bond formation by non-covalent interactions can serve as an excellent tool for developing efficient adaptive systems, where the formation of the host molecule is based on the structure of the guest.

Cucurbit[*n*]urils⁴ (CB) are non-toxic host molecules⁵ with a wide range of applications.^{1a,d,6} Mechanistic studies have shown that the formation of oligomers and larger CBs proceeds reversibly, indicating that the principles of DCC are applicable in CB chemistry.⁷ Hemicucurbiturils⁸ (HC) are a sub-group of the cucurbituril family (Fig. 1). HCs are known to form complexes with anions⁹ and unsubstituted HCs have been applied as catalysts in organic reactions.¹⁰ It has been shown that biotin[6]uril esters can be applied as transmembrane anion carriers.^{9e} Miyahara *et al.*^{9a} were the first to describe an efficient synthesis of HC[6] and HC[12].

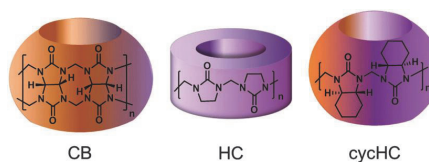


Fig. 1 Generalized shapes of normal CB, HC and chiral cycHC.

High selectivity towards the HC[6] was explained by the template effect of the chloride anion, which was recently confirmed in a biotin[6]uril synthesis.^{9f} The halogen anion is also the necessary template in the synthesis of bambus[6]urils (BU),¹¹ which can be classified as substituted HCs. Presently, besides HC[12], only 6-membered HCs⁸ and 4- and 6-membered BUs¹¹ have been isolated as main products. Until now, there has not been an efficient synthetic method available for the synthesis of 8-membered HCs. The existence of norbornahemicucurbit[8]uril^{8d} has been detected only by mass-spectrometry and (all-*R*)-cyclohexylhemicucurbit[8]uril (cycHC[8]) has only been isolated as a by-product in low yield.^{8e}

Herein we report an efficient synthesis of enantiomerically pure cycHC[8], starting either from its homologue cycHC[6] or (*R,R,N,N'*)-cyclohex-1,2-diyurea **1a** and paraformaldehyde. A mechanism of the transformation of cycHC[6] to cycHC[8] is proposed and proof of complexation with carboxylic acids is presented.

CycHC[6] was synthesized earlier in our group.^{8c} Subsequently, a small amount of its homologue cycHC[8]^{8e} was isolated from the crude product of cycHC[6]. Moreover, we noticed that in the chromatographic sample of cycHC[6] containing formic acid the amount of cycHC[8] gradually increased over time. The screening of reaction conditions for this conversion showed that cycHC[6] was transformed to cycHC[8] in the presence of sulphuric, formic and trifluoroacetic acid, but not acetic acid (S4, ESI†). The conversion of cycHC[6] to cycHC[8] by trifluoroacetic acid catalysis is approximately ten times faster than by formic acid (Table 1, entries 1 and 2). Nevertheless, the isolated yield of cycHC[8] was in both cases 71% in gram scale.

^a Department of Chemistry, Tallinn University of Technology, Akadeemia tee 15, 12618 Tallinn, Estonia. E-mail: riina.aav@ttu.ee

^b National Institute of Chemical Physics and Biophysics, Akadeemia tee 23, 12618 Tallinn, Estonia

^c University of Jyväskylä, Department of Chemistry, Nanoscience Center, P.O. Box. 35, FI-40014 Jyväskylä, Finland

† Electronic supplementary information (ESI) available: A detailed description of synthesis, MS, NMR, crystallographic and computational details. CCDC 1053111. For ESI and crystallographic data in CIF or other electronic format see DOI: 10.1039/c5cc04101e

Table 1 Selected reaction conditions and the list of templates for cycHC synthesis

No.	Starting comp.	(Additive)/acid/solvent ^a	Template	Time (h), T	Ratio ^b of cycHC[8] to cycHC[6]	Product	Isolated yield of product (%)
1	cycHC[6]	HCOOH/CH ₃ CN	HCO ₂ ⁻	24, rt	92:8	cycHC[8]	71
2	cycHC[6]	CF ₃ COOH/CH ₃ CN	CF ₃ CO ₂ ⁻	1.5, rt	95:5	cycHC[8]	71
3	cycHC[6]	NaPF ₆ (50 eq.)/CH ₃ COOH/CH ₃ CN	PF ₆ ⁻	24, rt	99:1	cycHC[8]	90
4	1a	HCOOH/CH ₃ CN	HCO ₂ ⁻	24, rt	92:8	cycHC[8]	7
5	1a	NaPF ₆ (50 eq.)/CH ₃ COOH/CH ₃ CN	PF ₆ ⁻	24, rt	95:5	cycHC[8]	55
6	1a	CF ₃ COOH/CH ₃ CN	CF ₃ CO ₂ ⁻	2, rt	96:4	cycHC[8]	73
7 ^c	1a	HCl/H ₂ O	Cl ⁻	24, 70 °C	0:100	cycHC[6] + HCl	85
8	cycHC[8]	HCl/H ₂ O	Cl ⁻	24, 70 °C	5:95	cycHC[6] + HCl	71
9	cycHC[8]	NaCl (50 eq.)/CH ₃ COOH	Cl ⁻	24, 70 °C	40:60	cycHC[6] + HCl	21

^a Generally 300 eq. of organic acid or 4 M HCl were used. ^b Determined by HPLC. ^c Described previously in ref. 8c.

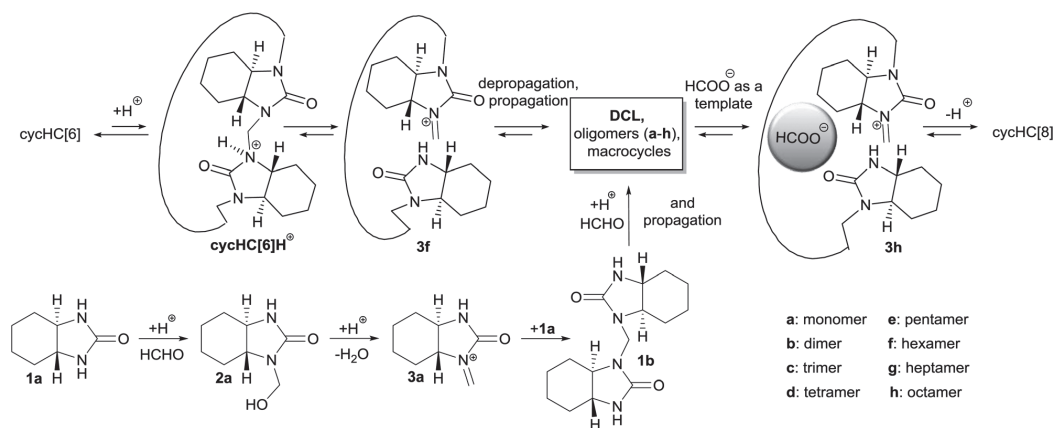
The kinetic data for the conversion of cycHC[6] to cycHC[8] revealed that the overall reaction was pseudo first-order, with a plateau. The fact, that the transformation of cycHC[6] to cycHC[8] proceeds faster in stronger acids (Table 1, compare entries 1 and 2) in combination with the results from DFT computational study of model structures (S29, ESI[†]) allows us to state, that the rate-limiting step of this process is protonation of the macrocycle. Occurrence of side reactions was minimal and no intermediates were detected by NMR (S16, ESI[†]).

Pittelkow *et al.* have shown that dimers are the main intermediates in the formation of biotin[6]uril.^{8f} Also, since cycHC[6] and cycHC[8] differ from each other by a dimer unit, we wanted to examine whether the cycHC[8] formation proceeds *via* dimer addition. We thus introduced ¹³C labels to methylene bridges of cycHC[6]^{8c} and subsequently used a 1:1 mixture of ¹³C-labelled and non-labelled cycHC[6] in cycHC[8] synthesis. The number of ¹³C-labelled methylene groups in isolated cycHC[8] varied from 0 to 8, following a normal distribution, thus confirming that beside dimers, other oligomers or monomers are involved in the reaction (S7, ESI[†]).

HRMS analysis of the reaction mixture showed the presence of cycHC[6–10]¹² and various oligomers (up to an octamer, S14, ESI[†]). The large number of observed intermediates pointed to the presence of a dynamic combinatorial library (DCL).^{3b}

According to DFT-calculated Gibbs' energies of cycHCs it is not the cycle strain, but the inclusion complex with formate anions that induces a preference towards the formation of cycHC[8] (S27, ESI[†]). Based on the experimental observations described above and the energy calculations on a model system (S29, ESI[†]), we propose that the transformation of cycHC[6] to cycHC[8] proceeds through the key steps outlined in Scheme 1. First, a reaction rate-limiting protonation of cycHC[6] occurs, then breakage of the first methylene bridge of cycHC[6]H⁺ takes place, forming the iminium **3f**. The DCL, whose members have been observed by HRMS, is generated through depropagation and propagation reactions. A formate acts as an anionic template and shifts the thermodynamic equilibrium between DCL members towards the formation of cycHC[8].

To verify that an anionic template is necessary to drive the reaction towards the formation of cycHC, we selected an anion that possessed the size and shape suitable for the cavity of cycHC[8], the hexafluorophosphate, in combination with acetic acid. Acetic acid alone was shown not to facilitate the formation of cycHC[8] (S4, ESI[†]). As expected, in the presence of NaPF₆ in acetic acid/acetonitrile, cycHC[6] was efficiently converted to cycHC[8] (Table 1, entry 3). This observation confirmed that even though reaction rate depends on the acid strength, the macrocycle formation is controlled by the anion, acting as a template.

**Scheme 1** Proposed reaction mechanism of the cycHC[8] formation catalysed by formic acid.

And with catalysis of formic and trifluoroacetic acid, their conjugate anions act as templates (Table 1, entries 1 and 2).

Next, based on the proposed mechanism, we envisioned that the DCL members could be generated starting from monomers **1a**. Indeed, using either formic acid, trifluoroacetic acid, or NaPF_6 /acetic acid as catalysts afforded cycHC[8] (Table 1, entries 4–6). The lower rate of formation of cycHC[8] from **1a** than from cycHC[6], was due to the additional acid-promoted reactions necessary for building methylene bridges. The best yield and selectivity were achieved with trifluoroacetic acid, giving the cycHC[8] from **1a** on a gram scale in 73% yield. This synthetic method allowed for the preparation of enantiopure chiral macrocycle cycHC[8] very efficiently, in only two steps, starting from commercially available 1,2-cyclohexanediamine.¹³

According to the proposed mechanism, the conversion of cycHC[8] to cycHC[6] in the presence of a halide template, should also be possible. Indeed, using the classic conditions of CB formation (Table 1, entry 8), cycHC[8] was efficiently converted to cycHC[6] with the aid of the chloride anion. Similarly, using NaCl as a templating additive in acetic acid at elevated temperature, cycHC[8] was also converted to cycHC[6] (Table 1, entry 9), again highlighting the role of the templating anion in the reaction.

The crystal structure confirmed the barrel-like shape of cycHC[8] (Fig. 2). According to the crystal structure, the cavity of cycHC[8], similar in size to that of CB[6], is of sufficient size for the encapsulation of a number of organic and inorganic guests (Table 2).

Complexation studies of the cycHC[8] with carboxylic acids were performed by diffusion NMR in CDCl_3 . The comparative results of the complexation of cycHC[6] and cycHC[8] are presented in Table 3. The association constants of simple carboxylic acids – acetic, formic and trifluoroacetic acids – follow the order of their acidity (Table 3, entries 1–3) for both hosts.

Analogously to small carboxylic acids, complexation with the more acidic α -methoxy- α -trifluoromethylphenylacetic acid (MTPA) was stronger than with α -methoxyphenylacetic acid (MPA) (Table 3, entries 5 and 6). The opposite preference of complexation of *R*-handed cycHC[6] and cycHC[8] toward MPA enantiomers may suggest different geometries of complexes in these cases. Nevertheless *R*-handed cycHC[8] showed nearly double affinity for *S*-MPA, compared to the *R*-MPA. This result confirms that cycHC[8] forms complexes enantioselectively.

In conclusion, we have presented the first highly efficient synthesis of an 8-membered representative of the cucurbituril family, the (all-*R*)-cyclohexylhemicucurbit[8]uril. We have shown that the reversibility of

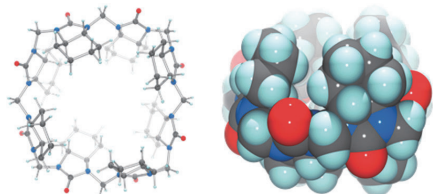


Fig. 2 Crystal structure of cycHC[8]: top view in ball and stick (left) and side view in CPK (right) representations (colour code: C grey, N blue, O red, H turquoise).

Table 2 Dimensions of cycHC[6,8] and CB[6,8]

Parameters ^a	CycHC[6] ^b	CycHC[8]	CB[6] ^c	CB[8] ^c
Opening diameter (Å)	2.2	4.6	3.9	6.9
Cavity diameter (Å)	5.3	8.5	5.8	8.8
Height (Å)	12.1	12.5	9.1	9.1
Cavity volume (Å ³)	35 ^d	123 ^d	119 ± 21	356 ± 16

^a Dimensions account for the van der Waals radii of the various atoms.

^b Opening, cavity and height values are from ref. 14a and cavity volume from ref. 14b.

^c Opening, cavity and height values are from ref. 8c and cavity volume from ref. 14b.

^d Cavity volume of cycHC[6] from ref. 8c and cycHC[8] calculated by analysing the solvent accessible voids in the respective crystal structures using PLATON¹⁵ with a probe radius of 1.2 Å³ and grid steps of 0.2 Å.

Table 3 Association constants K_a (M^{-1}) of carboxylic acids with cycHC[6] and cycHC[8] in 1:1 mixtures in CDCl_3

No.	Guest	CycHC[6] K_a	CycHC[8] K_a
1	CH_3COOH	8.0 ± 0.5^a	17 ± 2
2	HCOOH	97 ± 1	72.6 ± 0.5
3	CF_3COOH	$21(\pm 3) \times 10^3$	$29(\pm 1) \times 10^3$
4	<i>R</i> -MPA	27.2 ± 0.8^a	27.0 ± 0.5
5	<i>S</i> -MPA	20.1 ± 0.2^a	53 ± 3
6	<i>R</i> -MTPA	n.d.	$3.3(\pm 0.1) \times 10^2$
7	<i>S</i> -MTPA	n.d.	$3.0(\pm 0.1) \times 10^2$

^a Association constants from ref. 8c; n.d. - not determined.

the methylene bridge formation allows the size of the cycHC macrocycles to be controlled by the anionic templates, with halides driving the equilibrium towards the formation of cycHC[6], while carboxylates and PF_6^- promoted the formation of cycHC[8].

Chiral cycHC[8] and cycHC[6] were obtained very efficiently in one step, starting from enantiomerically pure (*R,R,N,N'*)-cyclohex-1,2-diyurea **1a** or either homologue. (all-*R*)-cycHC[8] enantioselectively formed complexes with chiral carboxylic acids, demonstrating chiral discrimination ability. CycHC[8] shows potential for application in host-guest chemistry.^{9g,10,16}

In the present study, DCL members were formed from identical monomeric units. It can be envisioned that by utilizing a mixture of different monomeric ureas and suitable templates, a very efficient yet diverse library of useful hemicucurbituril hosts could become accessible *via* dynamic covalent chemistry.

The authors would like to thank Tiina Aid, Marina Kudrjašova and Jasper Adamson for experimental assistance and Aivar Lõokene, Mart Reimund and Omar Parve for help with the manuscript. This research was supported by the Academy of Finland (KR, grants 263256 and 265328), the Estonian Ministry of Education and Research through Grants IUT19-32, IUT19-9, IUT23-7 and PUT692, TUT grant no. B25, the ESF DoRa, and the EU European Regional Development Fund (3.2.0101.08-0017). Computations were performed on the HPC cluster at TUT, which is part of the ETAIS. FT acknowledges support from NGS-NANO through a PhD fellowship.

Notes and references

- (a) X. Ma and Y. Zhao, *Chem. Rev.*, 2015, DOI: 10.1021/cr500392w;
- (b) Special Issue: Responsive Host-Guest Systems, *Acc. Chem. Res.*, 2014, 47, 1923; (c) G. Ghale and W. M. Nau, *Acc. Chem. Res.*, 2014, 47, 2150; (d) J. Hu and S. Liu, *Acc. Chem. Res.*, 2014, 47, 2084.

- 2 (a) C. J. Pedersen, *Angew. Chem., Int. Ed. Engl.*, 1988, **27**, 1021; (b) J.-M. Lehn, *Angew. Chem., Int. Ed. Engl.*, 1988, **27**, 89; (c) D. J. Cram, *Angew. Chem., Int. Ed. Engl.*, 1988, **27**, 1009; (d) J.-M. Lehn, *Angew. Chem., Int. Ed.*, 2013, **52**, 2836.
- 3 (a) J.-M. Lehn, *Chem. – Eur. J.*, 1999, **5**, 2455; (b) S. J. Rowan, S. J. Cantrill, G. R. L. Cousins, J. K. M. Sanders and J. F. Stoddart, *Angew. Chem., Int. Ed.*, 2002, **41**, 898; (c) P. T. Corbett, J. Leclaire, L. Vial, K. R. West, J. L. Wietor, J. K. M. Sanders and S. Otto, *Chem. Rev.*, 2006, **106**, 3652; (d) Y. Jin, C. Yu, R. J. Denman and W. Zhang, *Chem. Soc. Rev.*, 2013, **42**, 6634; (e) Y. Jin, Q. Wang, P. Taynton and W. Zhang, *Acc. Chem. Res.*, 2014, **47**, 1575; (f) A. Herrmann, *Chem. Soc. Rev.*, 2014, **43**, 1899; (g) M. Matache, E. Bogdan and N. D. Hádade, *Chem. – Eur. J.*, 2014, **20**, 2106.
- 4 (a) E. Masson, X. Ling, R. Joseph, L. Kyeremeh-Mensah and X. Lu, *RSC Adv.*, 2012, **2**, 1213; (b) K. I. Assaf and W. M. Nau, *Chem. Soc. Rev.*, 2015, **44**, 394.
- 5 (a) R. Oun, R. S. Floriano, L. Isaacs, E. G. Rowan and N. J. Wheate, *Toxicol. Res.*, 2014, **3**, 447; (b) U. Hoffmann, M. Grosse-Sundrup, K. Eikermann-Haerter, S. Zaremba, C. Ayata, B. Zhang, D. Ma, L. Isaacs and M. Eikermann, *Anesthesiology*, 2013, **119**, 317; (c) V. D. Uzunova, C. Cullinane, K. Brix, W. M. Nau and A. I. Day, *Org. Biomol. Chem.*, 2010, **8**, 2037.
- 6 (a) S. Walker, R. Oun, F. J. McInnes and N. J. Wheate, *Isr. J. Chem.*, 2011, **51**, 616; (b) A. I. Day and J. G. Collins, Cucurbituril receptors and drug delivery, in *Supramolecular Chemistry: From Molecules to Nanomaterials*, ed. J. W. Steed and P. A. Gale, John Wiley & Sons, Ltd, 2012, vol. 3, p. 983; (c) L. Peng, A. Feng, M. Huo and J. Yuan, *Chem. Commun.*, 2014, **50**, 13005; (d) V. Mandadapu, A. I. Day and A. Ghanem, *Chirality*, 2014, **26**, 712; (e) A. A. Elbashir and H. Y. Aboul-Enein, *Crit. Rev. Anal. Chem.*, 2015, **45**, 52; (f) S. Gürbüz, M. Idrisa and D. Tuncel, *Org. Biomol. Chem.*, 2015, **13**, 330.
- 7 (a) A. Day, A. P. Arnold, R. J. Blanch and B. Snusball, *J. Org. Chem.*, 2001, **66**, 8094; (b) A. Chakraborty, A. Wu, D. Witt, J. Lagona, J. C. Fettinger and L. Isaacs, *J. Am. Chem. Soc.*, 2002, **124**, 8297; (c) W.-H. Huang, P. Y. Zavalij and L. Isaacs, *J. Am. Chem. Soc.*, 2008, **130**, 8446; (d) L. Isaacs, *Chem. Commun.*, 2009, 619; (e) L. Isaacs, *Isr. J. Chem.*, 2011, **51**, 578; (f) D. Lucas, T. Minami, G. Iannuzzi, L. Cao, J. B. Wittenberg, P. Anzenbacher Jr. and L. Isaacs, *J. Am. Chem. Soc.*, 2011, **133**, 17966.
- 8 (a) Y. Miyahara, K. Goto, M. Oka and T. Inazu, *Angew. Chem., Int. Ed.*, 2004, **43**, 5019; (b) Y. Li, L. Li, Y. Zhu, X. Meng and A. Wu, *Cryst. Growth Des.*, 2009, **9**, 4255; (c) R. Aav, E. Shmatova, I. Reile, M. Borissova, F. Topić and K. Rissanen, *Org. Lett.*, 2013, **15**, 3786; (d) T. Fiala and V. Sindelar, *Synlett*, 2013, 2443; (e) M. Fomitsenko, E. Shmatova, M. Ören, I. Järving and R. Aav, *Supramol. Chem.*, 2014, **26**, 698; (f) M. Lisbjerg, B. M. Jessen, B. Rasmussen, B. Nielsen, A. U. Madsen and M. Pittelkow, *Chem. Sci.*, 2014, **5**, 2647.
- 9 (a) For anion binding of hemicucurbiturils see ref. 8 and H.-J. Buschmann, E. Cleva and E. Schollmeyer, *Inorg. Chem. Commun.*, 2005, **8**, 125; (b) H.-J. Buschmann, A. Zielesny and E. Schollmeyer, *J. Inclusion Phenom. Macrocyclic Chem.*, 2006, **54**, 181; (c) M. Sundararajan, R. V. Solomon, S. K. Ghosh and P. Venunalingam, *RSC Adv.*, 2011, **1**, 1333; (d) H.-J. Buschmann and A. Zielesny, *Comput. Theor. Chem.*, 2013, **1022**, 14; (e) M. Ören, E. Shmatova, T. Tamm and R. Aav, *Phys. Chem. Chem. Phys.*, 2014, **16**, 19198; (f) A. M. Lisbjerg, B. E. Nielsen, B. O. Milhøj, S. P. A. Sauer and M. Pittelkow, *Org. Biomol. Chem.*, 2015, **13**, 369; (g) M. Lisbjerg, H. Valkenier, B. M. Jessen, H. Al-Kerdi, A. P. Davis and M. Pittelkow, *J. Am. Chem. Soc.*, 2015, **137**, 4948.
- 10 (a) H. Cong, T. Yamato and X. Feng, *J. Mol. Catal. A: Chem.*, 2012, **181**; (b) H. Cong, T. Yamato and Z. Tao, *J. Mol. Catal. A: Chem.*, 2013, **287**; (c) H. Cong, T. Yamato and Z. Tao, *New J. Chem.*, 2013, **37**, 3778.
- 11 (a) J. Svec, M. Necas and V. Sindelar, *Angew. Chem., Int. Ed.*, 2010, **49**, 2378; (b) V. Havel, J. Svec, M. Wimmerova, M. Dusek, M. Pojarova and V. Sindelar, *Org. Lett.*, 2011, **13**, 4000; (c) J. Rivollier, P. Thuéry and M.-P. Heck, *Org. Lett.*, 2013, **15**, 480; (d) M. A. Yawer, V. Havel and V. Sindelar, *Angew. Chem., Int. Ed.*, 2015, **54**, 276; (e) M. Singh, E. Solel, E. Keinan and O. Reany, *Chem. – Eur. J.*, 2015, **21**, 536.
- 12 ref. 8e and ESI† for detailed MS data.
- 13 (a) Enantiopure 1,2-cyclohexanediamine can also be isolated from racemic mixture: J. F. Larrow, E. N. Jacobsen, Y. Gao, Y. Hong, X. Nie and C. M. Zepp, *J. Org. Chem.*, 1994, **59**, 1939; (b) J. F. Larrow and E. N. Jacobsen, *Org. Syn., Coll.*, 2004, **10**, 96.
- 14 (a) J. Kim, I.-S. Jung, S.-Y. Kim, E. Lee, J.-K. Kang, S. Sakamoto, K. Yamaguchi and K. Kim, *J. Am. Chem. Soc.*, 2000, **122**, 540; (b) W. M. Nau, M. Florea and K. I. Assaf, *Isr. J. Chem.*, 2011, **51**, 559.
- 15 A. L. Spek, *Acta Crystallogr.*, 2009, **D65**, 148.
- 16 (a) P. A. Gale, *Acc. Chem. Res.*, 2011, **44**, 216; (b) J. Lacour and D. Moraleda, *Chem. Commun.*, 2009, 7073; (c) R. J. Phipps, G. L. Hamilton and F. D. Toste, *Nat. Chem.*, 2012, **4**, 603; (d) K. Wichmann, B. Antonioli, T. Söhnel, M. Wenzel, K. Gloe, K. Gloe, J. R. Price, L. F. Lindoy, A. J. Blake and M. Schröder, *Coord. Chem. Rev.*, 2006, **250**, 2987; (e) T. J. Wenzel, *J. Inclusion Phenom. Macrocyclic Chem.*, 2014, **78**, 1.

Reprinted with permission from Royal Society of Chemistry

Part of Supporting Info of Publication III

E. Prigorchenko, M. Öeren, S. Kaabel, M. Fomitšenko, I. Reile, I. Järving, T. Tamm, F. Topić, K. Rissanen and R. Aav “Template-controlled synthesis of chiral cyclohexylhemicucurbit[8]uril” *Chem. Comm.*, 2015, 51, 10921–10924.

Table S8. Diffusion coefficients of the free and bound guest molecules and association constants with cycHC[6]

Guest	D_{free} ($10^{-10} \text{ m}^2\text{s}^{-1}$)	D_{obs} ($10^{-10} \text{ m}^2\text{s}^{-1}$)	D_1, D_{bound} ($10^{-10} \text{ m}^2\text{s}^{-1}$)	p	K_{as} M^{-1}
HCOOH	23.11 (± 0.03)	12.47 (± 0.02)	5.00 (± 0.06)	0.53 (± 0.01)	353 (± 3)
^a CF ₃ COOH	19.0 (± 0.1)	14.99 (± 0.1)	16.07 (± 0.07)	0,92	21 (± 3) $\times 10^3$

^a See comment under Table S7.

7 Computational details

7.1 Equilibrium between cycHC[6] and cycHC[8]

The equilibrium between cycHC[6] and cycHC[8] was studied by evaluating the equilibrium constant (K_{eq}) from experimental data (page S18) and computationally. It is suggested that the equilibrium is thermodynamically controlled due to the broad spectrum of observed oligomers during the transformation reaction. Despite the large number, there were no prevailing oligomers in the reaction mixture, thus it is presumed that the equilibria between intermediates do not dictate the equilibrium between cycHC[6] and cycHC[8]. The Jacobson–Stockmayer theory states that the macrocycles produced under thermodynamic control are strainless¹³ and their desired size is obtained by the aid of template molecules.¹⁴ We have shown previously that the formate anion can be encapsulated inside cycHC[6] and the formic acid can be bound outside of cycHC[6].¹⁵ To study whether the encapsulation drives the reaction towards cycHC[8], density functional theory calculations were used.

Geometry optimizations for local minima were carried out using the dispersion corrected B97-D functional,¹⁶ along with the def2-SV(P)¹⁷ basis set. Vibrational analysis was performed to ensure that all chosen geometries were at local minima. Additionally a single point calculation at the B97-D¹⁶/def2-TZVPD¹⁷ level of theory was performed for every stationary point, with inclusion of the solvation model COSMO ($\epsilon = 51,1$ – formic acid), to refine the energies. The total energies were calculated using the single point energies from the solvent phase calculation and adding the Gibbs free energy correction from the vibrational part of the gas phase calculation¹⁸. Gibbs free energy was estimated using the temperature 293.15 K and the pressure 0.1 MPa. The calculations were performed using the program package Turbomole 6.5.¹⁹

Complexation studies (Table 3 from the main text) have shown that cycHC[8] acts as a host for carboxylic acids. According to DFT calculations, the guest location preferences for cycHC[8] remained the same as for cycHC[6]¹⁵. Therefore the theoretical ΔG was calculated for a reaction involving inclusion complex with the formate anion,



The computationally derived ΔG is -177 kJ/mol in favour of cycHC[8], indicating that the complexation with formate anion induces a preference towards the formation of cycHC[8]. The calculation gives a qualitative explanation for the equilibrium preference of the system. Based on these findings, it can be proposed that complexation with formate anion may govern

the overall equilibrium between the 6- and 8-membered cycHCs and drive the aforementioned reaction towards the formation of cycHC[8].

Table S9. Calculated energies (in Hartrees) of the studied geometries.

Name	Energy	Gibbs Corr.	Total
cycHC[6]	-2980.157550 ^a	1.109313	-2979.048237
HCOO ⁻ @cycHC[6]	-3169.461130 ^b	1.127793	-3168.333337
[HCOOH+cycHC[6]]	-3169.948819 ^b	1.137799	-3168.811021
cycHC[8]	-3973.535695 ^a	1.474656	-3972.061039
HCOO ⁻ @cycHC[8]	-4162.866502 ^b	1.495944	-4161.370558
HCOO ⁻ @cycHC[8]	-4162.788348 ^a	1.495944	-4161.292404
[HCOO ⁻ +cycHC[8]]	-4162.748669 ^a	1.491423	-4161.257246
HCOOH@cycHC[8]	-4163.339071 ^b	1.507781	-4161.831289
HCOOH@cycHC[8]	-4163.292729 ^a	1.507781	-4161.784948
[HCOOH+cycHC[8]]	-4163.289851 ^a	1.503302	-4161.786549
HCOO ⁻	-189.284877 ^b	-0.004220	-189.289100

^a – calculated energies are in gas phase due to unsuitability of the continuum model for the guest-less cavity

^b – COSMO solvation model is included

The energy differences of cycHC[6] and cycHC[8] per monomer were compared to confirm that the Jacobson–Stockmayer theory applies. The difference of ΔG s is 1 kJ/mol in favour of cycHC[6] affirms that both macrocycles are strainless. Formic acid favours to be bound outside the cycHC[8] by 4 kJ/mol as can be seen on Figure S17. Formate anion favours to be bound inside the cycHC[8] by 92 kJ/mol.

The results do not include a basis set superposition error (BSSE) correction due to incompatibility between the continuum solvation model (COSMO) and the counterpoise (CP) approach to BSSE correction. In the CP workflow, COSMO energies of fragments with different cavities would be added, which would lead to physically meaningless results.

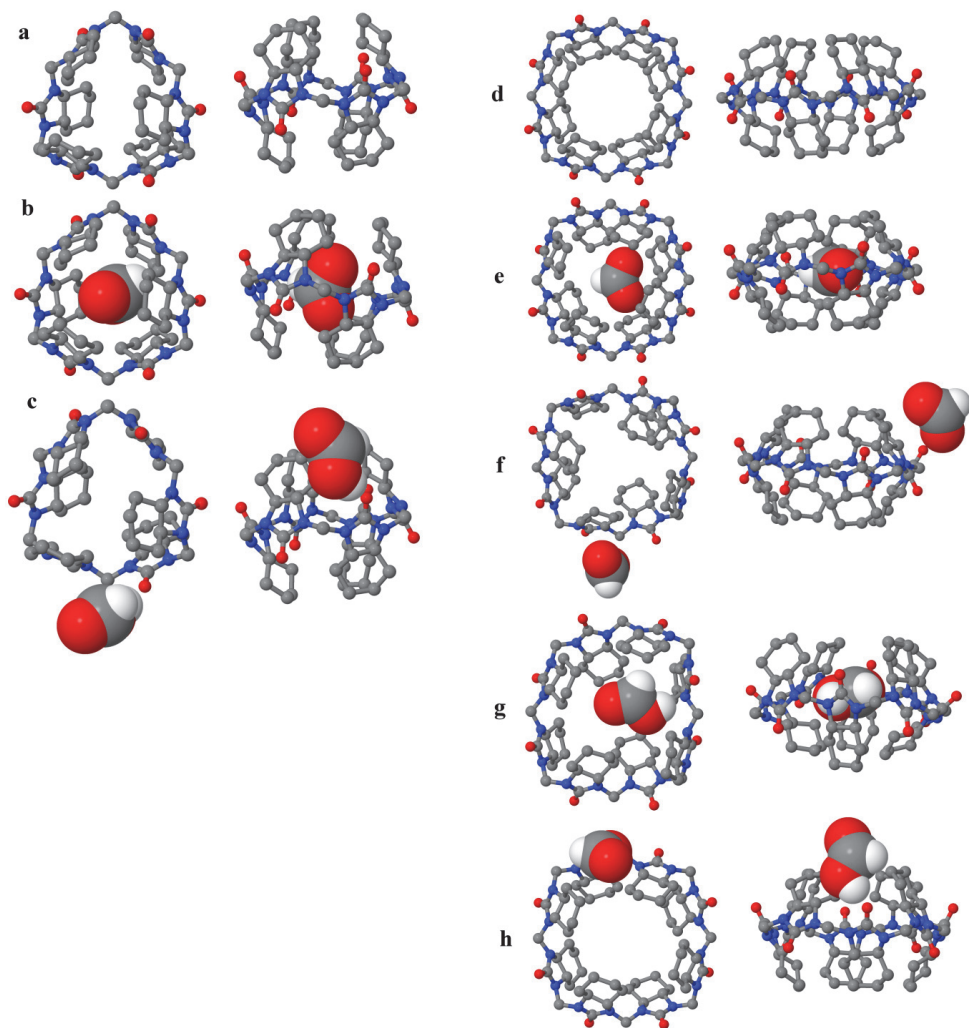


Figure S17. Geometries used in equilibrium calculations: a) cycHC[6], b) $\text{HCOO}^-@\text{cycHC}[6]$ (the anion bound outside the cycHC[6] is unfavoured – ref 15), c) $[\text{HCOOH}+\text{cycHC}[6]]$ (the formic acid bound inside the cycHC[6] is unfavoured – ref 15), d) cycHC[8], e) $\text{HCOO}^-@\text{cycHC}[8]$, f) $[\text{HCOO}^-@\text{cycHC}[8]]$, g) $\text{HCOOH}@\text{cycHC}[8]$ and h) $[\text{HCOOH}+\text{cycHC}[8]]$. Image was created using Jmol²⁰.

7.2 Equilibrium between cycHC[6] and cycHC[8]

To gain detailed insight into the reaction pathways of the transformation of cycHC[6] to cycHC[8], a computational study with model structures was performed. Irrespective of the vast number of possible reaction routes leading to the transformation of cycHC[6] to cycHC[8], they can be conceptually reduced to two basic steps: chain depropagation and chain propagation.

Because of its high efficiency, the density functional BP86²¹ in combination with the def2-SV(P)¹⁷ basis set was used to model the reaction pathways. Vibrational analysis was performed to ensure that all chosen geometries were at local minima or at first order saddle points, as appropriate. The transition states were verified using intrinsic reaction coordinate calculations. To refine the energies, a single point calculation at the B97-D/def2-TZVPD^{16,17} level of theory was performed for every stationary point, with inclusion of the solvation model COSMO ($\epsilon = 51,1$ – formic acid). The total energies were calculated using the single point energies from the solvent phase calculation and adding the Gibbs free energy correction from vibrational part of the gas phase calculation¹⁸. Gibbs free energy was estimated using the temperature 293.15 K and the pressure 0.1 MPa. The calculations were performed using the program package Turbomole 6.5.¹⁹

Figure S18 shows the relative energies and structures of the intermediates and transition states in the depropagation and propagation reaction. Due to the zig-zag orientation of the monomers in a macrocycle, there are two different types of methylene bridges and thus four different locations for the proton in cycHC[n] + H⁺. As we have shown in our previous work¹⁵, the protonation from inside of the macrocycle is energetically most favoured.¹⁵ The geometry of the dimer **1bH**⁺, protonated at the position corresponding to the inner protonation site, was chosen as starting geometry for computational depropagation and propagation studies. After the protonation, the chain depropagation can advance through two different reaction paths, differentiated on the reaction coordinate diagram in Figure S18 by continuous and dotted lines, respectively. The dissociation of the C–N bond (**TS2a** – continuous line) has lower transition state energy (64 kJ/mol) compared to substitution reaction (80 kJ/mol) (**TS2b** – dotted line). The product of dissociation is an iminium cation **3a**, which can be attacked by a formate anion, yielding the formyl-terminated **4a**. The second possible reaction path involves a nucleophilic attack on the methylene bridge by the formate (**TS2b** – dotted line). The energy of transition state of this substitution reaction is higher and the reaction path produces the formyl compound **4a** directly. Considering that the substitution reaction is energetically more demanding, one can suppose that the formation of formylated compounds proceeds through the iminium ion **3a**. All reactions can proceed also in the reverse direction, starting from the right hand side of the energy diagram (Figure S18). In addition, compound **4a** can be converted to iminium **3a** through protonation of the formyl group and subsequent fragmentation where formic acid leaves.

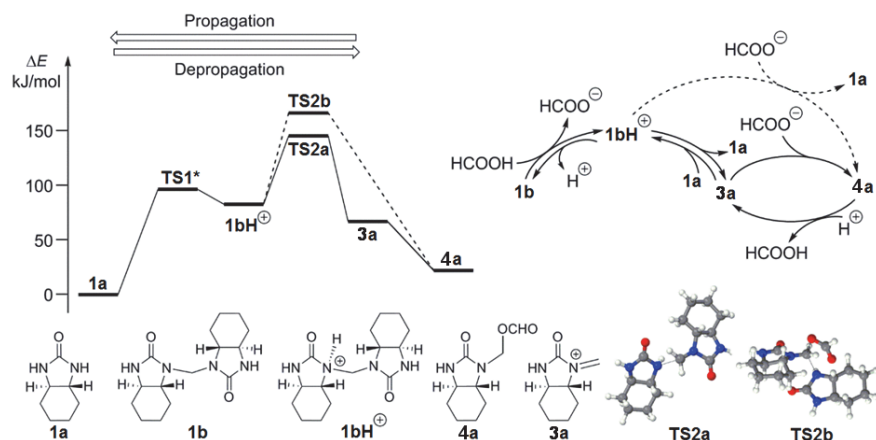


Figure S18. Propagation and depropagation reaction coordinate of the model structures.

Table S10. Calculated energies for the model system. Energies are in Hartrees (except for the last column which has the relative energies in kJ/mol).

Name	Energy	Gibbs correction	Total energy	Energy difference
1b	-955.298024	0.340361	-954.957662	0
TS1	-	-	-	96*
1bH⁺	-955.728298	0.352470	-955.375828	85
TS2a	-955.709673	0.349975	-955.359698	149
TS2b	-1145.006708	0.366083	-1144.640625	165
3a	-497.104069	0.171000	-496.933069	66
4a	-686.430878	0.191754	-686.239124	22

* - Energy obtained using the Eyring equation

Eyring equation

$$\Delta G = - \ln \left(\frac{kh}{k_B T} \right) RT$$

ΔG – Gibbs free energy

k – reaction rate constant ($5 \cdot 10^{-5} \text{ s}^{-1}$)

h – Planck's constant

k_B – Boltzmann constant

T – Temperature (293.15 K)

R – Gas Constant

Abstract

Cyclohexylhemicucurbiturils belong in the cucurbituril family and are suitable hosts for various molecules and ions. Cyclohexylhemicucurbiturils are composed of (*R,R,N,N'*)-cyclohex-1,2-diylurea monomers which are linked together by methylene bridges. Due to their “zig-zag” placement of the monomeric units they have the lowest unoccupied molecular orbital inside their cavity and thus prefer inclusion complexes with anionic guests. To isolate new homologues of cyclohexylhemicucurbiturils, a thorough study of complexation properties of cyclohexylhemicucurbiturils, cavities of cyclohexylhemicucurbiturils and the reversible macrocyclization from one homologue to another was conducted.

The studies of cyclohexylhemicucurbit[6]uril and its complexes showed that the anions (Cl^- , Br^- , I^- and HCOO^-) and the proton form inclusion complexes with the macrocycle. Non-dissociated acids (HCl, HBr, HI, HCOOH) preferred to be bound outside of the macrocycle. The order of binding preference of the studied anions was: $\text{Cl}^- > \text{Br}^- > \text{HCOO}^- > \text{I}^-$. In addition to the binding energy, the Quantum Theory of Atoms in Molecules showed interactions between anionic guests and cyclohexylhemicucurbit[6]uril (twelve interactions for Cl^- , Br^- and I^- and fourteen interactions HCOO^-). The strength of all interactions between the host and the guest is comparable to a couple of hydrogen bonds.

The studies of cyclohexylhemicucurbituril homologues (with the number of monomeric units of 6, 7, 8, 9 and 10) yielded images of the geometries, cavities and molecular orbitals of the homologues. While the six-, eight-, and ten-membered homologues barrel-shaped with equal dimensions of the openings, the seven and nine membered homologues were somewhat barrel-shaped with unequal dimensions of the openings. The six- and eight-membered homologues were energetically favoured, while the ten-membered homologue was energetically the least favoured.

The conversion mechanism from one homologue to another was studied using a simplified model system. When the cyclohexylhemicucurbituril is protonated, the methylene bridge breaks, this generates a linear intermediate. Through a series of analogous reactions, a dynamic combinatorial library is created from the intermediates which can be combined to form other homologues. The desired guest size is achieved through choice of the right template.

Kokkuvõte

Käesolevas doktoritöös uuritakse molekule, mis on võimelised enda sisse püüdma väiksemaid molekule (või ioone), moodustades külaline-võõrustaja komplekse ehk suluühendeid. Suluühendite moodustumine ei ole juhuslik ning sõltub külalise ning võõrustaja kujust ning nende vahelistest interaktsioonidest. Neid omadusi ära kasutades on võimalik disainida võõrustaja, mis moodustab suluühendeid vaid meid huvitavate molekulidega (või ioonidega). Võõrustajad on kasutuses erinevates valdkondades – toidutööstuses, keemilise sünteesi laborites, ravimitööstuses, jne. Võõrustajate lai kasutusala illustreerib nende tarvilikust meie igapäevaelus ning põhjendab vajadust inimkonna teadmisi selles valdkonnas laiendada.

Doktoritöö uurimisobjektiks on võõrustaja nimega tsükloheksüülhemikukurbituriil (cycHC). Esimene cycHC süntees avaldati aastal 2013 Riina Aava ning kaastöötajate poolt. Sünteesitud molekul koosnes kuue ühikulisest tsüklist, mis on omavahel ühendatud metüleensildade abil. Hilisemalt on sünteesitud ka kaheksa ühikuline cycHC. Et molekule omavahel eristada, märgitakse molekuli nimes ära ühikute arv: tsükloheksüülhemikukurbit[n]uriil (cycHC[n]), kus $n = 6, 8$. Lisaks on tuvastatud ka 7-, 9- ja 10 ühikuga molekule.

Käesoleva uurimustöö eesmärk oli uurida cycHC[n]-ide elektronstruktuuri, õõnsuseid, suluühendeid ning moodustumise reaktsiooni, kasutades arvutuskeemiat. Töö tähtsamad tulemused on:

- CycHC[6]-d moodustavasid suluühendeid anioonidega (Cl^- , Br^- , I^- ja HCOO^-) või liidavad enda sisse prootoni (H^+);
- Komplekseerumata kujul olid kõige stabiilsemad cycHC-d, kus oli 6 või 8 monomeeri. Kümne monomeeriga cycHC oli kõige ebastabiilsem (cycHC[6] > cycHC[8] > cycHC[7] = cycHC[9] > cycHC[10]);
- Lisades sünteesi keskkonda sobiva suurusega külalise, saab tekkiva cycHC ühikute arvu reguleerida;
- Happelistes tingimustes on võimalik lõhkuda cycHC[n]-i metüleensillad ning kasutades sobiva suurusega külalist on võimalik näiteks kuue monomeeriga cycHC-st sünteesida kaheksa monomeeriga cycHC.

Lisaks kirjeldati kõigi tsükloheksüülhemikukurbit[n]uriilide ($n = 6, 7, 8, 9, 10$) geomeetria, elektron-struktuuri ja õõnsuse kuju. Samuti kirjeldati uuritud suluühendite geomeetria ja elektronstruktuuri ning uuriti külalise ning võõrustaja vahelisi interaktsioone (interaktsioonide arv ning tugevus). Tehtud töö avardas teadmisi cycHC kohta ning võimaldab välja töötada selektiivsemaid võõrustajaid.

Acknowledgements

This work was conducted at the Department of Chemistry of Tallinn University of Technology. This work was financially supported by Estonian Science Foundation [grants 8255 and 8698], Tallinn University of Technology base financing [grant B25], the Ministry of Education and Research [grants IUT19-32, IUT19-9, IUT23-7 and PUT692], the EU European Regional Development Fund [grant 3.2.0101.08-0017] and the ESF DoRa. Computations were performed on the HPC cluster at Tallinn University of Technology, which is part of the ETAIS project.

I would like to thank my supervisor Associate Professor Toomas Tamm who introduced me to the world of quantum chemistry. I am grateful to him, because he has been supervising me for all these years I have been working in the scientific field. I also wish to thank Associate Professor Riina Aav who took me into her team and provided me with experimental input. I am grateful to Dr. Thomas Sandberg of Åbo Akademi (Finland) for reading the manuscript and providing many useful remarks. I would also like to thank my colleagues from the chairs of inorganic, organic and analytical chemistry, especially Dr. Merle Uudsemaa, who has been my close ally in doing science.

My sincere thanks go to my family and friends, especially my wife Mariliis, who has always motivated me and been by my side when I have drowned in work due to various deadlines.

Last but not least, I would like to thank my board game crew from the laboratory, with whom we spent countless evenings in the meeting room digging up resources from Mars, building cities in southern France, fighting for influence on Westeros, *etc.* The lingo from the games made their way into our everyday work and the conversations amongst us kept up my motivation and mood even if the calculations constantly failed.

Fus-Ro-Dah – Dovahkiin

Elulookirjeldus

1. Isikuandmed

Nimi Mario Öeren
Sünniaeg ja -koht 18.02.1987, Tallinn

2. Haridus

Tallinna Tehnikaülikool 2011 *MSc*
Tallinna Tehnikaülikool 2009 *BSc*
Tallinna Nõmme Gümnaasium 2006 keskharidus

3. Keelteoskus

Eesti keel kõrgtase
Inglise keel kõrgtase

4. Teenistuskäik

2009–2013 TTÜ, õppelabori assistant
2009–2012 Tallinna Nõmme Gümnaasium, keemiaõpetaja

5. Juhendatud lõputöö

2015 Viktoria Tisleri bakalaureuse töö,
kaitstud TTÜ-s

6. Teadustöö

Arvutuskeemiliste meetodite rakendamine molekulide geomeetria leidmisel, konformatsioonianalüüsil, vibratsiooniliste spektrite (IR, VCD) modelleerimisel ja reaktsioonimehhanismide modelleerimisel.

Curriculum Vitae

1. Personal Data

Name Mario Öeren
Date and place of birth 18.02.1987, Tallinn

2. Education

Tallinn University of Technology 2011 *MSc*
Tallinn University of Technology 2009 *BSc*
Tallinn Nõmme High School 2006 secondary education

3. Language competence

Estonian fluent
English fluent

4. Professional appointments

2009–2013 Department of Chemistry, TUT, teaching assistant
2009–2012 Tallinn Nõmme High School, Chemistry teacher

5. Supervised thesis

2015 Viktoria Tisler *BSc* thesis, defended in TUT

6. Scientific work

Using computational chemical methods for finding geometries of molecules; conformational analysis; modelling of vibrational spectra (IR and VCD); and modelling of reaction mechanisms.

Original publications

- 1) S. Žari, T. Kailas, M. Kudrjashova, M. Öeren, I. Järving, T. Tamm, M. Lopp and T. Kanger “Organocatalytic Asymmetric Addition of Malonates to Unsaturated 1,4-diketones” *Beilstein Journal of Organic Chemistry*, 2012, **8**, 145–1457.
- 2) A. Noole, M. Ošek, T. Pehk, M. Öeren, I. Järving, M. R. J. Elsegood, A. V. Malkov, M. Lopp and T. Kanger “3-Chlorooxindoles: Versatile Starting Materials for Asymmetric Organocatalytic Synthesis of Spirooxindoles” *Advanced Synthesis and Catalysis*, 2013, **355**, 829–835.
- 3) I. Osadchuk, T. Pehk, A. Paju, M. Lopp, M. Öeren and T. Tamm “Isomers and Conformers of Complexes of $Ti(OiPr)_4$ with Cyclopentane-1,2-Dione: NMR Study and DFT Calculations” *International Journal of Quantum Chemistry*, 2014, **114**, 1012–1018.
- 4) M. Ošek, A. Noole, S. Žari, M. Öeren, I. Järving, M. Lopp and T. Kanger “Asymmetric Diastereoselective Synthesis of Spirocyclopropane Derivatives of Oxindole” *European Journal of Organic Chemistry*, 2014, **17**, 3599–3606.
- 5) M. Fomitšenko, E. Shmatova, M. Öeren, I. Järving and R. Aav “New Homologues of Chiral Cyclohexylhemicurbit[*n*]urils” *Supramolecular Chemistry*, 2014, **26**, 698–703.
- 6) M. Öeren, E. Shmatova, T. Tamm and R. Aav “Computational and ion mobility MS study of (all-S)-cyclohexylhemicurbit[6]uril structure and complexes” *Physical Chemistry Chemical Physics*, 2014, **16**, 19198–19205.
- 7) E. Prigorchenko, M. Öeren, S. Kaabel, M. Fomitšenko, I. Reile, I. Järving, T. Tamm, F. Topić, K. Rissanen and R. Aav “Template Controlled Synthesis of Chiral Cyclohexylhemicurbit[8]uril” *Chemical Communications*, 2015, **51**, 10921–10924.

**DISSERTATIONS DEFENDED AT
TALLINN UNIVERSITY OF TECHNOLOGY ON
NATURAL AND EXACT SCIENCES**

1. **Olav Kongas**. Nonlinear Dynamics in Modeling Cardiac Arrhythmias. 1998.
2. **Kalju Vanatalu**. Optimization of Processes of Microbial Biosynthesis of Isotopically Labeled Biomolecules and Their Complexes. 1999.
3. **Ahto Buldas**. An Algebraic Approach to the Structure of Graphs. 1999.
4. **Monika Drews**. A Metabolic Study of Insect Cells in Batch and Continuous Culture: Application of Chemostat and Turbidostat to the Production of Recombinant Proteins. 1999.
5. **Eola Valdre**. Endothelial-Specific Regulation of Vessel Formation: Role of Receptor Tyrosine Kinases. 2000.
6. **Kalju Lott**. Doping and Defect Thermodynamic Equilibrium in ZnS. 2000.
7. **Reet Koljak**. Novel Fatty Acid Dioxygenases from the Corals *Plexaura homomalla* and *Gersemia fruticosa*. 2001.
8. **Anne Paju**. Asymmetric oxidation of Prochiral and Racemic Ketones by Using Sharpless Catalyst. 2001.
9. **Marko Vendelin**. Cardiac Mechanoenergetics *in silico*. 2001.
10. **Pearu Peterson**. Multi-Soliton Interactions and the Inverse Problem of Wave Crest. 2001.
11. **Anne Menert**. Microcalorimetry of Anaerobic Digestion. 2001.
12. **Toomas Tiivel**. The Role of the Mitochondrial Outer Membrane in *in vivo* Regulation of Respiration in Normal Heart and Skeletal Muscle Cell. 2002.
13. **Olle Hints**. Ordovician Scolecodonts of Estonia and Neighbouring Areas: Taxonomy, Distribution, Palaeoecology, and Application. 2002.
14. **Jaak Nõlvak**. Chitinozoan Biostratigraphy in the Ordovician of Baltoscandia. 2002.
15. **Liivi Kluge**. On Algebraic Structure of Pre-Operad. 2002.
16. **Jaanus Lass**. Biosignal Interpretation: Study of Cardiac Arrhythmias and Electromagnetic Field Effects on Human Nervous System. 2002.
17. **Janek Peterson**. Synthesis, Structural Characterization and Modification of PAMAM Dendrimers. 2002.
18. **Merike Vaher**. Room Temperature Ionic Liquids as Background Electrolyte Additives in Capillary Electrophoresis. 2002.
19. **Valdek Mikli**. Electron Microscopy and Image Analysis Study of Powdered Hardmetal Materials and Optoelectronic Thin Films. 2003.
20. **Mart Viljus**. The Microstructure and Properties of Fine-Grained Cermets. 2003.
21. **Signe Kask**. Identification and Characterization of Dairy-Related *Lactobacillus*. 2003
22. **Tiiu-Mai Laht**. Influence of Microstructure of the Curd on Enzymatic and Microbiological Processes in Swiss-Type Cheese. 2003.
23. **Anne Kuuskalu**. 2–5A Synthetase in the Marine Sponge *Geodia cydonium*. 2003.

24. **Sergei Bereznev**. Solar Cells Based on Polycrystalline Copper-Indium Chalcogenides and Conductive Polymers. 2003.
25. **Kadri Kriis**. Asymmetric Synthesis of C₂-Symmetric Bimorpholines and Their Application as Chiral Ligands in the Transfer Hydrogenation of Aromatic Ketones. 2004.
26. **Jekaterina Reut**. Polypyrrole Coatings on Conducting and Insulating Substrates. 2004.
27. **Sven Nömm**. Realization and Identification of Discrete-Time Nonlinear Systems. 2004.
28. **Olga Kijatkina**. Deposition of Copper Indium Disulphide Films by Chemical Spray Pyrolysis. 2004.
29. **Gert Tamberg**. On Sampling Operators Defined by Rogosinski, Hann and Blackman Windows. 2004.
30. **Monika Übner**. Interaction of Humic Substances with Metal Cations. 2004.
31. **Kaarel Adamberg**. Growth Characteristics of Non-Starter Lactic Acid Bacteria from Cheese. 2004.
32. **Imre Vallikivi**. Lipase-Catalysed Reactions of Prostaglandins. 2004.
33. **Merike Peld**. Substituted Apatites as Sorbents for Heavy Metals. 2005.
34. **Vitali Syritski**. Study of Synthesis and Redox Switching of Polypyrrole and Poly(3,4-ethylenedioxythiophene) by Using *in-situ* Techniques. 2004.
35. **Lee Põllumaa**. Evaluation of Ecotoxicological Effects Related to Oil Shale Industry. 2004.
36. **Riina Aav**. Synthesis of 9,11-Secosterols Intermediates. 2005.
37. **Andres Braunbrück**. Wave Interaction in Weakly Inhomogeneous Materials. 2005.
38. **Robert Kitt**. Generalised Scale-Invariance in Financial Time Series. 2005.
39. **Juss Pavelson**. Mesoscale Physical Processes and the Related Impact on the Summer Nutrient Fields and Phytoplankton Blooms in the Western Gulf of Finland. 2005.
40. **Olari Ilison**. Solitons and Solitary Waves in Media with Higher Order Dispersive and Nonlinear Effects. 2005.
41. **Maksim Säkki**. Intermittency and Long-Range Structurization of Heart Rate. 2005.
42. **Enli Kiipli**. Modelling Seawater Chemistry of the East Baltic Basin in the Late Ordovician–Early Silurian. 2005.
43. **Igor Golovtsov**. Modification of Conductive Properties and Processability of Polyparaphenylene, Polypyrrole and polyaniline. 2005.
44. **Katrin Laos**. Interaction Between Furcellaran and the Globular Proteins (Bovine Serum Albumin β -Lactoglobulin). 2005.
45. **Arvo Mere**. Structural and Electrical Properties of Spray Deposited Copper Indium Disulphide Films for Solar Cells. 2006.
46. **Sille Ehala**. Development and Application of Various On- and Off-Line Analytical Methods for the Analysis of Bioactive Compounds. 2006.
47. **Maria Kulp**. Capillary Electrophoretic Monitoring of Biochemical Reaction Kinetics. 2006.

48. **Anu Aaspõllu.** Proteinases from *Vipera lebetina* Snake Venom Affecting Hemostasis. 2006.
49. **Lyudmila Chekulayeva.** Photosensitized Inactivation of Tumor Cells by Porphyrins and Chlorins. 2006.
50. **Merle Uudsemaa.** Quantum-Chemical Modeling of Solvated First Row Transition Metal Ions. 2006.
51. **Tagli Pitsi.** Nutrition Situation of Pre-School Children in Estonia from 1995 to 2004. 2006.
52. **Angela Ivask.** Luminescent Recombinant Sensor Bacteria for the Analysis of Bioavailable Heavy Metals. 2006.
53. **Tiina Lõugas.** Study on Physico-Chemical Properties and Some Bioactive Compounds of Sea Buckthorn (*Hippophae rhamnoides* L.). 2006.
54. **Kaja Kasemets.** Effect of Changing Environmental Conditions on the Fermentative Growth of *Saccharomyces cerevisiae* S288C: Auxo-accelerostat Study. 2006.
55. **Ildar Nisamedtinov.** Application of ¹³C and Fluorescence Labeling in Metabolic Studies of *Saccharomyces* spp. 2006.
56. **Alar Leibak.** On Additive Generalisation of Voronoi's Theory of Perfect Forms over Algebraic Number Fields. 2006.
57. **Andri Jagomägi.** Photoluminescence of Chalcopyrite Tellurides. 2006.
58. **Tõnu Martma.** Application of Carbon Isotopes to the Study of the Ordovician and Silurian of the Baltic. 2006.
59. **Marit Kauk.** Chemical Composition of CuInSe₂ Monograin Powders for Solar Cell Application. 2006.
60. **Julia Kois.** Electrochemical Deposition of CuInSe₂ Thin Films for Photovoltaic Applications. 2006.
61. **Iiona Oja Açıık.** Sol-Gel Deposition of Titanium Dioxide Films. 2007.
62. **Tiia Anmann.** Integrated and Organized Cellular Bioenergetic Systems in Heart and Brain. 2007.
63. **Katrin Trummal.** Purification, Characterization and Specificity Studies of Metalloproteinases from *Vipera lebetina* Snake Venom. 2007.
64. **Gennadi Lessin.** Biochemical Definition of Coastal Zone Using Numerical Modeling and Measurement Data. 2007.
65. **Enno Pais.** Inverse problems to determine non-homogeneous degenerate memory kernels in heat flow. 2007.
66. **Maria Borissova.** Capillary Electrophoresis on Alkylimidazolium Salts. 2007.
67. **Karin Valmsen.** Prostaglandin Synthesis in the Coral *Plexaura homomalla*: Control of Prostaglandin Stereochemistry at Carbon 15 by Cyclooxygenases. 2007.
68. **Kristjan Piirimäe.** Long-Term Changes of Nutrient Fluxes in the Drainage Basin of the Gulf of Finland – Application of the PolFlow Model. 2007.
69. **Tatjana Dedova.** Chemical Spray Pyrolysis Deposition of Zinc Sulfide Thin Films and Zinc Oxide Nanostructured Layers. 2007.
70. **Katrin Tomson.** Production of Labelled Recombinant Proteins in Fed-Batch Systems in *Escherichia coli*. 2007.

71. **Cecilia Sarmiento**. Suppressors of RNA Silencing in Plants. 2008.
72. **Vilja Mardla**. Inhibition of Platelet Aggregation with Combination of Antiplatelet Agents. 2008.
73. **Maie Bachmann**. Effect of Modulated Microwave Radiation on Human Resting Electroencephalographic Signal. 2008.
74. **Dan Huvonen**. Terahertz Spectroscopy of Low-Dimensional Spin Systems. 2008.
75. **Ly Villo**. Stereoselective Chemoenzymatic Synthesis of Deoxy Sugar Esters Involving *Candida antarctica* Lipase B. 2008.
76. **Johan Anton**. Technology of Integrated Photoelasticity for Residual Stress Measurement in Glass Articles of Axisymmetric Shape. 2008.
77. **Olga Volobujeva**. SEM Study of Selenization of Different Thin Metallic Films. 2008.
78. **Artur Jõgi**. Synthesis of 4'-Substituted 2,3'-dideoxynucleoside Analogues. 2008.
79. **Mario Kadastik**. Doubly Charged Higgs Boson Decays and Implications on Neutrino Physics. 2008.
80. **Fernando Pérez-Caballero**. Carbon Aerogels from 5-Methylresorcinol-Formaldehyde Gels. 2008.
81. **Sirje Vaask**. The Comparability, Reproducibility and Validity of Estonian Food Consumption Surveys. 2008.
82. **Anna Menaker**. Electrosynthesized Conducting Polymers, Polypyrrole and Poly(3,4-ethylenedioxythiophene), for Molecular Imprinting. 2009.
83. **Lauri Ilison**. Solitons and Solitary Waves in Hierarchical Korteweg-de Vries Type Systems. 2009.
84. **Kaia Ernits**. Study of In₂S₃ and ZnS Thin Films Deposited by Ultrasonic Spray Pyrolysis and Chemical Deposition. 2009.
85. **Veljo Sinivee**. Portable Spectrometer for Ionizing Radiation "Gammamapper". 2009.
86. **Jüri Virkepu**. On Lagrange Formalism for Lie Theory and Operadic Harmonic Oscillator in Low Dimensions. 2009.
87. **Marko Piirsoo**. Deciphering Molecular Basis of Schwann Cell Development. 2009.
88. **Kati Helmja**. Determination of Phenolic Compounds and Their Antioxidative Capability in Plant Extracts. 2010.
89. **Merike Sõmera**. Sobemoviruses: Genomic Organization, Potential for Recombination and Necessity of P1 in Systemic Infection. 2010.
90. **Kristjan Laes**. Preparation and Impedance Spectroscopy of Hybrid Structures Based on CuIn₃Se₅ Photoabsorber. 2010.
91. **Kristin Lippur**. Asymmetric Synthesis of 2,2'-Bimorpholine and its 5,5'-Substituted Derivatives. 2010.
92. **Merike Luman**. Dialysis Dose and Nutrition Assessment by an Optical Method. 2010.
93. **Mihhail Berezovski**. Numerical Simulation of Wave Propagation in Heterogeneous and Microstructured Materials. 2010.
94. **Tamara Aid-Pavlidis**. Structure and Regulation of BDNF Gene. 2010.

95. **Olga Bragina**. The Role of Sonic Hedgehog Pathway in Neuro- and Tumorigenesis. 2010.
96. **Merle Randrüüt**. Wave Propagation in Microstructured Solids: Solitary and Periodic Waves. 2010.
97. **Marju Laars**. Asymmetric Organocatalytic Michael and Aldol Reactions Mediated by Cyclic Amines. 2010.
98. **Maarja Grossberg**. Optical Properties of Multinary Semiconductor Compounds for Photovoltaic Applications. 2010.
99. **Alla Maloverjan**. Vertebrate Homologues of Drosophila Fused Kinase and Their Role in Sonic Hedgehog Signalling Pathway. 2010.
100. **Priit Pruunsild**. Neuronal Activity-Dependent Transcription Factors and Regulation of Human *BDNF* Gene. 2010.
101. **Tatjana Knjazeva**. New Approaches in Capillary Electrophoresis for Separation and Study of Proteins. 2011.
102. **Atanas Katerski**. Chemical Composition of Sprayed Copper Indium Disulfide Films for Nanostructured Solar Cells. 2011.
103. **Kristi Timmo**. Formation of Properties of CuInSe_2 and $\text{Cu}_2\text{ZnSn}(\text{S},\text{Se})_4$ Monograin Powders Synthesized in Molten KI. 2011.
104. **Kert Tamm**. Wave Propagation and Interaction in Mindlin-Type Microstructured Solids: Numerical Simulation. 2011.
105. **Adrian Popp**. Ordovician Proetid Trilobites in Baltoscandia and Germany. 2011.
106. **Ove Pärn**. Sea Ice Deformation Events in the Gulf of Finland and This Impact on Shipping. 2011.
107. **Germo Väli**. Numerical Experiments on Matter Transport in the Baltic Sea. 2011.
108. **Andrus Seiman**. Point-of-Care Analyser Based on Capillary Electrophoresis. 2011.
109. **Olga Katargina**. Tick-Borne Pathogens Circulating in Estonia (Tick-Borne Encephalitis Virus, *Anaplasma phagocytophilum*, *Babesia* Species): Their Prevalence and Genetic Characterization. 2011.
110. **Ingrid Sumeri**. The Study of Probiotic Bacteria in Human Gastrointestinal Tract Simulator. 2011.
111. **Kairit Zovo**. Functional Characterization of Cellular Copper Proteome. 2011.
112. **Natalja Makarytsheva**. Analysis of Organic Species in Sediments and Soil by High Performance Separation Methods. 2011.
113. **Monika Mortimer**. Evaluation of the Biological Effects of Engineered Nanoparticles on Unicellular Pro- and Eukaryotic Organisms. 2011.
114. **Kersti Tepp**. Molecular System Bioenergetics of Cardiac Cells: Quantitative Analysis of Structure-Function Relationship. 2011.
115. **Anna-Liisa Peikolainen**. Organic Aerogels Based on 5-Methylresorcinol. 2011.
116. **Leeli Amon**. Palaeoecological Reconstruction of Late-Glacial Vegetation Dynamics in Eastern Baltic Area: A View Based on Plant Macrofossil Analysis. 2011.

117. **Tanel Peets**. Dispersion Analysis of Wave Motion in Microstructured Solids. 2011.
118. **Liina Kaupmees**. Selenization of Molybdenum as Contact Material in Solar Cells. 2011.
119. **Allan Olsper**. Properties of VPg and Coat Protein of Sobemoviruses. 2011.
120. **Kadri Koppel**. Food Category Appraisal Using Sensory Methods. 2011.
121. **Jelena Gorbatšova**. Development of Methods for CE Analysis of Plant Phenolics and Vitamins. 2011.
122. **Karin Viipsi**. Impact of EDTA and Humic Substances on the Removal of Cd and Zn from Aqueous Solutions by Apatite. 2012.
123. **David Schryer**. Metabolic Flux Analysis of Compartmentalized Systems Using Dynamic Isotopologue Modeling. 2012.
124. **Ardo Illaste**. Analysis of Molecular Movements in Cardiac Myocytes. 2012.
125. **Indrek Reile**. 3-Alkylcyclopentane-1,2-Diones in Asymmetric Oxidation and Alkylation Reactions. 2012.
126. **Tatjana Tamberg**. Some Classes of Finite 2-Groups and Their Endomorphism Semigroups. 2012.
127. **Taavi Liblik**. Variability of Thermohaline Structure in the Gulf of Finland in Summer. 2012.
128. **Priidik Lagemaa**. Operational Forecasting in Estonian Marine Waters. 2012.
129. **Andrei Errapart**. Photoelastic Tomography in Linear and Non-linear Approximation. 2012.
130. **Külliki Krabbi**. Biochemical Diagnosis of Classical Galactosemia and Mucopolysaccharidoses in Estonia. 2012.
131. **Kristel Kaseleht**. Identification of Aroma Compounds in Food using SPME-GC/MS and GC-Olfactometry. 2012.
132. **Kristel Kodar**. Immunoglobulin G Glycosylation Profiling in Patients with Gastric Cancer. 2012.
133. **Kai Rosin**. Solar Radiation and Wind as Agents of the Formation of the Radiation Regime in Water Bodies. 2012.
134. **Ann Tiiman**. Interactions of Alzheimer's Amyloid-Beta Peptides with Zn(II) and Cu(II) Ions. 2012.
135. **Olga Gavrilova**. Application and Elaboration of Accounting Approaches for Sustainable Development. 2012.
136. **Olesja Bondarenko**. Development of Bacterial Biosensors and Human Stem Cell-Based *In Vitro* Assays for the Toxicological Profiling of Synthetic Nanoparticles. 2012.
137. **Katri Muska**. Study of Composition and Thermal Treatments of Quaternary Compounds for Monograin Layer Solar Cells. 2012.
138. **Ranno Nahku**. Validation of Critical Factors for the Quantitative Characterization of Bacterial Physiology in Accelerostat Cultures. 2012.
139. **Petri-Jaan Lahtvee**. Quantitative Omics-level Analysis of Growth Rate Dependent Energy Metabolism in *Lactococcus lactis*. 2012.

140. **Kerti Orumets.** Molecular Mechanisms Controlling Intracellular Glutathione Levels in Baker's Yeast *Saccharomyces cerevisiae* and its Random Mutagenized Glutathione Over-Accumulating Isolate. 2012.
141. **Loreida Timberg.** Spice-Cured Sprats Ripening, Sensory Parameters Development, and Quality Indicators. 2012.
142. **Anna Mihhalevski.** Rye Sourdough Fermentation and Bread Stability. 2012.
143. **Liisa Arike.** Quantitative Proteomics of *Escherichia coli*: From Relative to Absolute Scale. 2012.
144. **Kairi Otto.** Deposition of In₂S₃ Thin Films by Chemical Spray Pyrolysis. 2012.
145. **Mari Sepp.** Functions of the Basic Helix-Loop-Helix Transcription Factor TCF4 in Health and Disease. 2012.
146. **Anna Suhhova.** Detection of the Effect of Weak Stressors on Human Resting Electroencephalographic Signal. 2012.
147. **Aram Kazarjan.** Development and Production of Extruded Food and Feed Products Containing Probiotic Microorganisms. 2012.
148. **Rivo Uiboupin.** Application of Remote Sensing Methods for the Investigation of Spatio-Temporal Variability of Sea Surface Temperature and Chlorophyll Fields in the Gulf of Finland. 2013.
149. **Tiina Kriščiunaite.** A Study of Milk Coagulability. 2013.
150. **Tuuli Levandi.** Comparative Study of Cereal Varieties by Analytical Separation Methods and Chemometrics. 2013.
151. **Natalja Kabanova.** Development of a Microcalorimetric Method for the Study of Fermentation Processes. 2013.
152. **Himani Khanduri.** Magnetic Properties of Functional Oxides. 2013.
153. **Julia Smirnova.** Investigation of Properties and Reaction Mechanisms of Redox-Active Proteins by ESI MS. 2013.
154. **Mervi Sepp.** Estimation of Diffusion Restrictions in Cardiomyocytes Using Kinetic Measurements. 2013.
155. **Kersti Jääger.** Differentiation and Heterogeneity of Mesenchymal Stem Cells. 2013.
156. **Victor Alari.** Multi-Scale Wind Wave Modeling in the Baltic Sea. 2013.
157. **Taavi Päll.** Studies of CD44 Hyaluronan Binding Domain as Novel Angiogenesis Inhibitor. 2013.
158. **Allan Niidu.** Synthesis of Cyclopentane and Tetrahydrofuran Derivatives. 2013.
159. **Julia Geller.** Detection and Genetic Characterization of *Borrelia* Species Circulating in Tick Population in Estonia. 2013.
160. **Irina Stulova.** The Effects of Milk Composition and Treatment on the Growth of Lactic Acid Bacteria. 2013.
161. **Jana Holmar.** Optical Method for Uric Acid Removal Assessment During Dialysis. 2013.
162. **Kerti Ausmees.** Synthesis of Heterobicyclo[3.2.0]heptane Derivatives *via* Multicomponent Cascade Reaction. 2013.

163. **Minna Varikmaa**. Structural and Functional Studies of Mitochondrial Respiration Regulation in Muscle Cells. 2013.
164. **Indrek Koppel**. Transcriptional Mechanisms of BDNF Gene Regulation. 2014.
165. **Kristjan Pilt**. Optical Pulse Wave Signal Analysis for Determination of Early Arterial Ageing in Diabetic Patients. 2014.
166. **Andres Anier**. Estimation of the Complexity of the Electroencephalogram for Brain Monitoring in Intensive Care. 2014.
167. **Toivo Kallaste**. Pyroclastic Sanidine in the Lower Palaeozoic Bentonites – A Tool for Regional Geological Correlations. 2014.
168. **Erki Kärber**. Properties of ZnO-nanorod/In₂S₃/CuInS₂ Solar Cell and the Constituent Layers Deposited by Chemical Spray Method. 2014.
169. **Julia Lehner**. Formation of Cu₂ZnSnS₄ and Cu₂ZnSnSe₄ by Chalcogenisation of Electrochemically Deposited Precursor Layers. 2014.
170. **Peep Pitk**. Protein- and Lipid-rich Solid Slaughterhouse Waste Anaerobic Co-digestion: Resource Analysis and Process Optimization. 2014.
171. **Kaspar Valgepea**. Absolute Quantitative Multi-omics Characterization of Specific Growth Rate-dependent Metabolism of *Escherichia coli*. 2014.
172. **Artur Noole**. Asymmetric Organocatalytic Synthesis of 3,3'-Disubstituted Oxindoles. 2014.
173. **Robert Tsanev**. Identification and Structure-Functional Characterisation of the Gene Transcriptional Repressor Domain of Human Gli Proteins. 2014.
174. **Dmitri Kartofelev**. Nonlinear Sound Generation Mechanisms in Musical Acoustic. 2014.
175. **Sigrid Hade**. GIS Applications in the Studies of the Palaeozoic Graptolite Argillite and Landscape Change. 2014.
176. **Agne Velthut-Meikas**. Ovarian Follicle as the Environment of Oocyte Maturation: The Role of Granulosa Cells and Follicular Fluid at Pre-Ovulatory Development. 2014.
177. **Kristel Hälvin**. Determination of B-group Vitamins in Food Using an LC-MS Stable Isotope Dilution Assay. 2014.
178. **Mailis Päre**. Characterization of the Oligoadenylate Synthetase Subgroup from Phylum Porifera. 2014.
179. **Jekaterina Kazantseva**. Alternative Splicing of *TAF4*: A Dynamic Switch between Distinct Cell Functions. 2014.
180. **Jaanus Suurväli**. Regulator of G Protein Signalling 16 (RGS16): Functions in Immunity and Genomic Location in an Ancient MHC-Related Evolutionarily Conserved Synteny Group. 2014.
181. **Ene Viiard**. Diversity and Stability of Lactic Acid Bacteria During Rye Sourdough Propagation. 2014.
182. **Kristella Hansen**. Prostaglandin Synthesis in Marine Arthropods and Red Algae. 2014.
183. **Helike Lõhelaid**. Allene Oxide Synthase-lipoxygenase Pathway in Coral Stress Response. 2015.
184. **Normunds Stivrins**. Postglacial Environmental Conditions, Vegetation Succession and Human Impact in Latvia. 2015.

185. **Mary-Liis Kütt.** Identification and Characterization of Bioactive Peptides with Antimicrobial and Immunoregulating Properties Derived from Bovine Colostrum and Milk. 2015.
186. **Kazbulat Šogenov.** Petrophysical Models of the CO₂ Plume at Prospective Storage Sites in the Baltic Basin. 2015.
187. **Taavi Raadik.** Application of Modulation Spectroscopy Methods in Photovoltaic Materials Research. 2015.
188. **Reio Pöder.** Study of Oxygen Vacancy Dynamics in Sc-doped Ceria with NMR Techniques. 2015.
189. **Sven Siir.** Internal Geochemical Stratification of Bentonites (Altered Volcanic Ash Beds) and its Interpretation. 2015.
190. **Kaur Jaanson.** Novel Transgenic Models Based on Bacterial Artificial Chromosomes for Studying BDNF Gene Regulation. 2015.
191. **Niina Karro.** Analysis of ADP Compartmentation in Cardiomyocytes and Its Role in Protection Against Mitochondrial Permeability Transition Pore Opening. 2015.
192. **Piret Laht.** B-plexins Regulate the Maturation of Neurons Through Microtubule Dynamics. 2015.
193. **Sergei Žari.** Organocatalytic Asymmetric Addition to Unsaturated 1,4-Dicarbonyl Compounds. 2015.
194. **Natalja Buhhalko.** Processes Influencing the Spatio-temporal Dynamics of Nutrients and Phytoplankton in Summer in the Gulf of Finland, Baltic Sea. 2015.
195. **Natalia Maticiuc.** Mechanism of Changes in the Properties of Chemically Deposited CdS Thin Films Induced by Thermal Annealing. 2015.